공학박사학위논문

Rheological behavior of particulate suspensions containing carbon black nanoparticles

카본블랙 나노입자를 포함하는 입자 분산계 재료의 유변학적 거동 연구

2019년 8월

서울대학교대학원
화학생물공학부
성상훈

Rheological behavior of particulate suspensions containing carbon black nanoparticles

SANG HOON SUNG

School of Chemical and Biological Engineering, Seoul National University

Abstract

Rheological properties of carbon black dispersions are essential from both academic and industrial points of view, and recently getting more attention due to the growth of the Li-ion battery industry. Despite numerous research works on the carbon black dispersions, there are still some features unclear or misunderstood. In this thesis, rheological behavior of various suspensions containing carbon black was studied, particularly in a viewpoint of industrial processing of the electrode slurries for the Li-ion battery. Differences between NMP-based and water-based slurries was first examined, and neutralization-dependent changes in a slurry with PAA binder was demonstrated similarly. For both cases, the slurries showed gel-like and liquid-like rheology according to the difference in the interaction between particles and binders. It was found that the gel-like behavior of the slurries with non-adsorbing polymers is dominant on CB particles, thus showing similar rheological behaviors with CB gels. Based on the understanding on the inter-component interactions, unexpected rheological change of the NMP-based cathode slurries was studied. Mechanism of the rheological changes was identified to be

attributed to CB agglomeration, and processing conditions for the agglomeration were suggested in terms of hydrodynamic stress of the suspending media. In the following chapters, model colloidal gels composed of CB and Newtonian media were used to study rheological characteristics of the dispersions containing CB. The CB gels in various suspending media show universal scaling behavior where the effect of medium viscosity could be normalized regarding relaxation timescale. Moreover, utilizing orthogonal superposition rheometry, it was observed that the CB gels under steady shear exhibit a universal relaxation behavior regardless of the shear rate, suggesting a "time-shear rate superposition."

Keywords: rheology, carbon black suspension, colloidal gel, Li-ion battery, electrode slurry, orthogonal superposition rheology

Student number: 2011-21041

Table of contents

List of figures

1. INTRODUCTION

Carbon black (CB) is a generic term for a family of carbonaceous particles that have been widely used as an additive for plastics or rubbers to impart key characteristics such as electrical conductivity, thermal conductivity, lubrication, reinforcement, etc. They also serve various applications printing inks, paints, coatings, and electrochemical energy storage such as primary and secondary batteries.

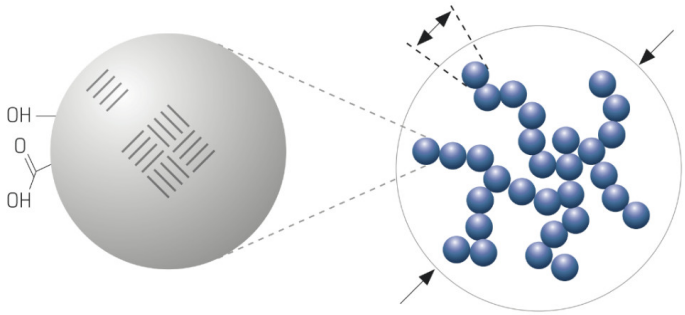

Figure 1.1 Schematic drawing on the structure of carbon black particles.

Rheological properties of CB/polymer compounds and CB suspensions are very important from both academic and industrial points of view. In attempting to elucidate these rheological responses, extensive studies have been carried out for the CB/polymer compounds and CB suspensions. The occurrence of both yield stress and thixotropy for these systems has been found. In general, an increase in the CB concentration and a decrease in the particle size enhance the agglomerate formation thereby increase the viscosity.

The CB particle morphology is specified at different levels: ‘‘particle’’, ‘‘aggregate’’, and ‘‘agglomerate’’ (Figure 1.1). CB is initially formed as roughly spherical primary particles, which covalently fused to form the fundamental structural unit in the CB suspension: aggregates. The CB aggregates exist in a variety of shape types from the higher-structure CB grades consisting of more branched structures to the lower structure grades containing more compact structures, and generally they are considered unbreakable during the normal processing of the materials. The aggregates can bind together by van der Waals forces in more loosely associated. The magnitude of this binding force may change with the chemical properties of the CB particles (such as surface chemistry and surface area), interparticle interaction as well as the suspending media, and presence of additives. In contrast to the aggregates, these agglomerates are characterized by weak bonding between the aggregates and therefore do not retain their integrity during processing. The rheological properties might change with not only the CB agglomerate structure, but also the aggregate structure.

Because of the industrial importance and the complex relationships between microstructure, processing, and rheology, there has been a need for a well-defined reference system that is reproducible for use in scientific investigations. A model carbon black suspension was proposed and characterized by Dullaert et al.[1–3], and studies on many additional carbon black suspensions have been reported by Amari et al,[4] Aoki et al.,[5–9] and Yearsley et al.,[10] Youssry et al.,[11] and Armstrong et al.[12]

The model colloidal gel suggested by Dullaert et al. is composed of carbon black dispersed in nonpolar hydrocarbon oil which shows high reproducibility with careful sample preparation. A model system for the weakly attractive colloidal gel to show universal scaling behavior suggested by Trappe et al.[13] also consists of carbon black dispersed in hydrocarbon oil. A novel approach to study rheological behavior of the model systems under flow will be introduced in the chapter 5 in the current thesis.

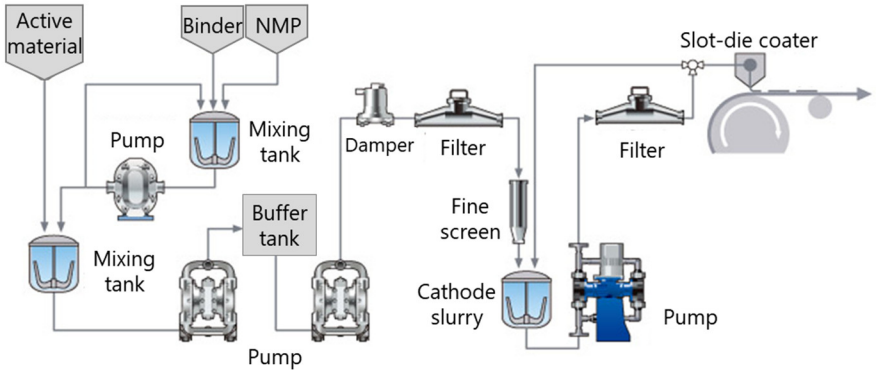

Figure 1.2 Electrode manufacturing process scheme

Meanwhile the importance of rheological behavior of electrode slurries containing CB as well as other various components are getting attention as Li-ion battery industry is growing rapidly. Electrode manufacturing process of the Li-ion battery generally consists of (1) preparing electrode slurry, (2) coating the slurry on current collector, (3) drying, (4) pressing steps. Step 1 and step 2 which are the process utilizing electrode slurries in liquid state were shown in Figure 1.2. Reducing the battery manufacturing cost remains a challenge in the current industries, and detailed attention to fundamental and applied science is required. Strategies for overcoming manufacturing costs include implementing low-

cost processing and adequate quality control tools to reduce the scrap rate in larger format batteries.[14] In the processing of the electrode slurries, control of dispersion stability and rheological properties are very important in terms of quality control Dispersion stability of the slurries can be a crucial factor in the scale up from laboratory to industrial scale since it influences processing issues such as mixing, viscosity control, filter clogging, and uniformity of the electrode.[15,16] For example, in case that the slurry viscosity changes during process (e.g. Figure 1.3), coating thickness can show variation so that the scrap rate and cost of manufacture significantly increase. In particular, it has been reported that the aggregation of carbon nanomaterials used as a conductive agent causes practical problems in the processing of electrode slurries.[17,18] Dispersion quality of the slurries also affects the mechanical strength and electrical conductivity of the electrode, resulting in a significant influence on the performance of a battery such as a cycle life.[19–21]

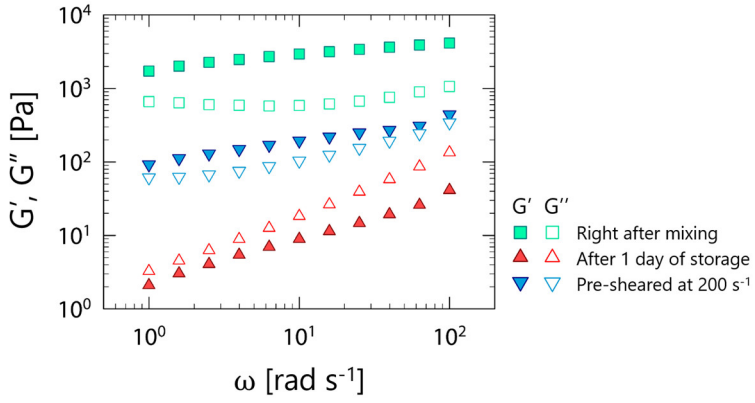

Figure 1.3 Change in rheological characteristics of an NMP-based cathode slurry during storage under mild agitation.

Moreover, many novel flow-assisted battery technologies such as

redox flow batteries [22,23], semi-solid flow cells [24], and electrochemical flow capacitors (EFCs)[25] have been considered to address the issue by offering low cost, high output, and scalability for grid-scale energy storage. In the flow batteries, good dispersion of active materials and conductive carbon black particles is critical to ensure homogeneity and equal distribution of electron conduction paths.

However, only the limited numbers of studies related to the dispersion quality and rheological characteristics of the electrode slurries have been published. Relationship between interparticle interactions in microscopic viewpoint and rheological behavior in macroscopic viewpoint is still far from understanding. The microstructural changes and viscoelastic response of the slurries under flow is far more difficult to understand compared to those at rest, notwithstanding the importance in both industrial and scientific perspective.

Accordingly, we find a great necessity to: (1) study the rheological behavior of the electrode slurries containing carbon black as well as many constituents to clarify the role of each constituents and (2) better understand the flow–structure relationships in colloidal gels composed of carbon black dispersions.

In this thesis, we will navigate the studies on electrode slurries and model slurries containing carbon black as following, which are motivated by complex rheological behavior of the electrode slurries:

In chapter 2, water-based and NMP-based slurries will be compared in terms of rheology and binder adsorption. In addition, effect of viscosity

of the suspending media will be elucidated by comparing rheological behavior of model CB gels

In chapter 3, unexpected rheological changes of the NMP-based slurries under flow will be introduced and the mechanism will be suggested.

In chapter 4, we will investigate the dispersion quality control of the particles in water-based anode slurries containing poly(acrylic acid) as a binder. The slurries show dramatic changes depending on neutralization.

In chapter 5, viscoelastic response of the model CB gels under flow will be studied utilizing a novel technique. It will be discussed that the steady shear flow applied on the CB gel controls overall timescale of the system.

I hope the discussion throughout the chapters will bring us one step closer to the understanding of physical behavior of the complex fluids containing carbon black nanoparticles so that we can control the materials in the beneficial way.

2. Rheological behavior of NMP-based and water-based electrode slurries for Li-ion battery

Overview

In this chapter, we show that NMP-based and water-based electrode slurries have unexpectedly disparate rheological characteristics and investigate the origin of the difference in terms of physicochemical interaction between particle surface and polymeric binder. Polyvinylidene fluoride (PVDF) binder in NMP only work as a thickening agent in the slurry without stabilization effect for the particles, thus rheological characteristics of the slurry highly depend on the particle concentration. Meanwhile, water-soluble binders such as carboxymethyl cellulose (CMC) does a role of dispersant as well as thickener, so that rheology of the water-based slurry is less dependent on the particles.

2.1. Introduction

2.1.1. Solvent and binder systems for the electrode slurries

Electrodes of Li-ion battery consist of active materials and inactive materials coated and onto current collectors. The inactive materials are polymeric binder and conductive additive. The conductive additive contributes to the electronic conductivity, and the binder plays the role of gluing the active materials and the conductive additive together to the current collector.[26] Although a solvent is not a constituent of the electrode composite, the solvent does an important role in the manufacturing process, since the electrodes are manufactured by casting a slurry onto a metallic current collector followed by drying process. The slurry contains active material, conductive carbon, and binder in a solvent. The binder, most commonly polyvinylidene fluoride (PVDF), are pre-dissolved in the solvent, most commonly N-Methyl-2-pyrrolidone (NMP). One of the factors that increase cost is the use of organic solvents such as N-methyl-2-pyrrolidone (NMP) which involves significant capital expense from material purchasing, processing energy (e.g. heated air flow), and process for recovery and treatment of NMP. Therefore, water-based processing of electrodes has been gaining attention as it has advantages such as low cost and environmental compatibility. Transition to an aqueous processing accompanies usage of a water-soluble binder that complies the requirements of an electrode of Li-ion battery.[27] The interactions between the constituents in the slurries have been of less interest in spite of

their substantial influences on the quality of the electrodes.

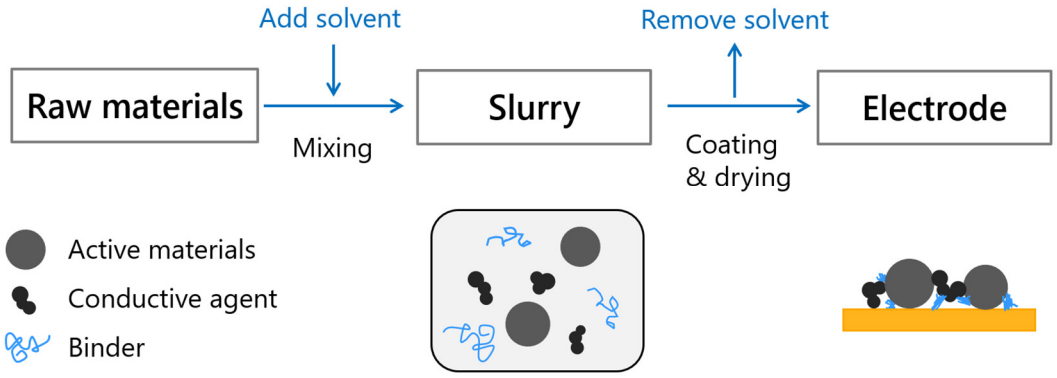

Figure 2.1 Simplified schematic on the manufacturing process and the components of the electrode.

2.1.2. Particle-binder interactions in the electrode slurries

The prime role of the binder is to provide adhesion of particles with current collector such that the electrode does not lose mechanical and electrical integrity.[28] However, in the viewpoint of the manufacturing process, the polymeric binder plays an important role in dispersing the particles to enhance phase stability as well as conferring rheological properties adapted for the coating process.[29,30] Dispersion stability of the slurries can be a crucial factor in scale up from a laboratory to industrial scale since it influences processing issues such as mixing process, viscosity control, filter clogging, and uniformity of the electrode.[15,16] In particular, it has been reported that the aggregation of carbon nanomaterials used as a conductive agent causes practical problems in the processing of electrode slurries.[17,18] Dispersion quality of the slurries also affects the mechanical strength and electrical conductivity of the

electrode, resulting in a significant influence on the performance such as a cycle life.[19–21] In addition to the dispersion quality, rheological behavior of the electrode slurry is known to strongly affect the processing of the slurry such that coating of the electrode in uniform thickness.

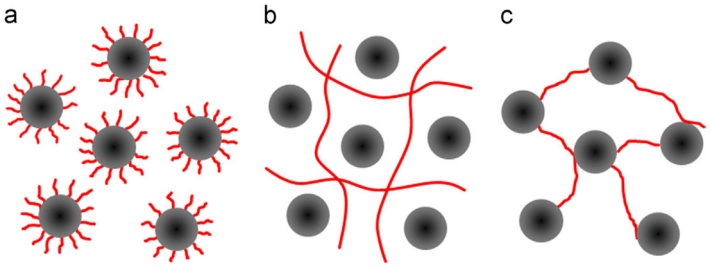

Figure 2.2 Particle–polymer-interaction in a dispersion with (a) sterically stabilizing dispersant, (b) thickener and (c) coagulating binder, as suggested by [31].

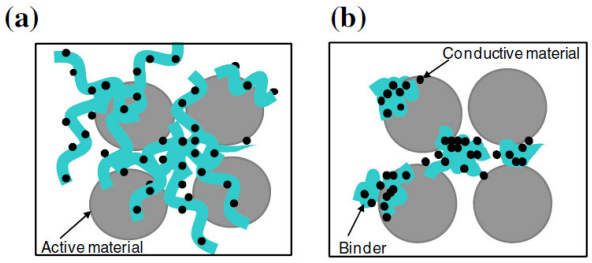

Figure 2.3 Schematic description of the internal structure of the electrode slury: (a) initial sample and (b) aged sample, as suggested by [32].

There have been only few literature reports those addressed the issues related with either on polymer-binder interaction or the rheological control of the slurry. Most of the literatures described the PVDF binder in NMP-based slurry as a typical adsorbing polymer that does a critical role on the microstructural change of the dispersion and the corresponding rheological properties.[31–35] It has been demonstrated that the addition of a high molecular weight PVDF binder can establish gel formation by

bridging flocculation (Figure 2.2). It has also been argued that the internal structure of the slurry is determined by the interaction of particle and polymeric binders, which can lead to the aggregation of the particles as shown in Figure 2.3.[32,33] It is notable that they are arguing such mechanism with no evidence of adsorption or interaction of PVDF binder on the particles.

2.1.3. Roadmap of the current chapter

The present work is dedicated to the analysis of particle-binder interactions in the NMP-based and water-based electrode slurries. We mainly compare the slurries by means of rheological testing. In particular, model slurries consisting of active material and carbon black are used to study the role of each particle on the rheological characteristics of the electrode slurry. The results are expected to provide correct understanding on the role of constituents and interactions in the electrode slurries, which have been hardly- or mis-understood.

2.2. Materials and methods

Slurries for the manufacturing of cathode coatings were prepared by mixing active materials and CB powder with binder solutions. As a cathode active material, $Li(Ni_{1/3}Mn_{1/3}Co_{1/3})O_2$ (NMC, Gelon, China) with a mean particle size of 10 μm were used. Graphite (SG-BH8, Ito graphite, Japan) with 8 μm were used as a negative active material. As a conductive additive,

carbon black (Super C65, Timcal Ltd., Switzerland) with a BET surface of 62 m^2/g and a mean TEM particle size of 35 nm was used.

PVDF homopolymer (Polyvinylidene fluoride; Solef 6020, 700,000 g/mol, Solvay, Belgium) was dissolved in NMP (N-Methyl-2-pyrrolidone; Daejung) for 6 h by means of a magnetic stirrer at 60 °C. CMC (carboxymethyl cellulose, 250,000 g/mol, degree of substitution 0.7) was dissolved in water for 24 h at room temperature. The carbon black powders were first pre-mixed using a rotor-stator homogenizer (Ultra-Turrax T18, IKA, Germany) at 8000 rpm for 5 min. Consequently, an active material was added and mixed using an anchor-type overhead stirrer at 1000 rpm for 15 min. Volume fraction of each particle was calculated based on the density of the materials provided by the manufacturers.

Rheological characterization is conducted in strain-controlled mode using an AR-G2 stress-controlled rheometer (TA Instrument) in 40 mm serrated parallel plate geometry to reduce wall-slip, or 60 mm parallel plate geometry, depending on the rheology of the sample. Steady-state flow viscosities were measured from $\dot{\gamma}$ = 464.1 s-1 to 0.01 s-1 using varied equilibration time from 10 s at the highest shear rate to 60 s at the lowest shear rate. Frequency sweep tests were carried out within the linear viscoelastic regime for each sample.

The amount of adsorbed polymer was determined by quantifying the polymer concentration in the medium before and after polymer adsorption. Model slurries with different concentrations of PVDF/NMP and

CMC/water, respectively, were prepared and centrifuged at 10,000 rpm for at least 3 hours. When all the particles are settled, the supernatant phase becomes transparent. The concentrations of residual polymer remaining in the supernatant solution were obtained by the gravimetric analysis. The solvent was evaporated by drying in a convection oven at 110 °C, and the residue was weighed with a microbalance. The total amounts of polymer adsorbed on the particles were obtained by calculating the difference between the amount of polymer in the initial solution and the supernatant solution after centrifuge.

2.3. Results and discussion

2.3.1. Comparison between NMP-based and water-based slurries

We start with a representative example of a comparison between water-based and NMP-based electrode slurries containing same solid contents. Figure 2.4 shows the frequency-dependent linear viscoelastic moduli of the cathode slurries which contain 19 vol% of NMC as an active material and 1.3 vol% of C65 carbon black as a conductive agent. The slurries show significant difference in rheological characteristics despite the same volume fraction of particles. Higher slope of G' that crossovers at high frequency shown for the water-based slurry indicates the slurry is a viscoelastic liquid similar to a polymer solution (Figure 2.4a). Meanwhile, the NMP-based slurry shows nearly frequency-independent G' and

minima of G", which is a typical behavior of colloidal gels (Figure 2.4b).

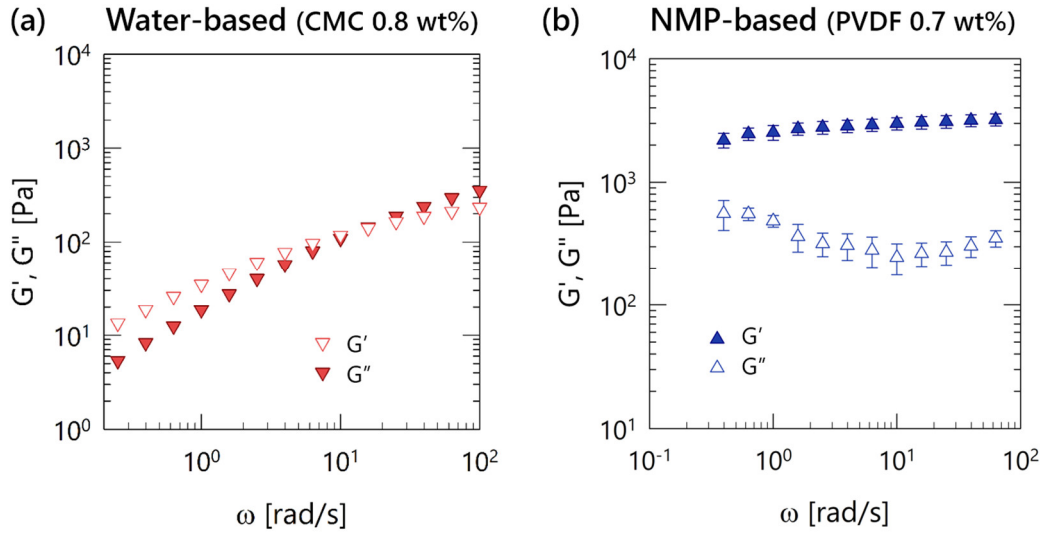

Figure 2.4 Storage (G') and loss (G'') moduli as a function of frequency of cathode slurries with CB 1.6 wt%(=1.3 vol%), NMC 51 wt%(=19vol%) dispersed in CMC/water (a) and PVDF/NMP system.

To see the effect of the binder/solvent system on the rheological characteristics of the slurries, both cathode and anode slurries with lower volume fraction were prepared. Figure 2.5 shows the frequency-dependent viscoelastic moduli of the slurries. The difference between water-based and NMP-based slurry is clearly seen for both cathode and anode slurries: NMP-based slurries show obviously gel-like response with much higher level of G' in a whole frequency range, while water-based slurry show liquid-like (though which can be ambiguous yet) response. Difference between cathode (NMC as an active material) and anode (graphite as an active material) slurries are not significant aside from the G' level difference in NMP-based slurries.

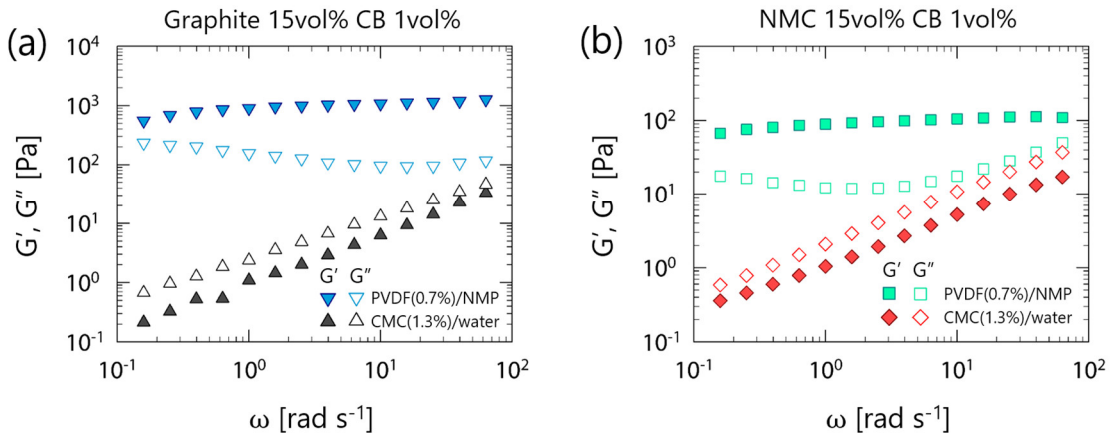

Figure 2.5 Comparison of G' and G'' as a function of frequency between NMP-based and water-based anode slurry (a) and cathode slurry (b). All the slurries contain 15 vol% of active material and 1 vol% of carbon black.

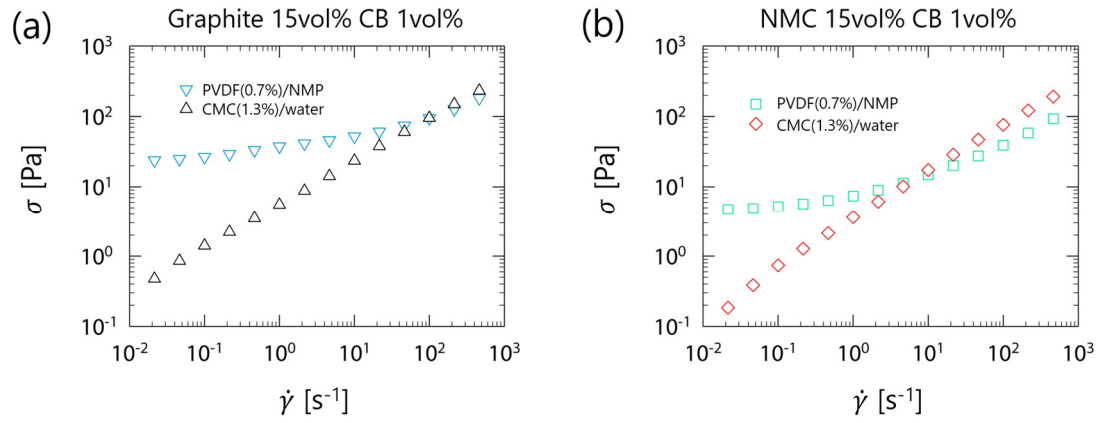

Figure 2.6 Shear stress as a function of steady shear rate between NMP-based and water-based anode slurry (a) and cathode slurry (b). All the slurries contain 15 vol% of active material and 1 vol% of carbon black.

Figure 2.6 shows steady state shear stress in terms of shear rate of the slurries same as those used in Figure 2.5.[a] NMP-based slurries show

[a] A cross-hatched upper plate and a sandpaper-attached lower plate were used for the steady flow measurements of the NMP-based slurries, because they show severe wall-

yielding behavior which can be translated into infinitely high viscosity at very low shear rate or stationary state. The results are consistent with the frequency dependent moduli data those indicate that NMP-based slurries are gel-like while water-based slurries are liquid-like.

From the results, it can be assumed that water-based slurry is composed of well-dispersed particles while NMP-based slurry is a gel consisting of flocculating particles. In other words, polymeric binder dominates the rheology of the water-based slurry and particles dominate the NMP-based slurry. The assumption will be verified in the following section.

2.3.2. Role of constituents in the NMP-based slurry on the rheological behavior

It is presented in the former section that the binder/solvent system does a crucial role on the rheological behavior of the slurries. Since it is not clear which component does which role in a slurry, the role of each component is figured out using the method of subtraction. For that purpose, one or two components were excluded from the NMP-based cathode slurry. Rheological behavior of model slurries containing NMC

slip when geometries with smooth surface are used.

only and CB only, respectively, will studied with respect to the influence of PVDF binder on each particle.

Figure 2.7 shows steady state viscosity of three suspensions with different compositions of particles are dispersed in 2.5% PVDF solution. Viscosity curve of the cathode slurry containing NMC 25 vol% and CB 1.3 vol% demonstrates a typical gel-like behavior similar as the data shown in the previous section. Slope of the viscosity at low shear rate is nearly -1, which means the material exhibits a yielding behavior. CB 1.3 vol% suspension shows a similar shape of the viscosity curve with the electrode slurry, as like the curve is shifted downward. Viscosity of NMC 25vol% suspension is nearly Newtonian, and the value is significantly lower than CB 1.3 vol% despite the larger volume fraction.

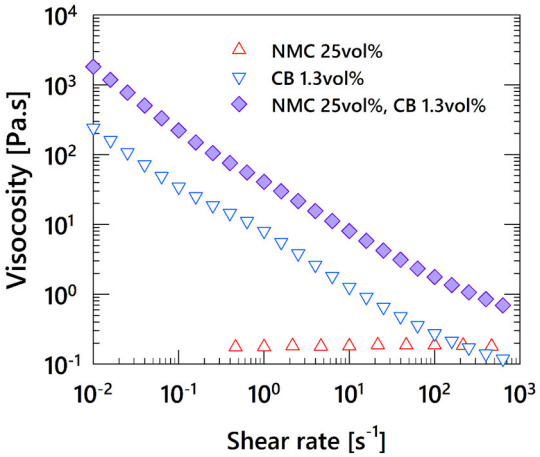

Figure 2.7 Viscosity as a function of steady shear rate of NMP-based model slurries containing NMC (25 vol%), CB (1.3 vol%) and both respectively.

The results can be unexpected for those who are not familiar with rheology of the electrode slurries. Many researchers have made a mistake assuming the active material dominate the bulk rheological properties of

the slurry[31,33,34,36] because the amount of active material is much higher than conductive agent: 20-30 times higher in weight fraction and 15-20 times higher in volume fraction. Meanwhile, it has already been presented that the carbon additive form colloidal gels and a high volume fraction of large non-Brownian active material particles has little effect on the rheology of the mixture [37].

Viscosity of NMC suspensions dispersed in 2.5% PVDF solution was measured for various volume fractions (Figure 2.8). Rate-dependent viscosity of the suspensions are nearly-Newtonian except that of 35 vol% which is slightly shear thinning. Even for the 35 vol% NMC suspension, level of the viscosity is much lower than 1.3 vol% CB suspension shown in Figure 2.7. The results suggest that active material (NMC) particles in NMP-based cathode slurry do not form the gel by themselves regardless of the volume fraction.

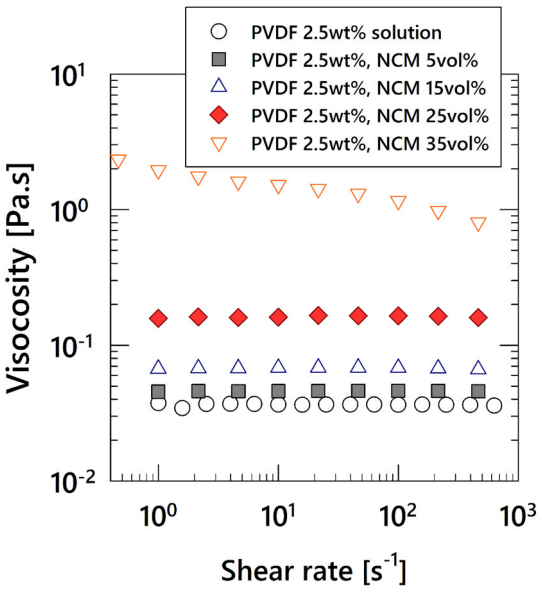

Figure 2.8 Steady shear viscosity as a function of shear rate of NMC/PVDF/NMP

suspensions for a various volume fractions as indicated.

An important issue can be suggested from the Newtonian viscosity of the NMC suspensions: fast sedimentation of NMC particle due to its large size (~10 μm) and high density (~4.7 g cm^{-3}). NMC particles in a slurry with absence of CB will possibly sediment before complete drying process, resulting in inhomogeneous distribution in the vertical direction. Measurement of the NMC suspensions demanded a special attention due to the fast sedimentation. All the measurements were performed as fastest as possible, and a concentric cylinder geometry was used to minimize the effect of sedimentation on the rheological properties. Such an issue does not occur for the slurries containing enough carbon black that forms gel and provides yield stress.

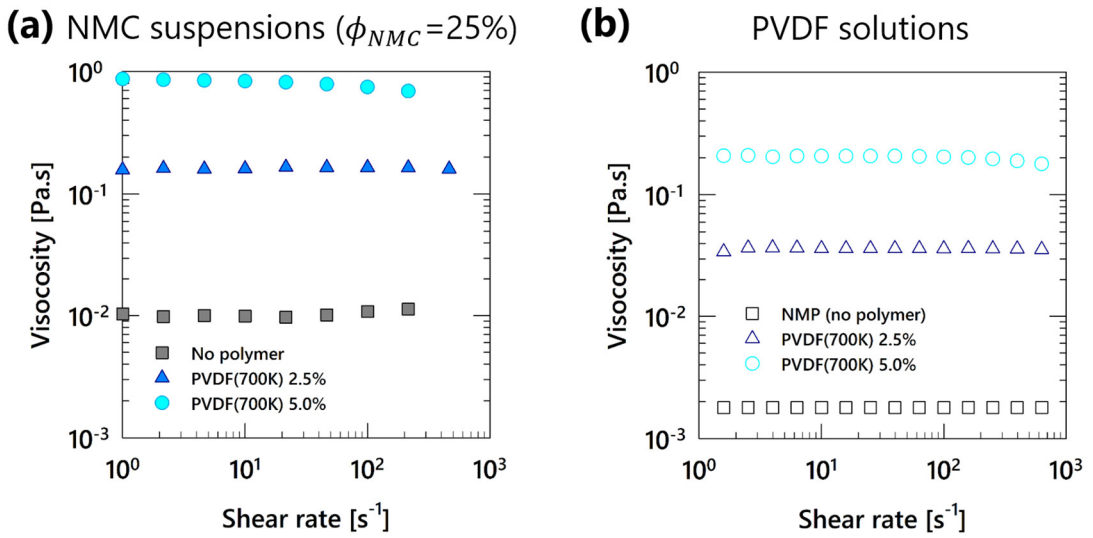

Figure 2.9 Steady shear viscosity as a function of shear rate of (a) NMC/PVDF/NMP (NMC 25 vol%) suspensions and (b) PVDF solutions with various concentrations as indicated.

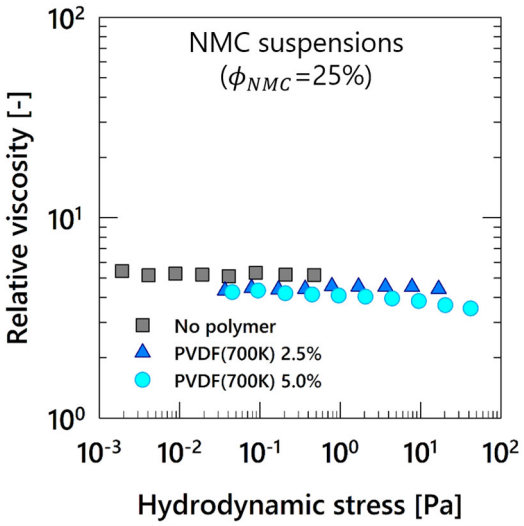

Figure 2.10 Relative viscosity as a function of hydrodynamic stress of NMC/PVDF/NMP (NMC 25 vol%) suspensions for a various PVDF concentrations.

To identify the role of PVDF in the NMC/PVDF/NMP suspension, the viscosity of the 25 vol% NMC suspensions according to PVDF concentration is shown in Figure 2.9a. The suspensions show nearly-Newtonian behavior with different viscosity levels and those viscosity levels are likely to be proportional to that the PVDF solutions (Figure 2.9b). For the verification, the viscosities are normalized by PVDF solution viscosity by plotting the relative viscosity η/η_{medium} in terms of hydrodynamic stress $\eta_{medium}\dot{\gamma}$ (Figure 2.10). The viscosities coincide into nearly a single curve when they are normalized by matrix viscosities.

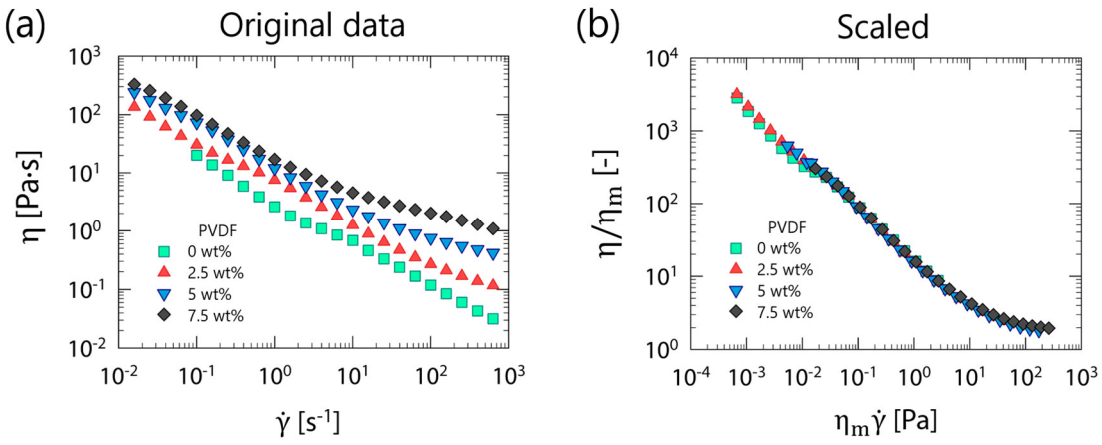

Figure 2.11 (a) Viscosity as a function of shear rate (a) and relative viscosity as a function of hydrodynamic stress (b) for 1.3 vol% CB suspensions dispersed in PVDF solutions.[b]

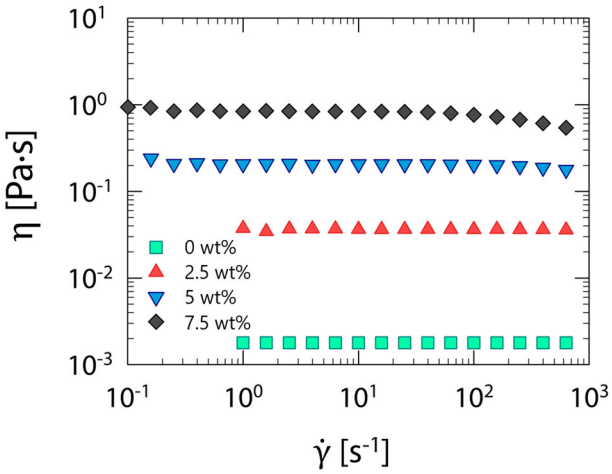

Figure 2.12 Viscosity as a function of shear rate for PVDF solution with no particle for different PVDF concentrations.

Rheological behavior of CB suspensions was investigated in a similar

[b] PVDF concentrations denoted in this section are not the weight fraction of the polymer in the slurry but in the solution only. Each polymer solution was used as a matrix with a fixed viscosity presuming that the polymer does not adsorb to the particle; which will be verified in the following.

manner to the NMC suspensions; viscosities of the CB suspensions were measured for various PVDF concentrations. All the suspensions show gel-like yielding behavior regardless of PVDF concentration (Figure 2.11a). The viscosity curves are similar in shape and coincide into a single curve when they are normalized by matrix viscosities, that is, relative viscosity in terms of hydrodynamic stress (Figure 2.11b). The viscosities for the PVDF solutions as matrices are shown in Figure 2.12. The overlapping means that the Brownian time of the system is dependent on the matrix viscosity.[38] Therefore, the dimensionless viscosity of the system follows the dimensionless shear rate or Peclet numbers $Pe = 6\pi a^3 \eta_m \dot{\gamma} / k_B T$ of the flow.c The single curve of the normalized flow curve demonstrates that the interparticle interaction or microstructure of the dispersions is identical despite the different polymer concentrations. The results also imply that PVDF does not adsorb to the particles, so that the solutions can be regarded as homogeneous matrices with different viscosities, which was presumed in the start of the section.

[c] Please note that the $\eta_m \dot{\gamma}$ is proportional to the Pe for the same particle dispersions.

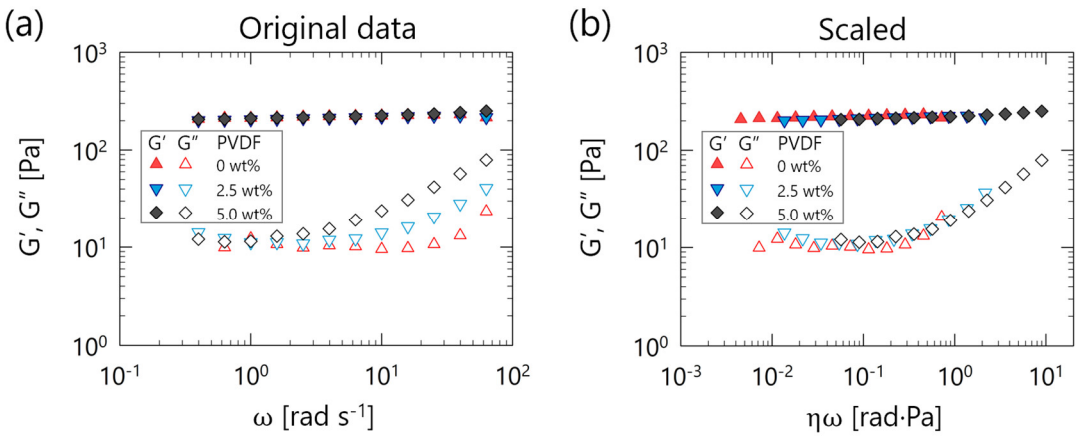

Figure 2.13 (a) Linear viscoelastic moduli G' and G'' as a function of frequency and (b) the moduli as a function of scaled frequency by the medium viscosity for CB suspensions with different PVDF concentration.

Frequency-dependent viscoelastic moduli of the slurries also confirm that the PVDF has only an effect of viscosity increase in the polymeric solution as suspending media. The moduli of the CB suspensions with different PVDF concentration are plotted against oscillation frequency in Figure 2.13a. G' are nearly overlapping for all the suspensions and G'' show deviation at high frequency range. It can be supposed that the difference in G'' is an effect of medium viscosity, similar to the steady flow seen in Figure 2.11. In addition, the moduli show superposition when the data are scaled in the frequency axis (Figure 2.13b). The scaling was carried out simply by multiplying the medium viscosity (=solution viscosity) to the frequency axis. More detailed study on the CB suspensions, including normalization of the rheological data in terms of medium viscosity, will be addressed in the chapter 5.

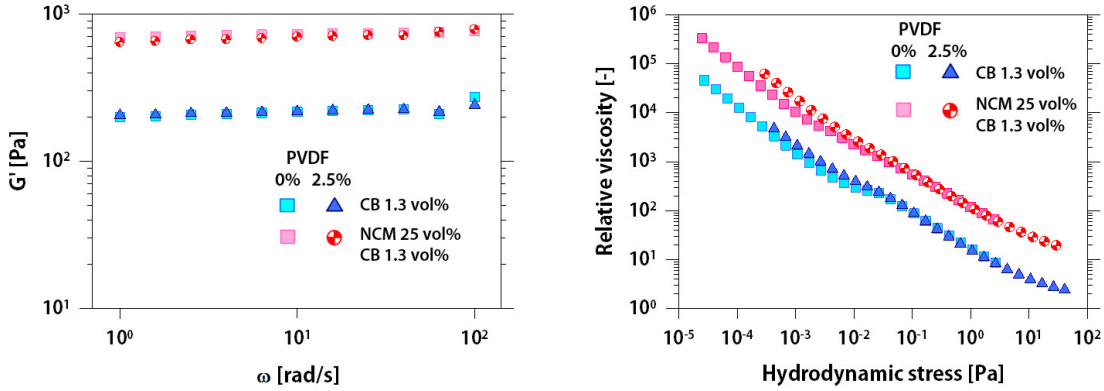

Figure 2.14 (a) Storage modulus G' as a function of frequency and (b) relative viscosity as a function of hydrodynamic stress for cathode slurries with CB 1.3 vol% and NMC 25 vol% dispersed in 2.5% PVDF solution and pure NMP (PVDF 0%).

As we have seen that rheological behaviors of both NMC suspension and CB suspension show little change according to the addition of PVDF, it can be expected that the NMP-based cathode slurry containing both particles will show the similar results. Rheological measurements data for the cathode slurry containing 25 vol% NMC and 1.3vol% CB are shown in Figure 2.14. For comparison, the data for the 1.3vol% CB suspension are plotted together. As expected, the cathode slurries with PVDF and without PVDF show very similar shape and value in both frequency-dependent moduli and $\eta_m\dot{\gamma}$-dependent η/η_m. It can be demonstrated that PVDF in the slurry only changes the viscosity of the dispersing matrix with no

influence on inter-particle interactions. Another significant feature shown in the Figure 2.14 is that the electrode slurry and the CB suspension show very similar shape in both frequency-dependent moduli and rate-dependent viscosity. It should be noted that the rheological characteristics of the cathode slurry is reproducible only when the sample preparation process is controlled strictly. The processing condition dependence will be addressed in detail in the following chapter. As previously shown in the Figure 2.7, small amount of CB dominates the rheological characteristic of the electrode slurry regardless of presence of PVDF.[d] Similar to our results, it was reported in a previous literature that the carbon additive forms strong colloidal gels, and the introduction of a high volume fraction of large non-Brownian particles has little effect on the gelation.[37]

[d] More details on rheological characteristics of the CB suspensions – including variation of loss moduli depending on matrix viscosity – are discussed in the chapter 5.

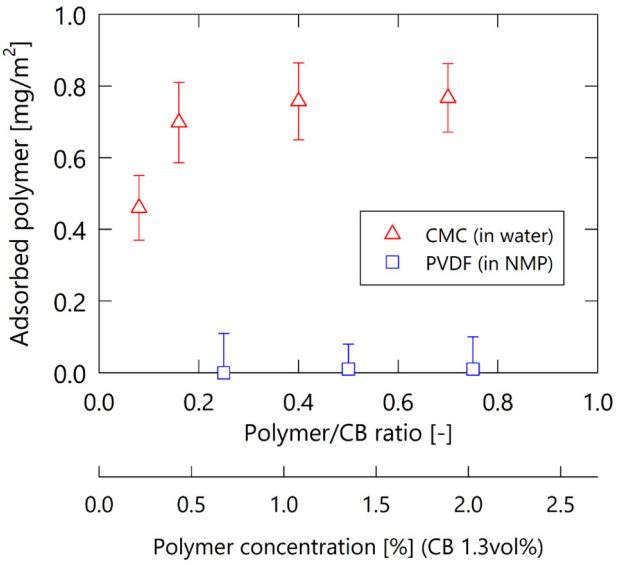

Figure 2.15 Adsorption isotherms of PVDF in NMP and CMC in water on CB surface for varied polymer concentration.

All the rheological data suggest that PVDF does not adsorb to NMC nor CB in NMP-based slurries. Nevertheless, direct measurement of the adsorption is needed for the clear conclusion. The adsorption amount of PVDF onto the CB surface measured using gravimetric analysis is shown as a function of polymer/particle ratio in Figure 2.15. The adsorption amount of CMC in water to the same CB particle was plotted together, to provide data of adsorbing case for comparison. The results clearly show that the PVDF in NMP does not adsorb to CB unlike CMC in water. Adsorption behavior of CMC will be discussed together with the rheological behavior of the water-based slurries in the following section.

So far, we have verified the non-adsorbing behavior of PVDF in NMP-based slurry and its effect on the rheological characteristics of the slurry.

One may raise a question on the binder adsorption in the NMP-based slurry: what about other polymers which dissolve in NMP? For example, though PVDF is major binder material, other polymers such as poly(methyl methacrylate) (PMMA) can be used as binders for the electrodes.[39] To check the adsorbing property, rheological characteristics of the NMP-based CB suspensions with different polymers – PVDF, polycarbonate(PC), PMMA – shown in Figure 2.16. The suspensions containing PVDF, PC, PMMA showed nearly identical G' and G'' suggesting the polymers do not adsorb to the CB particles. The only polymer that showed different effect on the rheological properties of the suspensions was polyvinylpyrrolidone (PVP). The CB suspension with PVP showed nearly-Newtonian behavior so that G' was not measured in our experimental setting and only G'' showed slope of 2, which indicates liquid-like rheological characteristics. Therefore, it can be inferred that PVP adsorbs to CB surface and provide steric stabilization, while the other polymers do not. To confirm that the polymers show different adsorbing behavior, electrical conductivity of the suspensions was compared for the PVDF- and PVP-containing suspension. The suspensions show substantial difference in electrical conductivity: CB suspension with PVDF is far more conductive, which indicates the percolation path is formed by contact of the conductive particles.

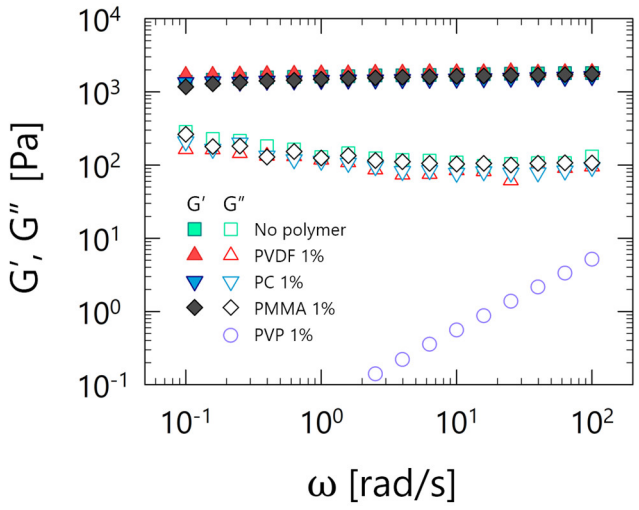

Figure 2.16 Frequency sweep measurements on C65 suspension (5 wt%) with various NMP-dissolving polymers.

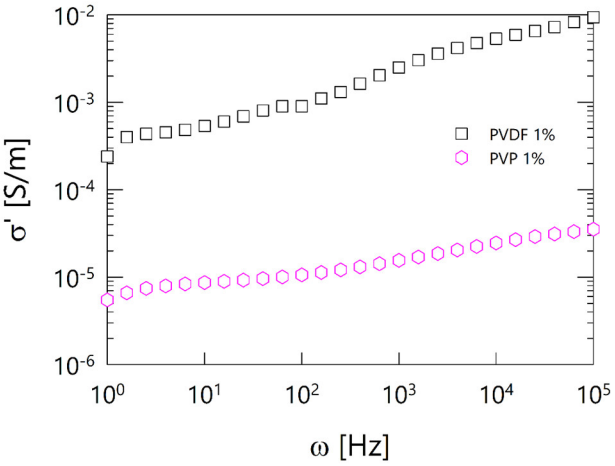

Figure 2.17 AC electrical conductivity measurements on C65 suspension (3 wt%) containing PVDF and PVP.

2.3.3. Role of constituents in the water-based slurry on the rheological behavior

As it was determined that CMC in water adsorb to the particles unlike PVDF in NMP (Figure 2.15), we can expect that the water-based slurries show completely different rheological behavior according to the addition of either binder or particles. We already know that the water-based slurries show liquid-like rheological properties compared to NMP-based slurries (Figure 2.4) and that the influence of the polymer solution is dominant. However, it is not clear yet how much dominant the polymer is compared to the particles.

In Figure 2.18, the rheological properties of the CMC solution and the water-based slurries containing the constituent particles are compared. What we can see in the results is that the influence of the particles is an increase of the moduli and viscosity. The increasing magnitude is nontrivial but very small when compared with the case of NMP-based slurries. Shape of the curve is retaining the shape for the polymer solution even when a large amount (corresponding to 25% in volume) of graphite particle is added. Rheological characteristics of the graphite suspension and the CB suspension were qualitatively similar.

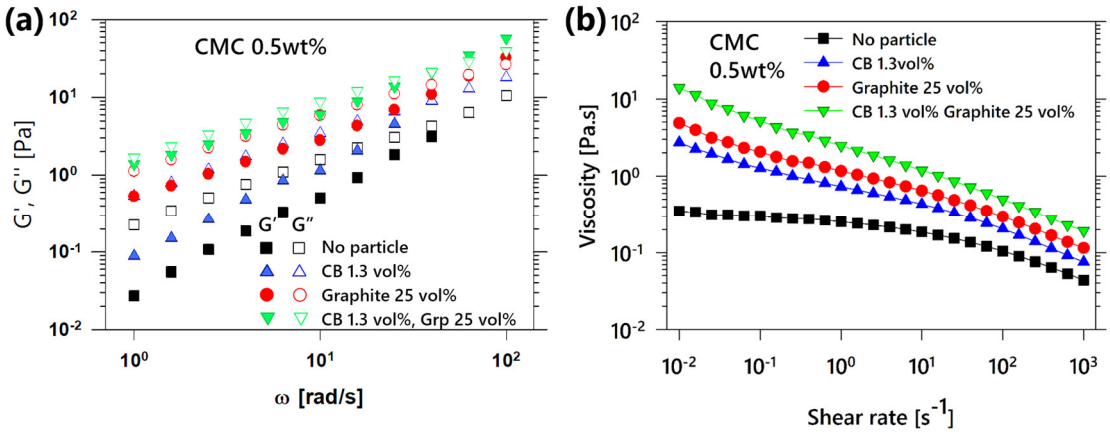

Figure 2.18 (a) Storage (G') and loss (G'') moduli as a function of frequency and (b) viscosity as a function of steady shear rate of the CMC/water-based model slurries containing different composition of particles as indicated.

Viscosity increase of the suspensions were observed according to the increase of the volume fraction or CB and graphite, respectively (Figure 2.19). The changes are monotonic and show little change in the shape, similar to what was seen in Figure 2.18b. For the purpose of comparing the influence of each particle on the viscosity of the electrode slurry, relative viscosity as a function of the particle volume fraction is shown in Figure 2.20. The substantial difference the difference in the hydrodynamic effective volume fraction, which of CB is much higher due to the fractal structure of the fused aggregates.

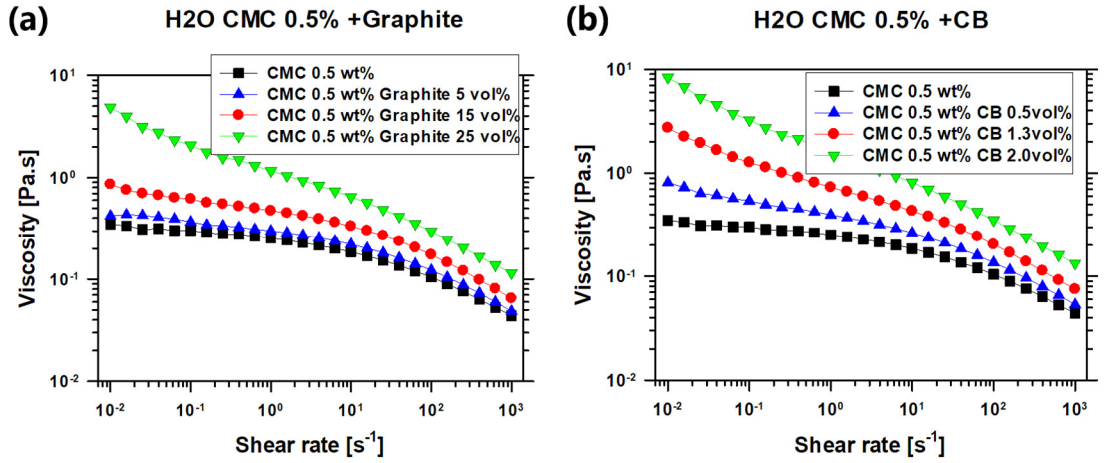

Figure 2.19 Viscosity as a function of steady shear rate of the CMC/water-based model slurries with varied volume fraction of (a) graphite and (b) CB.

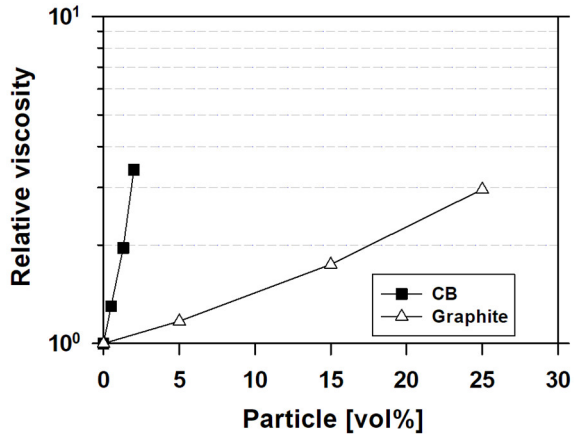

Figure 2.20 Relative viscosity of the CMC/water-based model slurries at shear rate $1s^{-1}$ in terms of volume fraction of the particles.

The gradual changes in suspension viscosity according to the particle volume fraction implies stabilization of the particles to form a well-dispersed system. To directly see the effect of CMC in the water-based slurry, frequency-dependent moduli of the model slurries containing CMC and containing only particles without polymer were plotted together in Figure 2.21. As expected from the adsorption measurement and the

previous results, effect of CMC on the rheological property is significant. The model slurries show nearly-plateau G' whose magnitude is several times higher than that of the slurries containing the polymer. The gel-like rheology of the polymer-free model slurries is due to the aggregation of particles which are naturally attractive. Therefore, we can conclude that the CMC binder in the water-based slurries works as a dispersant to alter the slurries from gel to liquid in rheological aspect. The dispersing effect of the polymer in water-based slurry is in contrary to the NMP-based slurry where the polymer only increases viscosity of the suspending medium with no change in the interparticle interactions.

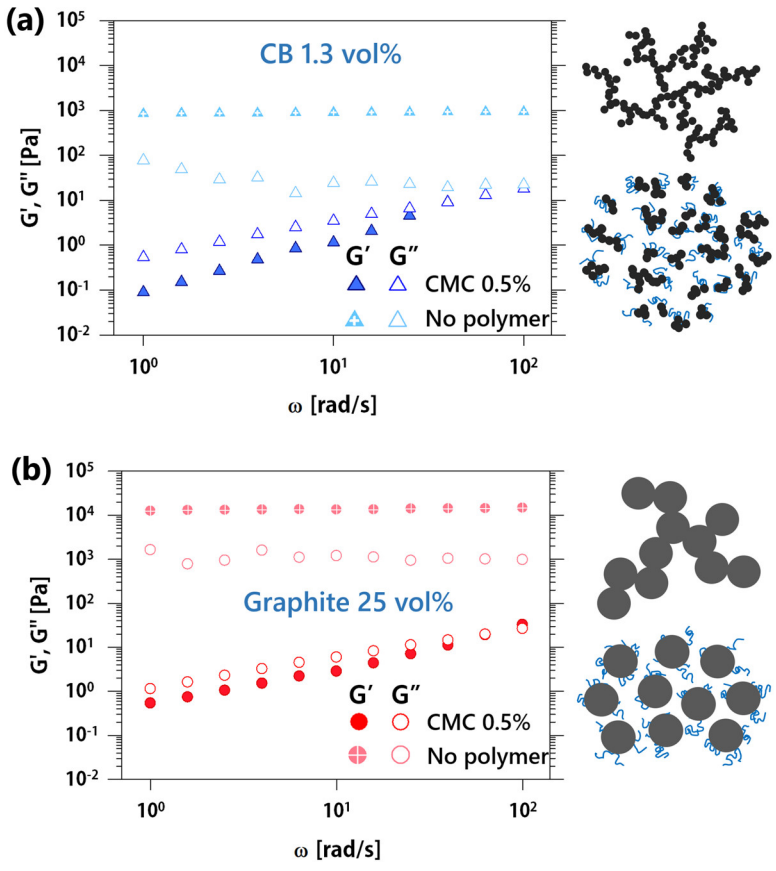

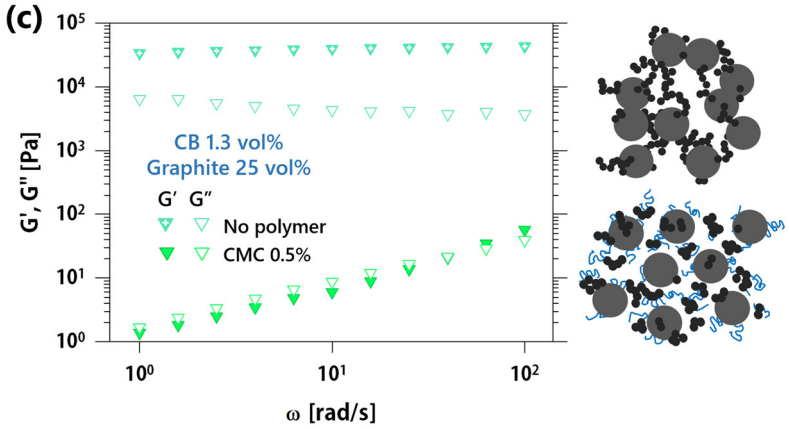

Figure 2.21 Comparison of G' and G'' as a function of frequency depending of the existence of CMC in model slurries composed of (a) CB only (b) graphite only and (c) both CB and graphite particles.

The dispersing effect of the polymeric additive on the suspension can change according to polymer/particle ratio, or grafting ratio of the polymer on the particle surface. For example, small amount of polymer may form bridges between the particles leading to the 'bridging flocculation' and excess amount of polymer can lead to the 'depletion flocculation', both results in gelation of the suspension. The adsorption isotherm (Figure 2.15) that shows saturation of adsorption at about 0.5 wt% of CMC suggests a possibility of bridging flocculation due to the partly adsorbed polymer in the model slurry containing smaller amount of CMC, and a possibility of depletion attraction due to the excessive polymers for the slurry with larger concentration of CMC.

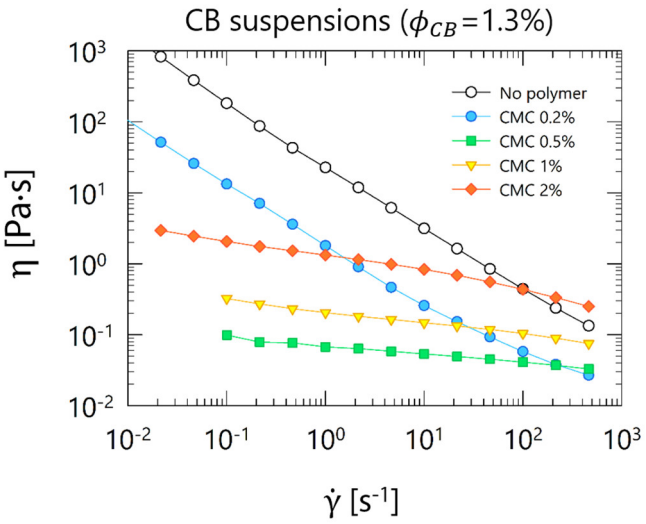

Figure 2.22 Viscosity as a function of steady shear rate of the 1.3 vol% CB suspension with varied concentration of CMC.

The results shown in the Figure 2.22 suggest that the bridging nor depletion is hardly occurring at whole concentration range of our experiments. At low concentration range, the gel-like yielding behavior gradually becomes liquid like until the CMC concentration reaches 0.5%. As the PAA concentration further increases, the viscosity increases over a wide shear rate range maintaining its nearly-Newtonian behavior, which is attributed to the viscosity of the polymer solution itself. The Newtonian behavior of the model slurry which is common in the stable dispersions suggests that CMC is effectively reducing the attractive interparticle interactions through the steric stabilization. The nearly-Newtonian viscosity of the slurry far beyond the adsorption saturation point indicates that the influence of depletion attraction due to free polymer is not existing or negligible.

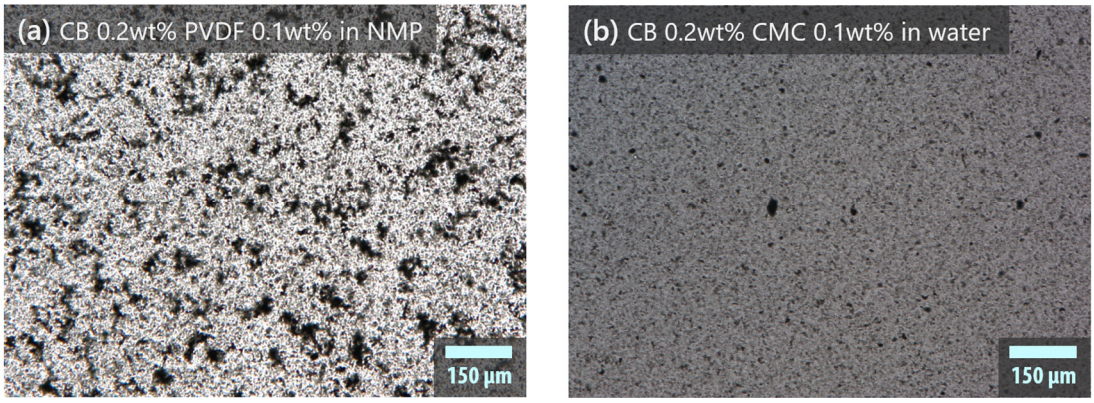

Figure 2.23 Optical microscopic images of diluted samples containing 0.2 wt% CB and 0.1 wt% binder for (a) NMP-based and (b) water-based model slurries.

2.4. Conclusion

Rheological characterization and polymer-particle adsorption measurements were conducted on the model electrode slurries for the clarification of the following questions: (1) Rheological difference between NMP-based and water-based slurries; (2) Microstructural origin of the difference depending on the formulation. Summarizing the results, PVDF in NMP and CMC in water play different roles on the dispersion of particles, leading to different influences on the rheological properties. In case of NMP-based slurries, PVDF binder does not adsorb to the particles. Rheological properties of the model slurries show a universal behavior when they were normalized by viscosity of PVDF solution. The universal

behavior indicates similarities in interparticle attraction and structure. In other words, dispersion states of NMP-based slurries are dominated by interaction between particles but not by polymeric additives. Nevertheless, the existence of PVDF in the slurry has a nontrivial influence on the dispersion stability. It will be further discussed in Chapter 3 that how come the non-adsorbing polymer affect the dispersion stability. Since the rheological properties of the NMP-based electrode slurries are dominated by CB, understanding the rheological properties and the structural changes of CB gels during flow will be helpful for understanding and improving the electrode manufacture process. In Chapter 5, fundamental understanding on the rheological response of the attractive CB dispersions under flow will be discussed.

Meanwhile, in case of the water-based slurries, CMC as a binder adsorbs to the particles, leading to significant changes both in rheology and microstructure. The adsorbed CMC provide steric stabilization to the dispersed particles, therefore attraction between particles become negligible. As a result, rheological behavior of the slurries is dominated by the polymeric binder rather than particles. The effect of binder adsorption is expected to lead to the difference in microstructure and electrochemical characteristics as well, though they are not directly compared in the current chapter because the materials systems are different. The effect of binder adsorption will be revisited in Chapter 4 where poly(acrylic acid) is used as a binder to control adsorption behavior without changing materials.

3. Flow-induced changes of NMP-based cathode slurry

Overview

In this chapter, a peculiar behavior of NMP-based cathode slurry will be explored. NMP-based slurries show many unexpected rheological variations depending on formulation and processing conditions, and the viscosity decrease during storage is one of them. Magnitude of the rheological change is large enough to make problems in continuous coating process, therefore the change should be avoided. From the rheological experiments, it was demonstrated that the low shear rate of flow accelerates the decrease of rheological properties of the slurry. The rheological change was attributed to the agglomeration of carbon black particles resulting to the large sphere. Origin of the flow-induced agglomeration was discussed by means of surface energy difference between carbon black and active material particles.

3.1. Introduction

In the electrode manufacturing process, it is beneficial to control dispersion stability and rheological properties adapted for the coating process.[29,30] Dispersion stability of the slurries can be a crucial factor in the scale up from laboratory to industrial scale since it influences processing issues such as mixing, viscosity control, filter clogging, and uniformity of the electrode.[15,16] In particular, it has been reported that the aggregation of carbon nanomaterials used as a conductive agent causes practical problems in the processing of electrode slurries.[17,18] Dispersion quality of the slurries also affects the mechanical strength and electrical conductivity of the electrode, resulting in a significant influence on the performance of a battery such as a cycle life. Change of slurry viscosity causes the inhomogeneity in electrode thickness which can result in variation in electrode balance locally and affect the cell performance. A problem is that the NMP-based cathode slurries sometimes shows unexpected variation in rheological properties. Most of the variation is due to the processing conditions such as mixing and storage conditions. In the current chapter, we focused on the effects of storage time and speed of agitation during storage. It has already been reported that the agitation accelerates the agglomeration of the binder and carbon conductive additive, resulting in a rheological change.[32] However, the previous literature did not provide clear mechanism of the agglomeration nor quantitative analysis on the flow condition where the agglomeration occurs. In the

current chapter, cathode slurry consisting of acetylene black (AcB) as a conductive agent and $LiNi_{0.8}Co_{0.15}Al_{0.05}O_2$ (NCA) as an active material was used as a standard slurry for the rheological experiments. The study will start with clarifying the combination of material that shows flow-induced changes. What will follow is unveiling the microstructural mechanism behind the rheological change. Finally, criteria on the flow condition to accelerate or prevent the change will be suggested.

3.2 Experimental

Slurries for the rheological and microstructural characterizations were prepared by mixing active materials and conductive agent with binder solutions. As a cathode active material, $LiNi_{0.8}Co_{0.15}Al_{0.05}O_2$ (NCA) (NCA, Gelon, China) with a mean particle size of 10 μm were used. As a conductive additive, acetylene black (AcB, Denka, Japan) with a mean particle size of 35 nm was used. PVDF homopolymer (Polyvinylidene fluoride; Solef 6020, 700,000 g/mol, Solvay, Belgium) was dissolved in NMP (N-Methyl-2-pyrrolidone; Daejung) for 6 hours by means of a magnetic stirrer at 60 °C.

A rotor-stator homogenizer (Ultra-Turrax T18, IKA, Germany) equipped with S18N-19G disperser unit was used as a standard dispersing device for nano-sized CB particles. The device has 12.7 mm of rotor diameter and 0.4 mm of gap size. The carbon black powders were first dispersed using the homogenizer at 8000 rpm for 3 min. Consequently, the

active material was added and mixed using an anchor-type overhead stirrer with 30 mm of diameter at 1000 rpm for 5 min. Volume fraction of each particle was calculated based on the density of the materials provided by the manufacturers. We prepared 35-40 g of the slurry for each batch using a 60 mL HDPE bottle. The slurries were subsequently sampled for the characterizations or agitated at varied rotation speed and time (Figure 3.1). From the geometry of the setting, shear rates exerted onto the sample between agitator and wall were calculated as follows: 50 rpm = 20 s^{-1} ; 100 rpm = 40 s^{-1} ; 200 rpm = 80 s^{-1} ; 400 rpm = 160 s^{-1}.

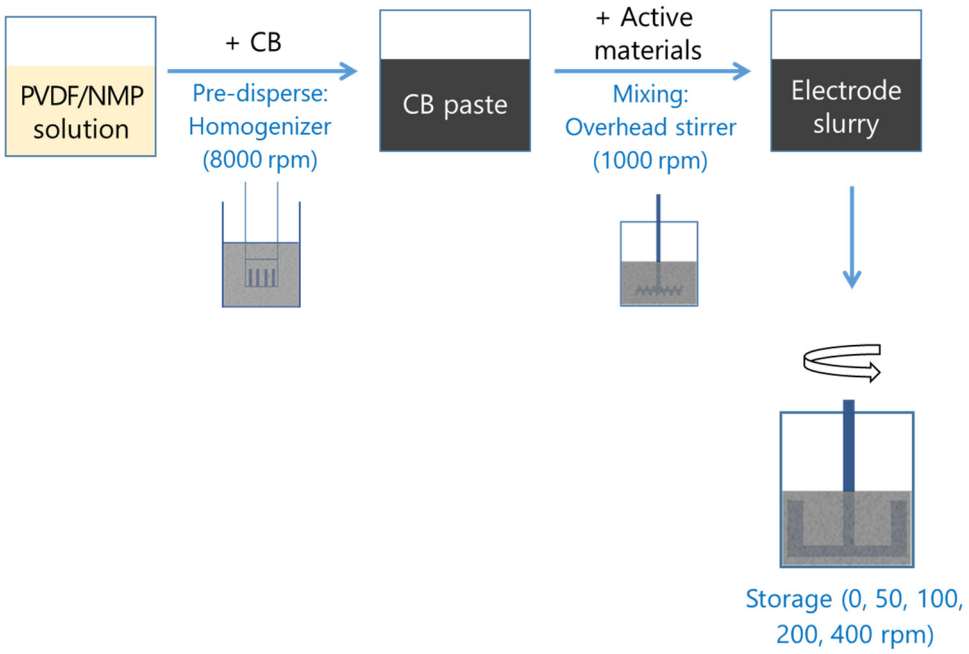

Figure 3.1 Simplified schematic of the procedure on sample preparation and storage with agitation.

Rheological characterization was conducted in strain-controlled mode using an AR-G2 stress-controlled rheometer (TA Instruments, USA). Two kinds of geometries were used for the measurements, depending on the rheological characteristics of the samples. 60mm parallel plates were used for the liquid-like samples while 40 mm serrated parallel plates were used for the gel-like samples to reduce wall-slip. Basically, these two geometries led to the identical results, except at low-torque limit and wall-slip-occurring regime. Steady-state flow viscosities were measured from $\dot{\gamma}$ = 464.1 s^{-1} to 0.01 s^{-1} using varied equilibration time from 10 s at the highest shear rate to 60 s at the lowest shear rate.

Field emission scanning electron microscopy (FE-SEM, Zeiss SUPRA 55VP) was used to characterize the surface microstructure of the electrode. For this purpose, the slurries were coated on a piece of Al foil using the doctor blade with 200 μm of wet thickness. Thereafter, the electrodes were dried overnight in a convection oven at 80 °C.

3.3 Results and discussion

Cathode slurry composed of 25 vol% NCA and 1.3 vol% AcB dispersed in PVDF/NMP solution was used as a standard slurry for the study on the effect of flow condition during storage. Comparison of rheological behavior between a slurry stored with mild agitation and a slurry stored at quiescent state was shown in Figure 3.2. The slurry under agitation exhibited a significant decrease of the moduli (Figure 3.2 a). G' of

the slurry after an hour of the agitation showed about 100 times smaller value than the initial state. Difference between 1 hour and 4 hours of agitation showed only a small difference, implying that the change was mainly done within an hour. Meanwhile, the slurry stored at quiescent state showed little change in rheological properties. G' of the slurry was decreased less than 50% from the initial value. However, even under the storage with no agitation, sedimentation of NCA particles was observed when the slurry was stored for 3 days.

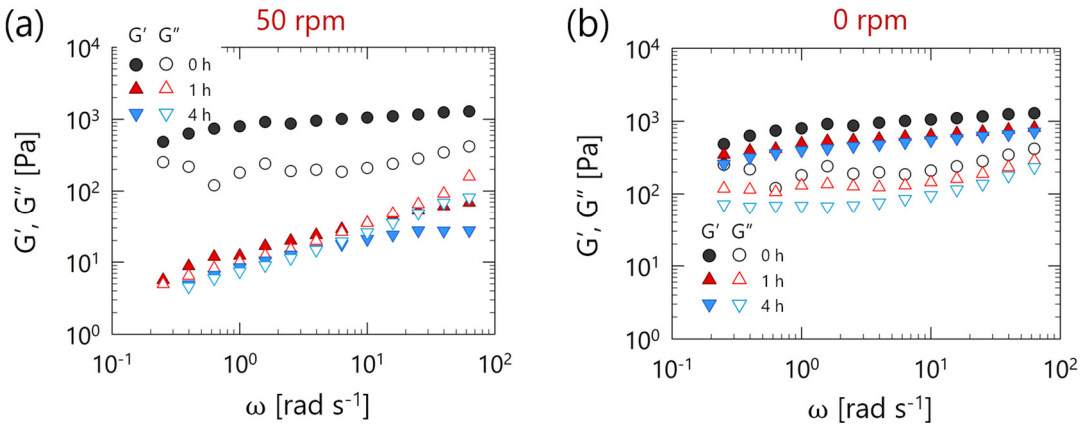

Figure 3.2 Storage (G') and loss (G'') moduli as a function of frequency of a cathode slurry (ϕ_{CB}=1.3%, ϕ_{NCA}=25% in PVDF 4.4%) depending on storage time: (a) stored with agitation (50 rpm), (b) stored with no agitation.

The results obviously show that the agitation has a significant impact on the rheological characteristics of the slurry, which reflects the structure in the microscopic scale. There has been a report in a previous literature that there is more change in rheological properties when there is agitation compared to storage without flow.[32] However, the literature suggests a mechanism of a 'degradation' of the slurry due to flocculation of particles

and polymers based on a false assumption – the adsorption of PVDF onto the particles. As explained in chapter 2 of this thesis, PVDF is not adsorbed on both CB and active material, so this explanation is difficult to establish. Instead, we suggest the interaction between different particles can be a key factor rather than the polymer-particle interaction.

Rheological experiments on the NMP-based model slurries show that the flow-induced rheological change is not a general behavior of the NMP-based slurries with PVDF as a binder. For example, Figure 3.3 compares rheological change under agitated storage for two NMP-based slurries: a cathode slurry containing NCA as an active material and an anode containing graphite as an active material. The slurries have similar composition except the surface characteristics of the active material particles – even the particle size is very similar. Unlike the cathode slurry that shows substantial decrease of G' and G'' (Figure 3.3 a), the anode slurry maintained its rheological properties after the storage with agitation (Figure 3.3 b). Considering that both slurries are composed of CB/AM binary dispersion in PVDF/NMP solution, the difference is significant. From the measurements, it can be proposed that the interaction between CB and active material determines whether a slurry shows rheological variation during storage.

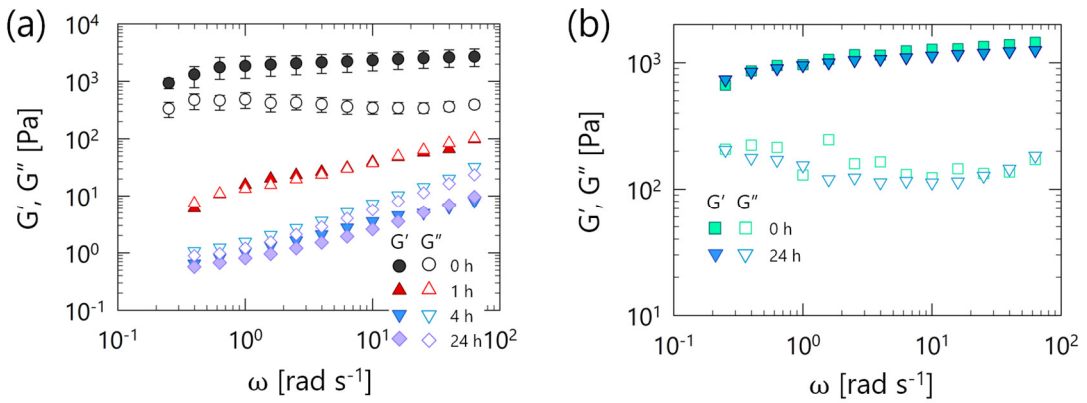

Figure 3.3 Storage (G') and loss (G'') moduli as a function of frequency of (a) a NMP-based cathode slurry (ϕ_{CB}=1.3%, ϕ_{NCA}=25% in PVDF 2.5%) and (b) a NMP-based anode slurry (ϕ_{CB}=0.5%, ϕ_{Grp}=20% in PVDF 2.5%) stored with agitation (50 rpm).

Since rheological responses in a bulk scale reflect microstructures of complex fluids, we can expect there is a microstructural change in the cathode slurry during agitated storage. For the observation of the microstructure, the electrodes were fabricated by coating and drying the cathode slurries right after preparation and after the storage. Scanning electron microscope was utilized to observe morphology of the electrode surfaces as shown in Figure 3.4. In the SEM image of electrode made of the fresh slurry, NCA particles with 5-15 μm size were observed at 1,000X magnification(Figure 3.4 a) and CB particles distributed over the electrode are observed at 10,000X magnification(Figure 3.4 c). In case of the electrode made of the slurry after agitated storage, we could find spheres with 30-50 μm size which were not found in the electrode from fresh slurry(Figure 3.4 b). Because only two kinds of particles comprise the cathode and size of the NCA is 5-15 μm, there is no other possibility than the large spheres are composed of CB. It can be verified in the SEM image

with 10,000X magnification that the spheres are agglomerates of CB (Figure 3.4 d). The amount of CB on the NCA surface is much smaller in Figure 3.4 c compared to Figure 3.4 d, because most of the CB particles are forming the large agglomerates.

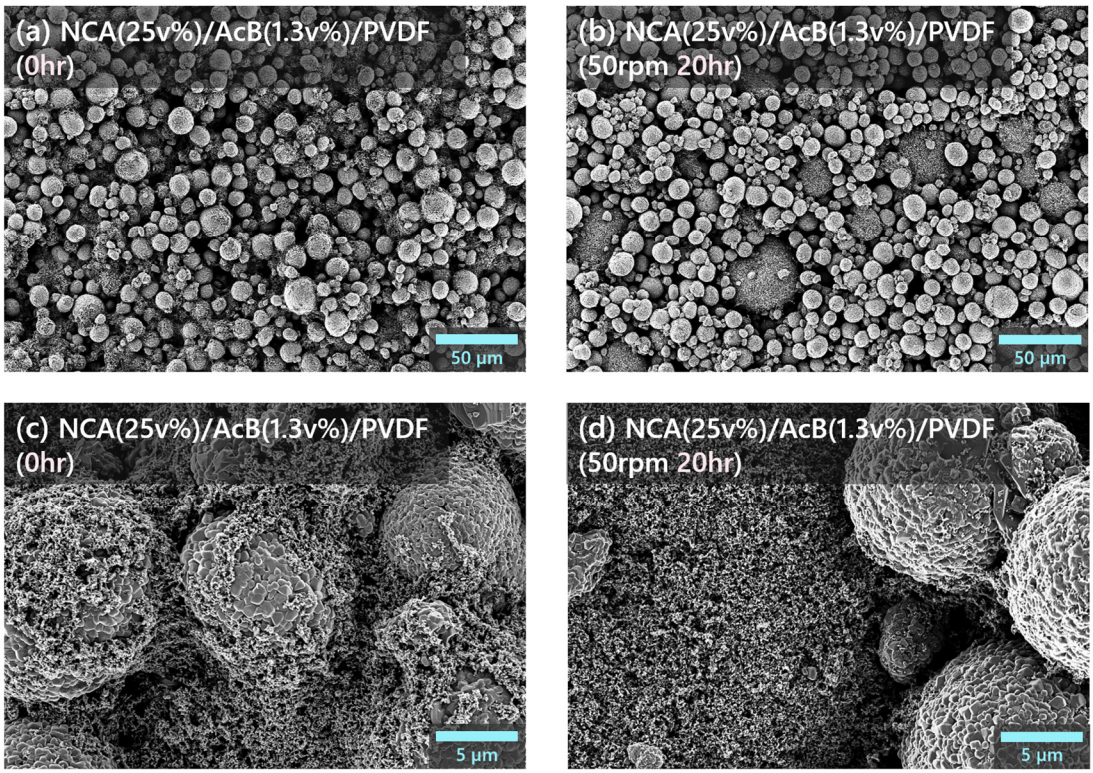

Figure 3.4 SEM images of the electrodes prepared by coating and drying the cathode slurry (ϕ_{CB}=1.3%, ϕ_{NCA}=25% in PVDF 2.5%) right after preparation and after agitated storage (50 rpm, 20 hours).

As we found that CB in the cathode slurry forms large agglomerates during a few hours of mild agitation, one may bring up a question: how critical the agglomeration can be in a viewpoint of homogeneous electrode formation? To deal with this question, it should be clarified that if the agglomeration is reversible, in other words, if the agglomerate can be broken up by mechanical dispersing process. For the purpose of the

clarification, the stored slurry was re-dispersed using the same dispersing condition of the initial slurry preparation (1000 rpm for 5 minutes). One can immediately notice that the liquid-like becomes gel-like during the re-dispersing process, and the change can be verified through the rheological measurement as shown in Figure 3.5. The viscoelastic moduli were 'recovered' close to the initial values by re-dispersing the slurry, though the 'recovered' moduli are still slightly lower than the initial moduli. The rheological recovery suggests the structural recovery – breakup of the large-size CB agglomerates – by the mechanical re-dispersing. Summarizing the results so far, microstructural mechanism on the rheological change of cathode slurries during mild agitation and re-dispersing can be suggested as shown in Figure 3.6: (1) agglomeration of CB occurs leading to the formation of large spherical shape during the mild agitation; (2) the agglomerates can easily breakup through the re-dispersing.

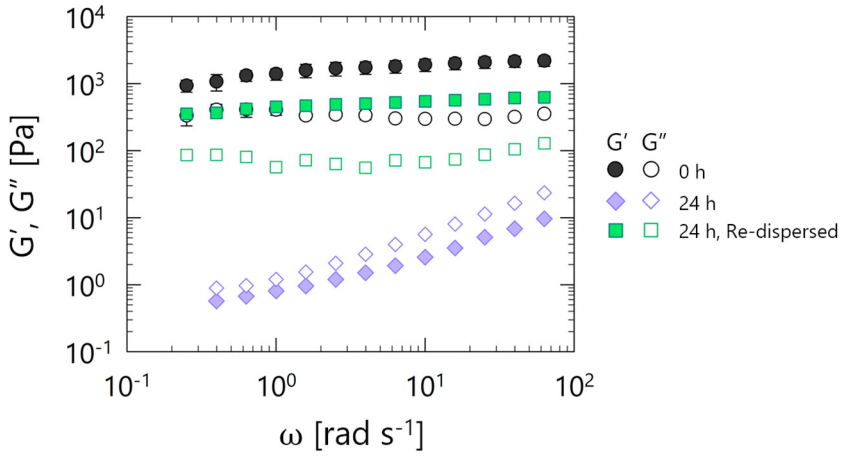

Figure 3.5 Storage (G') and loss (G'') moduli as a function of frequency of a NMP-based cathode slurry (ϕ_{CB}=1.3%, ϕ_{NCA}=25% in PVDF 2.5%) after agitated storage (50 rpm, 24 hours) and re-dispersing (1000 rpm, 5 min).

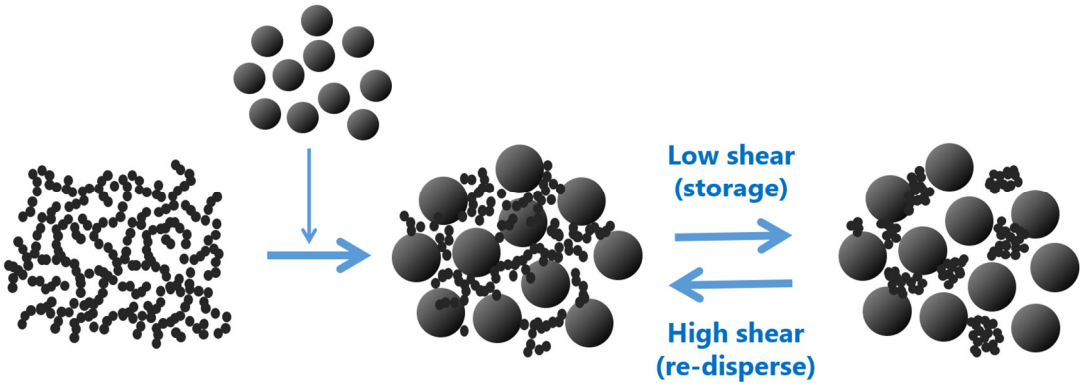

Figure 3.6 Shematic drawing on the suggested microstructural changes of the slurry under agitation and re-dispersing.

At this point, it would be meaningful to discuss detailed issues: (1) What is a cause for the agglomeration of CB in a large spherical shape? (2) Why CB forms large agglomerate in the cathode slurry while it does not in the anode slurry? (3) Why the rheological/structural changes occur only when the slurry is under flow? A possible scenario that explains the issues can be suggested in a perspective of a surface energy of the particles.

Surface energy quantifies the disruption of intermolecular bonds that occurs when a surface is created. Surfaces are intrinsically less energetically favorable than the bulk of a material. The surface energy may therefore be defined as the excess energy at the surface of a material compared to the bulk. Due to the fine particle size and inherently high surface energy, dispersed particles tend to attach to each other, or flocculate. The driving force of the flocculation can be explained as a Van der Waals interaction in a viewpoint of interparticle forces instead of surface energy. A wide variety of surface treatments have been used to prevent the flocculation, including

the adsorption of polymers of dispersants on the surfaces. In case of the NMP-based slurry used in the current study, PVDF does not play a role as a dispersant. Therefore, the particles directly interact with themselves with no force that hinders the interactions, which infers that the surface properties of the conductive agent and active material are crucial.

A key idea is that we can interpret the agglomeration in a similar approach to the mixing and phase separation of liquids. To estimate the affinity between particles, surface energy for the particles were used. Measured values for the dispersive and polar parts of the surface energy using the sessile drop method were adopted from a work by Ludwig et al. [40] The measured valued for LCO was used instead of NCA, for a rough estimation. The LCO shows a high polar component (~38 mN/m) and a low dispersive component (~13 mN/m). CB shows opposite characteristics with it having a large dispersive surface energy (~57 mN/m) and a very small polar surface energy (~0.5 mN/m). The work of adhesion can be calculated from the components of surface energy using Fowkes equation.

$$W_{12} = 2(\gamma_1^d \gamma_2^d)^{0.5} + 2(\gamma_1^p \gamma_2^p)^{0.5}$$

As AcB (or similar type of carbon black particles) and NCA (or the other cathode materials such as LCO, NCM, etc.) have significantly difference surface properties, it can be predicted that the binary dispersion system will tend separate into the agglomerate of each particles. The calculation of the work of adhesion confirms that AcB will preferably attach

to AcB itself and form agglomerates. Therefore, we can conclude that the agglomeration of AcB is originated from the thermodynamic aspect. We can also understand why the NMP-based anode slurry did not show the changes under shear flow (Figure 3.3): graphite particle has a very similar surface properties with carbon black.

Here one question can be raised: Why the rheological/structural changes occur only when the slurry is under flow? The reason can be found in the physical characteristics of the colloidal gel. The colloidal gel consisting of attractive particles are not in a thermodynamically stable state but a kinetically arrested state. In a quiescent state, microstructural changes toward lower energy state – phase separation – are very slow. However, external flow field can give the system an energy to overcome energy barriers. In the current case, the agitation flow accelerated the agglomeration by giving a lot more chance for the particles to contact themselves. Once an AcB particle attach to another AcB particle, they form an agglomerate and the agglomeration repeats leading to the formation of the large spherical shape.

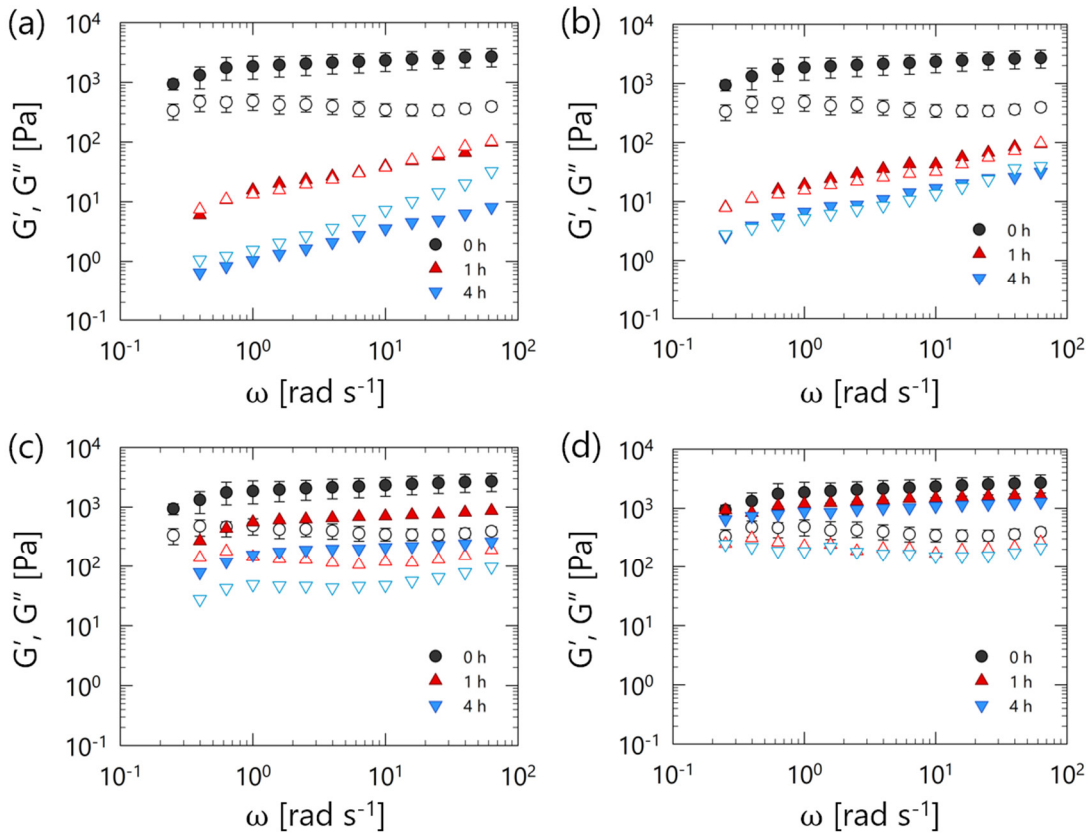

Figure 3.7 Storage (G') and loss (G'') moduli as a function of frequency of a NMP-based cathode slurry (ϕ_{CB}=1.3%, ϕ_{NCA}=25% in PVDF 2.5%) under storage with agitation at 50 rpm (a), 100 rpm (b), 200 rpm (c), and 400 rpm (d).

So far, we have demonstrated that the rheological change is attributed to the agglomeration of AcB and have discussed on the origin of the agglomeration. Next, flow condition for the agglomeration will be investigated. Different speeds of agitation – or different shear rates – were applied to the slurries for 1 h and 4 h, followed by the rheological measurements. Figure 3.7 shows the change of the viscoelastic moduli of the slurries during agitated storage at different speeds. It can be clearly demonstrated that the change under agitation is highly dependent on the agitation speed. G' of the slurry stored at 50 rpm decrease 1,000 times after

4 hours of agitation (Figure 3.7), whereas the one stored at 400 rpm maintained the initial value. From the results, it can be suggested that the shear rate of the flow determines whether the AcB agglomerate or not. In addition, it can be hypothesized that the agglomeration and breakup of the agglomerate is susceptible to hydrodynamic stress, similar to the case of model carbon black gels [41,42]. For the verification of the hypothesis, PVDF concentration in the slurries were varied to control the viscosity of the polymeric solutions as suspending media. The change of G' for the model slurries with different media viscosities are shown in Figure 3.8. The slurries showed different responses to the agitation speed variation; for example, the slurry with PVDF 3.5% showed substantial decrease in G' when agitated at 100 rpm, while the slurry with PVDF 4.5% showed much less change even at the same agitation speed. The slurry with PVDF 6.2% showed little decrease of G' even at 50 rpm, which indicate that the AcB in the slurry did not agglomerate. The critical hydrodynamic stress could be roughly estimated as ~5 Pa; shear flow below which induces agglomeration.

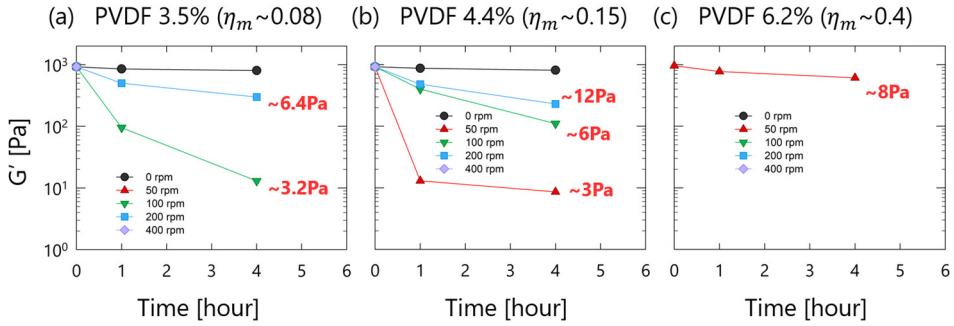

Figure 3.8 Agitation speed dependence of storage modulus (G') of the cathode slurries (ϕ_{CB}=1.3%, ϕ_{NCA}=25%) with PVDF 3.5% (a), 4.5% (b), and 6.2% (c).

3.4 Conclusion

In the current study, we unveiled that the microstructural mechanism behind the rheological change during agitated flow is the agglomeration of conductive agent particles. The origin of the agglomeration was suggested in a similar approach to the phase separation of liquids, utilizing the surface energy of the particles. In addition, it was revealed that the aggregation occurs by low shear agitation below a certain shear rate and that whether the aggregation occurs is determined by hydrodynamic stress of flow.

4. Effect of neutralization of poly(acrylic acid) binder on the negative electrode slurry

Overview

In this chapter, we examined dispersing effect of PAA in the water-based model electrode slurries by changing neutralization degree α*. Rheological properties of the model slurries with individual and multiple components were investigated with different* α *and PAA concentrations. Dispersion stability and microscopic observation were followed to reveal the dispersion quality. Mechanism of the* α*-dependent dispersion quality is discussed based on polymer adsorption measurements. The results provide a guideline that can be utilized for the water-based processing of the electrodes containing PAA-based binders.*

4.1. Background: PAA as a binder for the electrode

Poly(acrylic acid) (PAA)-based polymer has been receiving attention as one of the candidates for water-soluble binder material for electrodes.[43–45] Recently it received a particular attention as a binder for Si-based anode because of good adhesion and cycle life.[46–49] It is also possible to obtain crosslinked PAA-based copolymers with excellent cycling stability.[50–54] On the other hand, low molecular weight PAA can be used to improve the dispersion of the slurry, resulting in a reduction of the aggregation and an increase in rate capability of the electrode.[19,55]

Because the carboxyl group in the PAA chain is electrostatically associated/dissociated depending on the neutralization degree α (or on the pH values of their aqueous solutions), its conformation in water can be modulated. PAA without neutralization has a coiled conformation due to intramolecular hydrogen bonding, whereas neutralized PAA has extended conformation owing to the electrostatic repulsion between dissociated carboxyl group (Figure 4.1).[56–58] It has been reported that the optimization of α of PAA binder can be a significant factor for the improvement of the battery performance.[54,59,60] Adjustment of α of PAA in the slurries (and corresponding pH) can also influence the dispersion state of the carbon nanomaterials which are used as conductive agents.[61,62] Thus we can expect that neutralization of a slurry containing PAA binder is capable to adjust the slurry rheology that reflects the dispersion state of the particles.

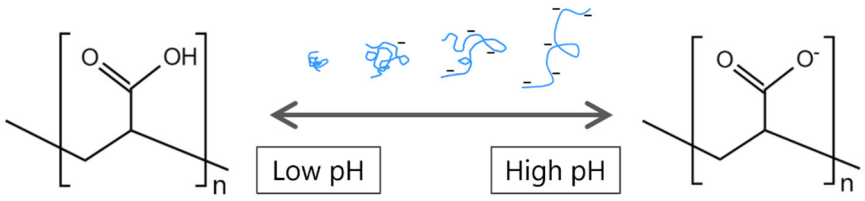

Figure 4.1 Schematic illustration of change of poly(acrylic acid) depending on neutralization degree or corresponding pH of the aqueous solution.

4.2. Materials and methods

Graphite (SG-BH8, Ito Graphite Co., Ltd.) with 8.1 μm of average particle size and 2.23 g/cm^3 of density was used as a negative active material. Carbon black (Conductex 7067 Ultra, Birla carbon; CB) was used as a conductive agent. The CB consists of submicrometer-sized permanently fused aggregates of spherical primary units with an average diameter of 42nm. Specific surface area of the CB particle is 54 m^2/g according to the manufacturer. The PAA used as a binder in the current study is linear poly(acrylic acid) (Sigma-Aldrich; PAA) with M_w of 250,000 g/mol in the form of 35 wt% aqueous solution.[e]

Three model slurries were prepared for the experiments. CB model slurry comprises 1.0 wt% PAA and 2.9 wt% CB, an estimated volume fraction of 1.3 vol% using the density of 2.25 g/cm^3. Graphite model slurry

e Weakly crosslinked PAA is more widely used as a binder, however, use of such crosslinked polymers make the interpretation of measured data difficult. For example, the role of particles and polymer in the rheological characteristics of a slurry can hardly be distinguished due to the gel-like nature of the crosslinked PAA.

is composed of 1.5 wt% PAA and 45 wt% graphite that corresponds to 26.8 vol% from the calculation using the density of 2.23 g/cm^3. The anode slurry contains 2.0 wt% CB, 40 wt% graphite particles, and 1.5 wt% PAA as a binder. PAA content in the slurry was controlled by dispersing a given quantity of dry particles to the PAA solution with a properly adjusted concentration and α.

A rotor-stator homogenizer (Ultra-Turrax T18, IKA, Germany) equipped with S18N-19G disperser unit was used as a standard dispersing device for nano-sized CB particles. The device has 12.7 mm of rotor diameter and 0.4 mm of gap size. Operation time and speed of the homogenizer were varied to control the mechanical dispersing intensity. For the strongest intensity, an ultrasonic processor (VCX 750, Sonics & Materials Inc., USA) equipped with a solid horn was used. A continuous sequence of 2 s pulses followed by 2 s rests was applied for 5 min, with the sonication power set at 40%. The graphite particle was mixed using a laboratory dissolver mixer at 1,500 rpm for 15 min. For the preparation of the anode slurry, CB was pre-dispersed using the Ultra-Turrax homogenizer at 6,000 rpm for 5 minutes, and subsequently graphite was mixed with the CB dispersion using the dissolver mixer at 1,500 rpm for 15 min. We prepared 35-40 g of the slurry for each batch. The neutralization degree α of PAA was adjusted by dropping the desired amount of 1 mol L^{-1} NaOH on the last step of the sample preparation, as follows:

$$\text{-}[CH_2\text{–}CH(COOH)]_n\text{-} + \alpha NaOH \rightarrow \text{-}[CH_2\text{–}CH(COOH)]_{n(1-\alpha)}\text{-}[CH_2\text{–}CH(COONa)]_{n\alpha}\text{-} + H_2O$$

For the preparation of electrodes, the slurries were coated on a copper foil using the doctor blade. Thereafter, the electrodes were dried overnight in a convection oven at 50 °C. By drying the anode slurries containing 2.0 wt% CB, 40 wt% graphite, and 1.5 wt% PAA, the electrodes containing 4.6 wt% CB, 92 wt% graphite and 3.4 wt% PAA were obtained. For the electrochemical characterization, composition was slightly changed to make sure the electrode does not fall apart from the copper foil during cell assembly. The electrodes for the electrochemical characterization contain 3 wt% CB, 92 wt% graphite, 4 wt% PAA, and 1 wt% SBR.

Rheological characterization was conducted in strain-controlled mode using an AR-G2 stress-controlled rheometer (TA Instruments, USA). Two kinds of geometries were used for the measurements, depending on the rheological characteristics of the samples. 60mm parallel plates were used for the liquid-like samples while 40 mm serrated parallel plates were used for the gel-like samples to reduce wall-slip. Basically, these two geometries led to the identical results, except at low-torque limit and wall-slip-occurring regime. All the measurements were performed at least 3 times to guarantee the reproducibility. Error bars are shown in the graphs unless the error range is negligibly small. Steady-state flow viscosities were measured from $\dot{\gamma}$ = 464.1 s^{-1} to 0.01 s^{-1} using varied equilibration time from 10 s at the highest shear rate to 60 s at the lowest shear rate.

Dispersion stability of CB was characterized using Turbiscan Lab Stability Analyzer (Formulaction, France) based on multiple light scattering. The model slurries were diluted by 1000 times because the scattering can hardly be detected in the original model slurries due to

highly light-adsorbing CB particles. The transmittance of the diluted samples is monitored for 12 hours.

Zeta potential of the CB dispersions was determined by laser Doppler method using ELSZ-2000 (Otsuka Electronics, Japan). The instrument measures the electrophoretic mobility of particles in dilute dispersions and then converts the mobility into zeta potential by utilizing the Smoluchowski equation. Dilute dispersions of CB with and without PAA for each, were prepared by dilution of the model slurries by 100 to 1000 times, depending on light absorbance of the sample. After dilution, samples were stored at room temperature for a day, and then pH was finally checked before the zeta measurement. Sedimentation of agglomerate was observed for some suspensions due to low dispersion stability, in which case supernatant suspension was sampled for the measurement.

To observe the aggregation of the CB particles, an inverted microscope (IX-71, Olympus, Japan) was used. The slurries were diluted by 20 times and loaded between microscope slides separated by 150 μm-thick spacers. Field emission scanning electron microscopy (FE-SEM, Zeiss SUPRA 55VP) was used to characterize the surface microstructure of the electrode. For this purpose, the slurries were coated on a piece of copper foil using the doctor blade with 150 μm of wet thickness. Thereafter, the electrodes were dried overnight in a convection oven at 80 °C.

Electrical conductivity of the electrodes was measured with an SI 1260 impedance/gain-phase analyzer and a 1296 dielectric interface (Solartron, Cambridge, UK). The measurements were made at frequencies $\omega = 10^{-1}$–

10^5 Hz. In the measurement, the amplitude of the oscillatory electric field was kept small (0.1 V) so as to ensure the linearity of the dielectric response of the samples.

Electrochemical performance of the anode was evaluated using half cells (2032-type coin cells) comprising the graphite anode and a Li metal electrode. Pre-cycling was conducted 10 mA g^{-1} and 30 °C for 5 cycles. After pre-cycling, galvanostatic charge/discharge cycling was performed at varied C-rate with the cell voltage maintained between 0.01 V and 2 V during the cycling.

The interactions between polymeric binder and particles were probed by adsorption measurements. The amount of adsorbed PAA was determined by quantifying the polymer concentration in the medium before and after polymer adsorption. Model slurries with different concentrations of PAA were prepared and centrifuged at 10,000 rpm for at least 3 hours. When all the particles are settled, the supernatant phase becomes transparent. The concentrations of residual PAA remaining in the supernatant solution were obtained by the gravimetric analysis. The solvent was evaporated by drying in a convection oven at 110 °C, and the residue was weighed with a microbalance. The total amounts of PAA adsorbed on CB were obtained by calculating the difference between the amount of PAA in the initial solution and the supernatant solution after centrifuge.

4.3. Results and discussion

We first examined the influence of neutralization degree α of a CB model slurry, while keeping CB and PAA concentrations constant. The PAA solution undergoes a conformational transition depending on α, resulting in a difference in viscosity level.[63–65] In order to examine the effect of particle dispersion, suspension viscosity divided by the solvent viscosity (i.e. relative viscosity) of the CB 2.9wt% PAA 1.0wt% slurry at varied α was plotted in Figure 4.2.

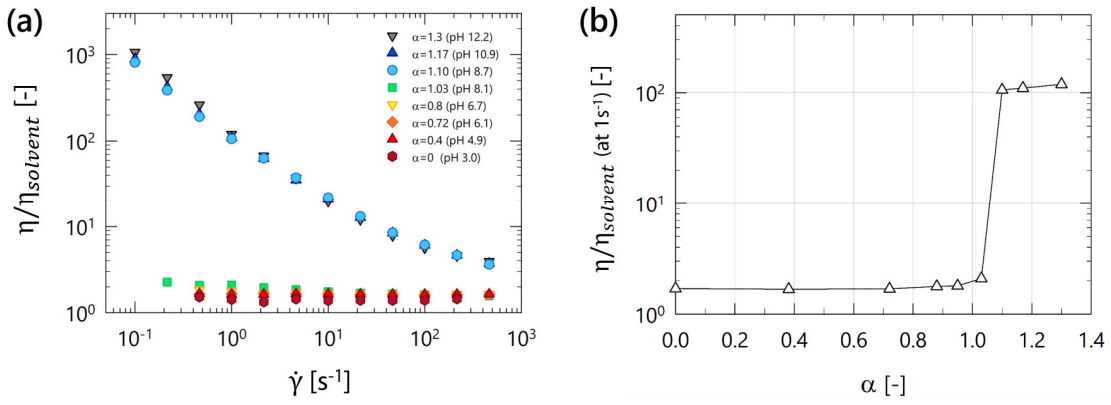

Figure 4.2 (a) Relative viscosity as a function of shear rate and (b) relative viscosity at 1 s^{-1} as a function of neutralization degree α in 2.9 wt% CB suspensions with 1.0 wt% PAA.

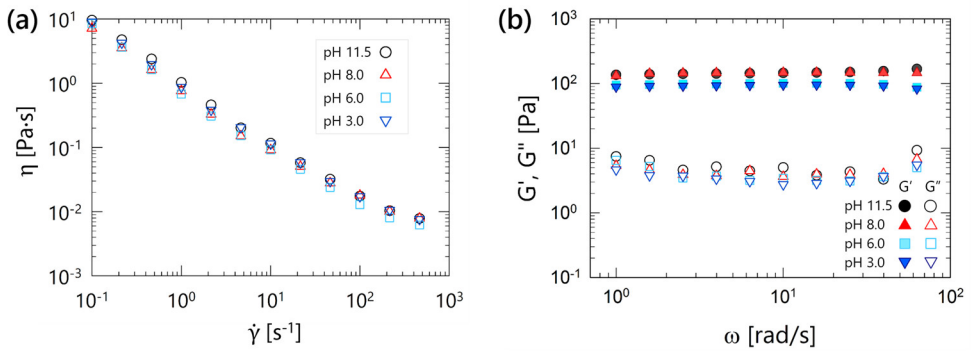

Figure 4.3 (a) Viscosity as a function of shear rate and (b) frequency dependent viscoelastic moduli for 2.9 wt% CB suspensions with no polymer.

Up to $\alpha \leq 1.0$, all the samples show nearly Newtonian behavior and the viscosity is almost constant. For $\alpha \geq 1.1$, the slurry shows a gel-like yielding behavior similar to the CB suspension with no polymer as shown in Figure 4.3. In other words, a sharp transition appears at the critical point at $1.0 < \alpha < 1.1$, as shown in Figure 4.2(b). On the other hand, the suspension with 2.9 wt% CB particles dispersed with no polymer always show a gel-like behavior regardless of the pH (Figure 4.3), while 1.0 wt% PAA solution is nearly-Newtonian liquid at all times (Figure 4.4). It can be deduced that the polymer-particle interaction is the cause of the α-dependent rheological difference since the rheological properties are α-dependent only when both CB and PAA are present together.

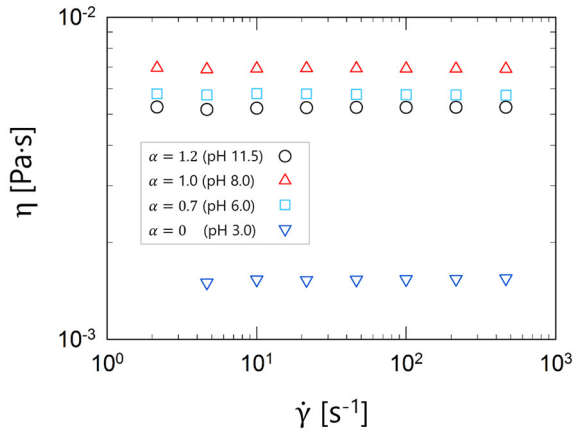

Figure 4.4 Viscosity of 1% PAA solutions with different neutralization degrees.

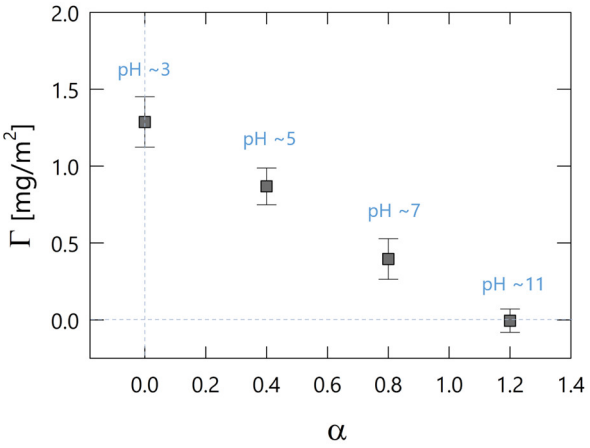

Figure 4.5 Adsorption amount of PAA on CB surface at a fixed concentration 2.9 wt% CB suspensions with 1.0 wt% PAA, which is the same as the one used in Figure 4.2.

The difference in polymer-particle interaction can be identified by measuring the amount of adsorbed polymer. Adsorbed amount of PAA on CB surface in the slurry containing 1.0wt% PAA and 2.9 wt% CB are presented in Figure 4.5. The largest amount of PAA is adsorbed at $\alpha = 0$ and the adsorption decreases as α increases, which agrees well with the former studies.[66,67] It was revealed that the adsorption does not occur at $\alpha = 1.2$. The absence of adsorption illustrates that the model slurry at $\alpha = 1.2$ shows a gel-like behavior similar to the CB suspension without PAA (Figure 4.2). Meanwhile, nearly Newtonian viscosity (Figure 4.2) and a significant amount of adsorption (Figure 4.5) at $\alpha \leq 1.0$ indicate that PAA adsorbed on CB provides a steric stabilization. It can be interpreted that the rheology of the CB model slurry is not dependent on how much the adsorption amount is, but on whether the polymer is adsorbed or not.

It is notable that the viscosity shows little variation (Figure 1) despite the significant difference in adsorption amount unless the measured value

is zero (Figure 2). If there is no difference in the dispersing efficacy provided by the polymer, dispersion quality is expected to decrease according to the adsorption amount reduction. However, it should be noted that a change in α (or corresponding pH) results in a transition of PAA chain between tightly coiled and highly extended conformations, by charge density variation from electrolytic dissociation of carboxylic group.[68] When the polymer forms an extended conformation, the adsorbed polymer can provide steric stabilization even at a lower density of adsorption when compared with the case of coiled conformation.[68] Moreover, the adsorbed PAA chains with high α also have negative charges, thus provide a significant electrostatic stabilization in addition to the steric stabilization, which is sometimes referred to as electrosteric stabilization.[69,70] Such electrosteric stabilization due to highly charged PAA can explain the stability of the system notwithstanding the low adsorption amount. Furthermore, lower adsorption at higher α can be explained due to a larger surface occupation of polymer molecules with extended conformation.

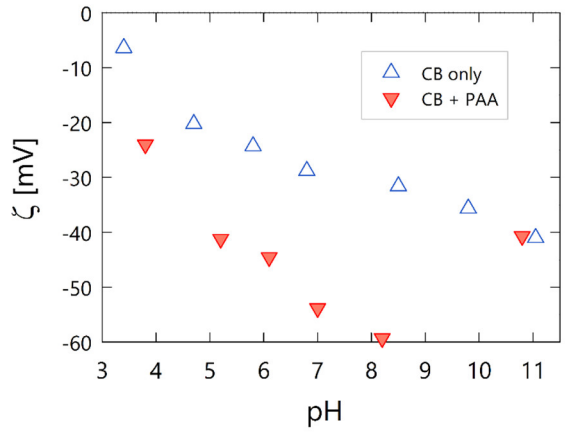

Figure 4.6 Zeta potential as a function of pH for CB only and CB with presence of PAA

To prove the charge density variation of the adsorbed PAA, we figured out the difference in the electrical charge of adsorbed PAA at various pH conditions, by comparing surface charge of bare CB and PAA-adsorbed CB. If there is a significant difference of surface charge between the bare particle and PAA-adsorbed particle, it means that PAA chain is electrically charged. Because conformational transition of PAA comes with ionization of polymer chain, the charge on the polymer is indicative of the extended conformation.[71]

In Figure 4.6, we compared the zeta potential ζ of CB in slurries with PAA and with no PAA, in terms of pH of the system. The negative charge of both samples gradually increased with pH. The ζ of PAA-adsorbed CB changed more rapidly compared to bare CB, leading to a larger difference in ζ between them. This increasing difference in zeta potential of two samples indicates the negative charge of adsorbed PAA that gradually increased depending on α (or corresponding value of pH). The difference in ζ exhibited a maximum at pH 8.2 and decreased again resulting in no difference at around pH 11. No difference in ζ can be interpreted as an absence of PAA on the CB surface, which is consistent with that the adsorption is not occurring at α = 1.2 which corresponds to about pH 11 (Figure 4.5). The reason for the absence of PAA adsorption at high pH is not clear yet, but a possible scenario is that the electrostatic repulsion arising from highly charged PAA can hinder the adsorption. The reason for the absence of PAA adsorption at high pH is not clear yet, however,

electrostatic repulsion between highly charged PAA and CB can be suggested as a possible cause.

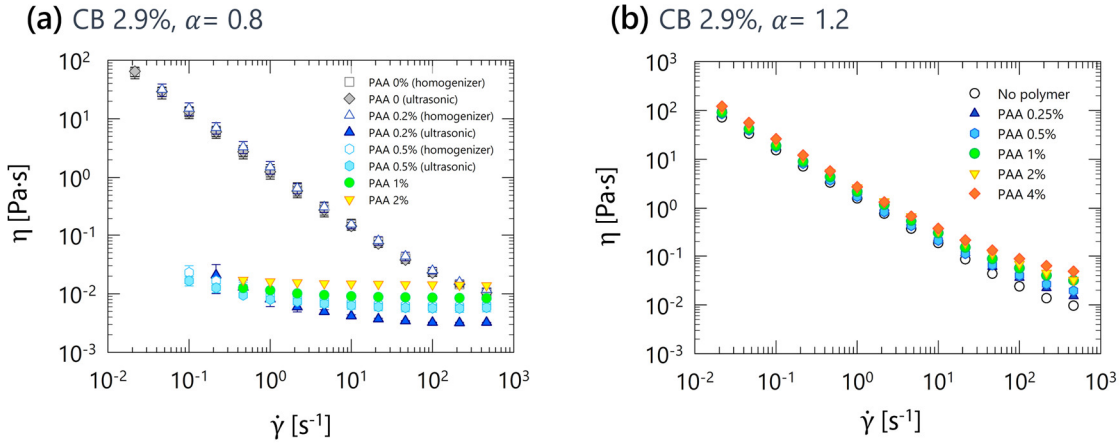

Figure 4.7 Viscosity of 2.9 wt% CB suspensions with various PAA concentrations at α = 0.8 (a), and α = 1.2 (b).

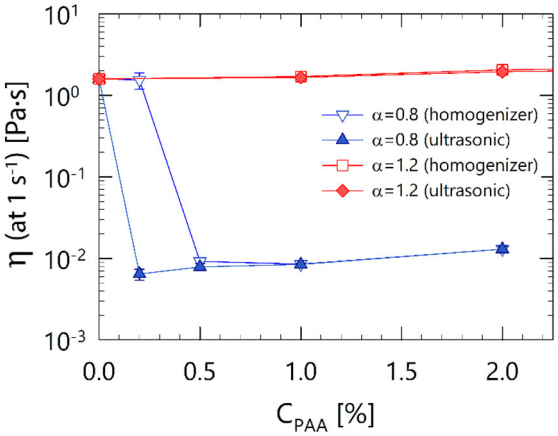

Figure 4.8 The viscosity of 2.9 wt% CB suspensions with various PAA concentrations; dispersed using Ultra Turrax homogenizer at 6000 rpm for 5 minutes, or horn-type ultrasonicator for 5 minutes.

To understand the influence of PAA concentration, the change in the rheological properties of CB slurry according to the PAA concentration for

a fixed CB concentration (2.9 wt%) was investigated for two conditions, α = 0.8 (adsorbing) and α = 1.2 (non-adsorbing) as shown in Figure 4.7 and Figure 4.8. In addition to the polymer concentration, the dispersing method was varied to compare the effect of dispersing intensity for the adsorbing and non-adsorbing cases. For ease of identification, only the viscosity at 1 s^{-1} is presented as a function of PAA concentration in Figure 4.8, from the viscosity data for the entire range of shear rates (Figure 4.7). The adsorption isotherms in terms of PAA concentration were obtained (Figure 4.9), to support the rheological changes according to the polymer adsorption.

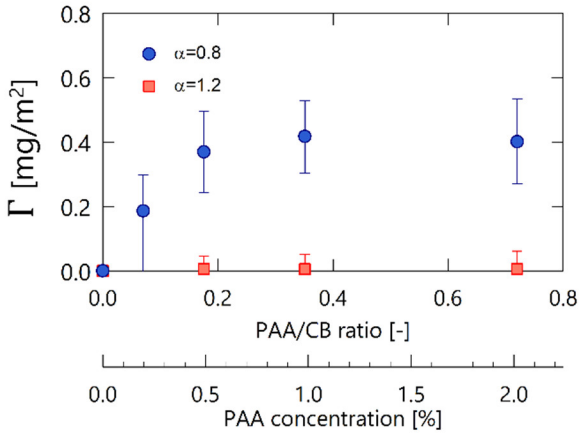

Figure 4.9 Adsorption isotherms of PAA on CB surface for α = 0.8 (adsorbing) and α = 1.2 (non-adsorbing).

At α = 0.8 (adsorbing), the rheological properties of the slurry exhibited a dramatic change with the increase in PAA concentration. The model slurry with only a small amount 0.2% of PAA showed a considerable dispersion intensity dependence (blue triangles in Figure 4.8), which is hardly observed in other model slurries. When dispersed using a rotor-

stator homogenizer (at 6000 rpm for 5 minutes), a gel-like behavior similar to that without a polymer was observed, whereas the slurry showed a nearly-Newtonian behavior when subjected to stronger ultrasonication (300 W for 5 minutes). Once the sample was liquefied by ultrasonic, it retained liquid-like properties without forming gelation again. The liquefaction implies a possibility of an existence of bridging flocculation, since it has been reported that a disruption of polymer bridge causes an irreversible liquefaction of the gel when very strong dispersing force is applied.[72] The adsorption isotherm (blue circle in Figure 4.9) that shows saturation of adsorption at about 0.5 wt% of PAA supports the possibility of bridging flocculation due to the partly adsorbed polymer in the model slurry containing 0.2 wt% PAA.

Above 0.5% of PAA, the dispersion intensity-dependence of the viscosity is remarkably reduced. It can be suggested that the bridging is hardly occurring at this concentration range in which the PAA adsorption on CB surface is saturated as confirmed by the adsorption measurements. As the PAA concentration further increases, the viscosity increases over a wide shear rate range maintaining its nearly-Newtonian shape (Figure 4.7(a)), which is attributed to the viscosity of the polymer solution itself (Figure 4.4). The Newtonian behavior of the model slurry which is common in the stable dispersions suggests that PAA is effectively reducing the attractive interparticle interactions through the steric stabilization. Adsorption isotherm shows that the adsorption is already saturated when PAA concentration is 0.5 wt%, thus the model slurry containing PAA 1wt% and CB 2.9wt% is expected to include both adsorbed and excessive free

polymers. The nearly-Newtonian viscosity of the slurry far beyond the adsorption saturation point indicates that the depletion attraction due to free polymer is negligible.

There is no significant viscosity change depending on the PAA concentration for α = 1.2 (non-adsorbing), contrary to α = 0.8 (adsorbing). All the model slurries with α = 1.2 are independent of dispersing intensity (red symbols in Figure 4.8) and show a gel-like yielding behavior regardless of PAA concentration (Figure 4.7(b)). The increase in PAA concentration only increases the viscosity over a wide shear rate range with little change in the shape of the viscosity curve. This type of flow curve change is similar to the case of the previous study in which only the medium viscosity was changed for the model colloidal gel using carbon black.[38] From this, it can be proved that the increase of the PAA concentration only increases the viscosity of the medium and does not cause additional change at α = 1.2.

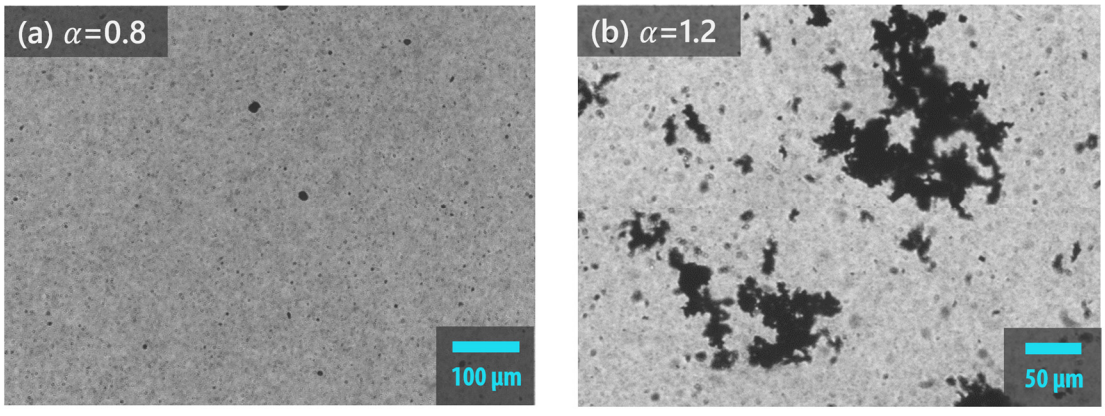

Figure 4.10 Optical microscopic images of samples of CB 0.14 wt% PAA 0.05 wt% with α = 0.8 (a) and α = 1.2 (b). Both samples were prepared by dispersing on Ultra Turrax homogenizer at 12,000 rpm for 10 minutes and then diluted 20 times from 2.9 wt% CB

suspensions with 1.0 wt% PAA.

To further characterize the dispersion quality of the CB, aggregate size distribution was observed using optical microscopy. CB model slurries prepared using the homogenizer at 12,000 rpm for 10 minutes were diluted 20 times and were observed in an optical microscope to compare $\alpha = 0.8$ and $\alpha = 1.2$ (Figure 4.10). At $\alpha = 0.8$, spherical aggregates with a few micrometers are observed. At $\alpha = 0.8$, though it is not distinguished in Figure 4.10(a), the light absorption rate is very high thus it is dark over the whole sample even when the maximum intensity of illumination was provided. This high light adsorption implies that a considerable amount of CB particles is dispersed in a submicron-scale which is difficult to observe with an optical microscope, besides the micro-scale agglomerates. On the other hand, fractal-like agglomerates of several tens to several hundreds of micrometers is observed at $\alpha = 1.2$ (Figure 4.10(b)), and the space without agglomerate is bright compared with $\alpha = 0.8$. Please note that the illumination intensity was far lower for Figure 4.10(b) comparing with Figure 4.10(a). A quantitative comparison of the light absorption will be seen in the Turbiscan Lab measurement later.

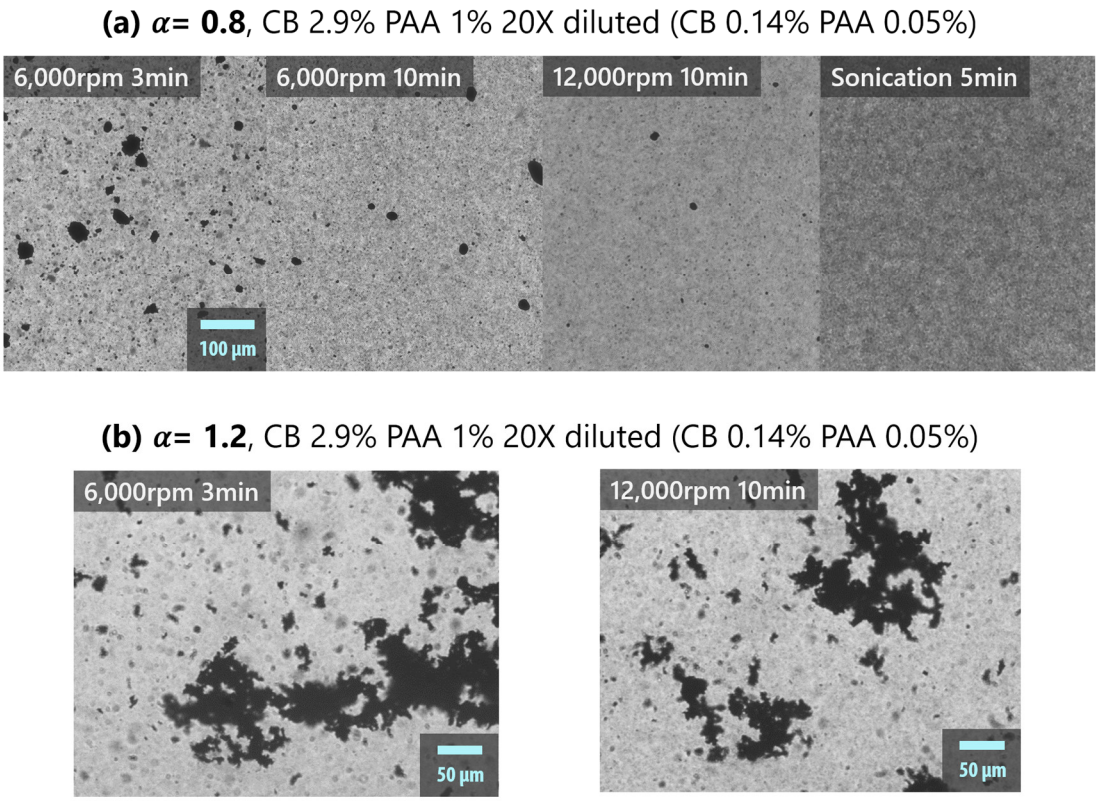

Figure 4.11 Optical microscope images showing the effect of mechanical dispersion intensity for CB/PAA dispersion with α = 0.8 (a) and α = 1.2 (b).

It is to be noted that the aggregate size changes in different ways when a mechanical dispersing intensity is varied as shown in Figure 4.11. At α = 0.8, the unbroken aggregates are observed when the dispersing intensity is weak, which is hardly visible since PAA adsorbs to prevent re-aggregation of CB once dispersed under a strong intensity (e.g. Ultrasonication). The result is in good agreement with a previous study that shows a decrease of aggregate size according to the dispersing strength when a sufficient dispersant is present.[73] On the other hand, at α = 1.2 there is nothing that can prevent the aggregation of CB particles. Therefore, large aggregates are observed irrespective of the dispersing intensity owing to the

immediate re-aggregation of the particles. However, those two slurries show little difference in viscosity (blue triangles in Figure 4.8) while they differ in the size of aggregates due to the difference in dispersing intensity (Figure 4.11). Therefore, it is to be noted that the measurement of the rheological properties alone is not sufficient to evaluate the dispersibility of the slurry. In order to confirm the presence of aggregates due to insufficient dispersing intensity, one can utilize some techniques such as confocal and SEM observations of dried samples, and light scattering using diluted samples, in addition to optical microscopy.

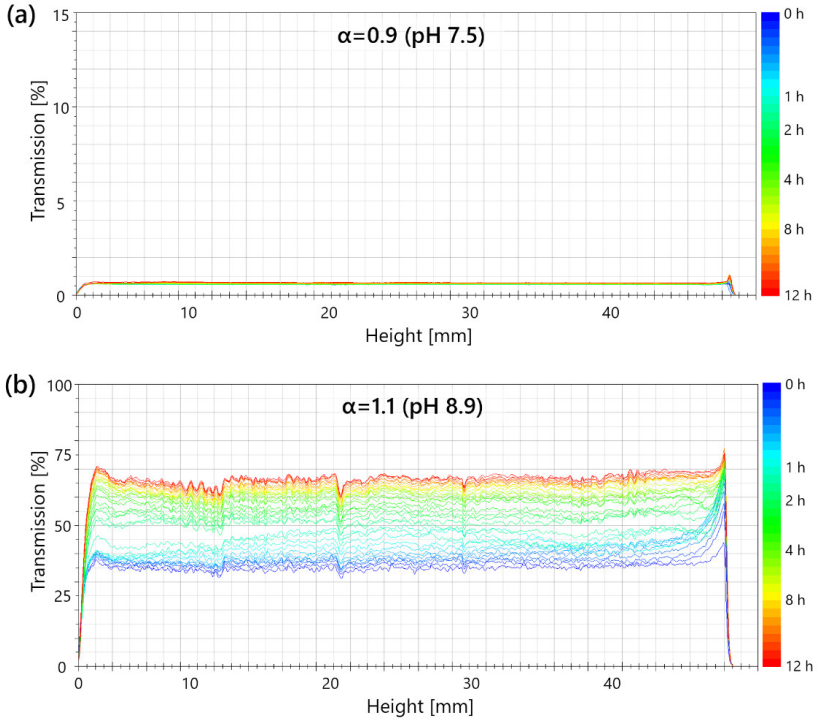

Figure 4.12 Variation of time-dependent transmission of 1000 times diluted CB model slurry (containing $2.9*10^{-3}$ wt% of carbon black and 10^{-3} wt% PAA) at two different neutralization degrees: (a) $\alpha = 0.9$ (b) $\alpha = 1.1$. Note that the scale range of the y-axis is different for the two cases.

Turbiscan Lab was utilized as a tool for directly observing the

occurrence of aggregation of particles according to time. This method gives an information on sedimentation and aggregate size increase of dispersion system over time. Due to the high level of light absorption of CB, very diluted samples were used for the measurement. Figure 4.12 is a transmission profile of 1000 times diluted model slurries measured for 12 hours. The diluted slurry at $\alpha = 1.1$ showed significantly higher values of both initial transmission and change of transmission over time, compared to the sample with $\alpha = 0.9$ that shows very low values for both measurements. The lower value of transmission indicates better dispersion of CB particles because a suspension with smaller aggregate size has higher light adsorption efficiency due to the increased surface area.[74] In addition, the smaller change of transmission over time indicates the smaller change in overall aggregate size, which represents better dispersion stability. In these regards, the higher initial value of transmission at $\alpha = 1.1$ reflects larger size of aggregates, while the increase of transmission mainly reflects further increase in size by continuous aggregation of CB particles over measurement time. Therefore, it can be concluded that the dispersion stability of CB slurry with PAA is very poor at $\alpha = 1.1$ where PAA does not adsorb to CB and fairly stable at $\alpha = 0.9$ where PAA adsorbs. The trend of the dispersion stability is consistent with that of rheology and optical microscopy measurements.

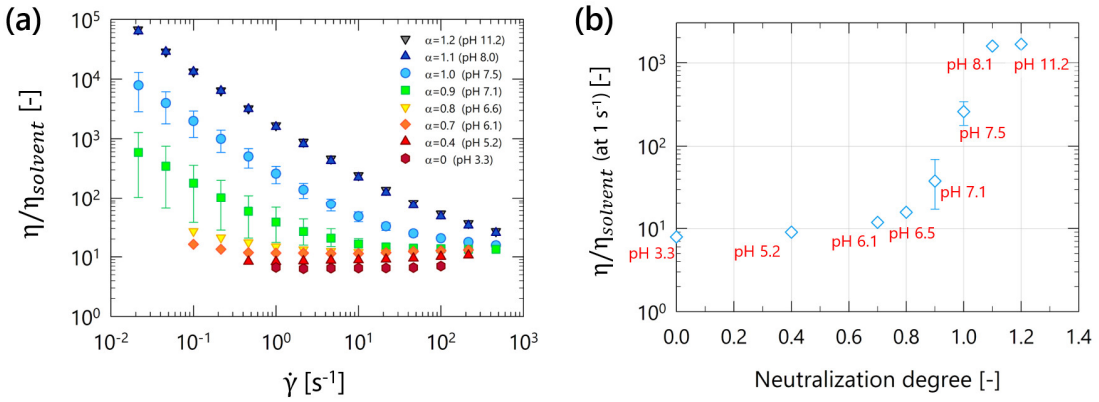

Figure 4.13 (a) Relative viscosity as a function of shear rate and (b) relative viscosity at 1 s^{-1} of graphite 45wt% suspensions with PAA 1.5wt% at varied neutralization degree α.

So far, we have investigated the α-dependent dispersion stability of the CB model slurry. In a similar way, a graphite model slurry and a model slurry containing both graphite and CB together were studied for varied α. In the case of the graphite slurry, α-dependent change is analogous to that of CB slurry, exhibiting a large change in the rheological properties from nearly Newtonian to gel-like yielding behavior depending on α (Figure 4.13). Different features from CB slurry are a relatively gradual change of viscosity depending on α and a large error range of the viscosity at α = 0.9. Meanwhile, little difference in dispersion quality of the slurry or microstructure of the electrode was observed despite the difference in rheology, possibly due to the large particle size and relatively weak interparticle attraction. For example, it is hard to see a clear difference between α = 0.6 and α = 1.1 in the microstructure of the electrode (Figure 4.14). Since it is nanometer-size CB rather than micrometer-size graphite that mainly causes aggregation problems in the processing of the electrode slurries, the aggregation of CB will be focused in the study using model

electrode slurries containing both particles.

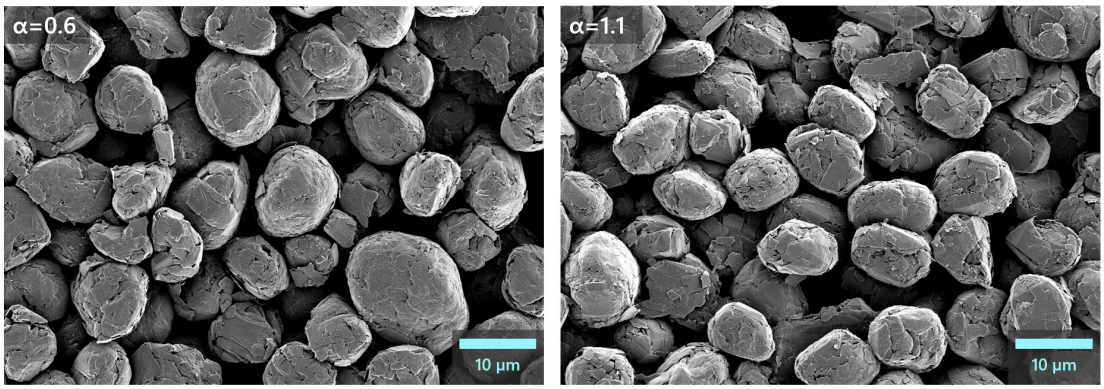

Figure 4.14 SEM images of the electrodes containing 96.7wt% graphite and 3.3wt% PAA with different neutralization degree α. Each electrode is prepared by coating and drying the slurry used in Figure S5.

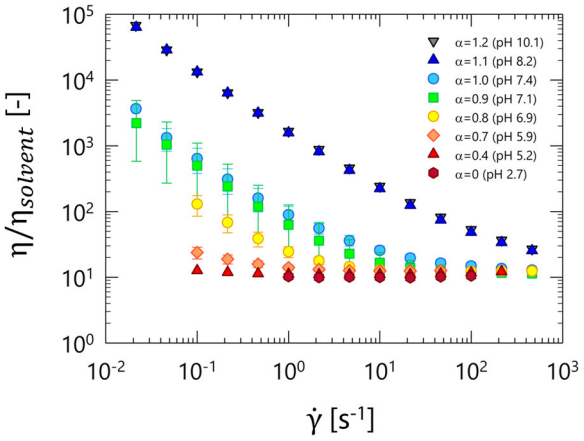

Figure 4.15 Relative viscosity at each α of the model electrode slurry containing 2.0 wt% CB, 40wt% graphite and 1.5wt% PAA.

Figure 4.15 shows the relative viscosity of the model electrode slurries containing 2wt% CB, 40wt% graphite and 1.5 wt% PAA at various α. The slurry exhibits nearly Newtonian behavior up to $\alpha \leq 0.7$, followed by a gradual increase in low shear viscosity at $\alpha \geq 0.7$ which indicates colloidal gelation, showing no further change at $\alpha \geq 1.1$. The α-dependent change can be more clearly seen in Figure 4.16 where the relative viscosity at shear

rate 1 s^{-1} is plotted separately in terms of α and pH.

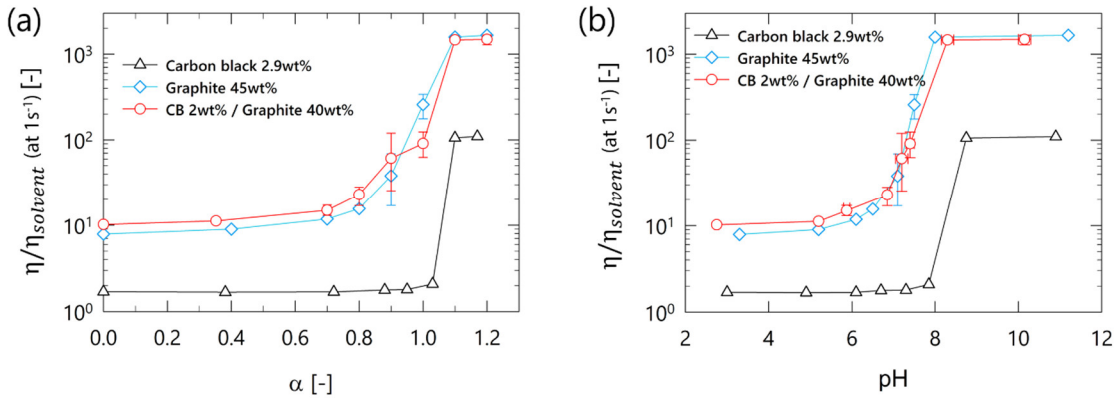

Figure 4.16 Relative viscosity at $1s^{-1}$ of three model slurries as a function of neutralization degree (a) and pH (b).

The relative viscosity of the CB 2wt% graphite 40wt% slurry shows a significant increase as α varies from 0.7 to 1.1 (Figure 4.16(a)) which corresponds to pH from 5.2 to 8.3 (Figure 4.16(b)). It is to be noted that a large error bar appears accompanied with an increase in viscosity around α = 0.9. It can be suggested that the error bar is an inherent characteristic of the sample, given that all the data shown are the values measured at least three times for each sample from at least two separate sets of experiments. In this study, the cause of such a big viscosity variation has yet to be clarified, but two factors could be suggested as possible causes. Since the graphite 45wt% slurry shows a large error bar at α = 0.9 (blue diamonds in Figure 4.16) while CB 2.9wt% slurry shows a very high reproducibility (black triangles in Figure 4.16), it can be deduced that the large error bar of the CB 2 wt% graphite 40wt% slurry (red circles in Figure 4.16) is attributed to the graphite and its interaction with CB particles. The other possibility can be pointed out in Figure 4.16(b), where the relative viscosity is plotted

in terms of pH instead of α. Since the relative viscosity shows a drastic change at around pH 7 which corresponds to α = 0.9, any small fluctuation in pH from local heterogeneity or time-dependent variation could result in a significant change in viscosity.

No matter what the exact reason behind it, the result proposes that the slurry around α = 0.9 (or pH 7) is likely to exhibit temporal and spatial inhomogeneity in the industrial processes as well as in the lab-scale experiments. In addition, the results suggest that a small difference in the quantity of NaOH input can lead to a significant change in rheological properties and dispersion quality, which may cause troubles in the coating process of the electrodes.

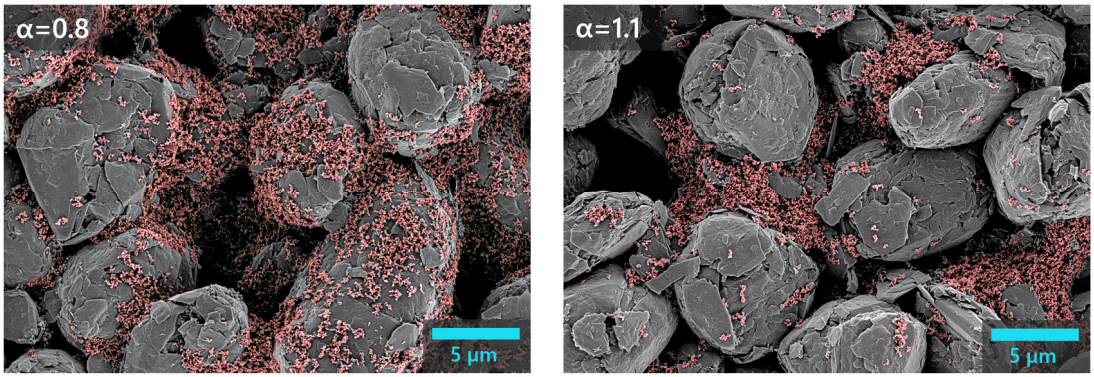

Figure 4.17 SEM images of the electrodes containing 4.6wt% CB, 92wt% graphite and 3.4wt% PAA with different neutralization degree α. Each electrode is prepared by coating and drying the slurry used in Figure 4.15 and Figure 4.16. CB particles are colored in red for better identification.

It has been demonstrated previously that the α-dependent rheological changes are related with the difference in the aggregating behavior of the

particles, especially nanometer-sized CB. To confirm the change in the aggregation tendency of CB, scanning electron microscope (SEM) images of the electrode made from the slurries of $\alpha = 0.8$ and $\alpha = 1.1$ are compared in Figure 4.17. Although there are some cases such that the dispersion state changes during drying process, [75,76] basically the microstructure of the slurry is reflected in the microstructure of the dried electrode composite.[16] Therefore, if the change in rheological properties is due to the change in particle aggregation, SEM images are also expected to reveal the difference. In Figure 4.17, only CB particles are colored in red by post-processing in Adobe Photoshop for easy identification of the distribution of CB particles. At $\alpha = 0.8$, CB particles cover the surface of the graphite with a relatively even distribution. On the other hand, at $\alpha = 1.1$, there are much fewer CB particles on the graphite surface, and most of them are forming aggregates of several μm or more. This difference in aggregation size of CB is in good agreement with our explanation that the difference in the adsorption of PAA depending on α results in the drastic change in the aggregation of particles and rheological properties of the slurry. Meanwhile, unlike CB, graphite particles showed little difference in the microstructure, which is consistent with the observation for the electrodes containing graphite only, as shown earlier in Figure 4.14. Summarizing the results, the change in α of the electrode slurry can give rise to a large difference in the CB distribution of the electrode as well as the rheological properties of the slurry.

The distribution of the carbon black also influences the electrical conductivity in two opposite effects: local aggregation of the conductive

particles can lower the chance of the existence of a neighboring particle, while the aggregation can increase direct contact between the particles forming electrical paths. AC conductivity measurements revealed that the samples with α=1.1 have higher electrical conductivity for both slurry and electrode (Figure 4.18), demonstrating the latter effect is dominant for the system in the current study. This is consistent with the results of existing studies where the inhomogeneous distribution of carbon black in electrodes led to higher electrical conductivity.[40,77,78] Moreover, electrochemical performance is also slightly higher for the electrode with α=1.1, though the difference is very small (Figure 4.19). The result is consistent with a previous study where the electrode having agglomeration exhibited higher rate capability.[14] From the results, it can be suggested that the difference of α leads to only a small change of the electrochemical performance, while it brings about significant increases in the viscosity and dispersion heterogeneity.

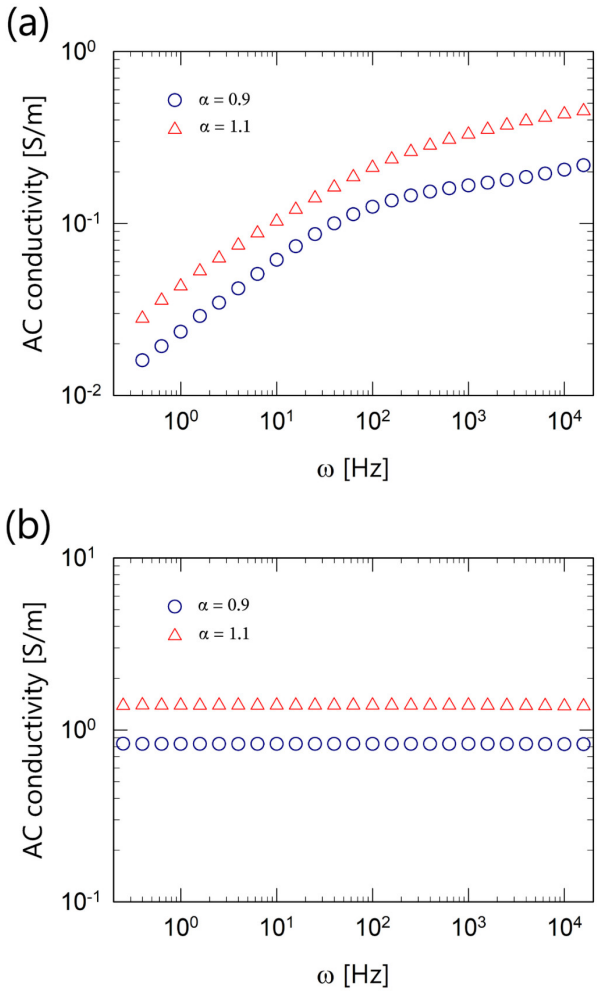

Figure 4.18 Comparison of AC conductivity depending on the neutralization degree α. (a) Electrode slurry containing 2.0 wt% CB, 40 wt% graphite and 1.5wt% PAA. (b) Electrode containing 4.6 wt% CB, 92 wt% graphite and 3.4 wt% PAA.

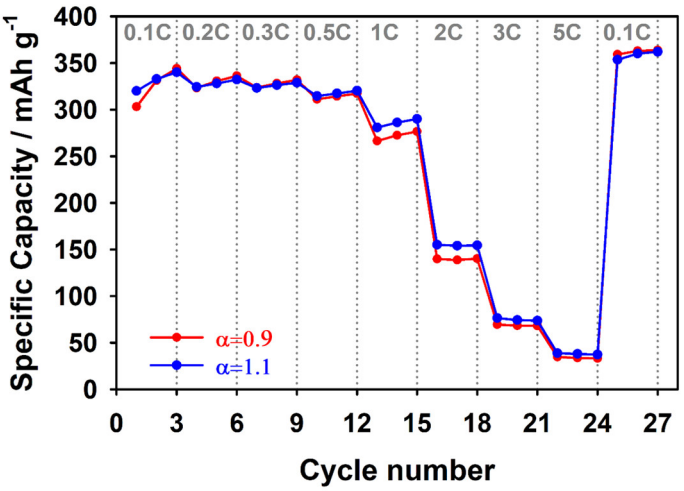

Figure 4.19 Comparison of rate performance of the anodes with α=0.9 and α=1.1. The anodes are composed of 3 wt% CB, 92 wt% graphite, 4 wt% PAA, and 1 wt% SBR.

4.4. Conclusion

This study presents that the rheological properties and dispersion quality of the model electrode slurries using PAA as a binder show considerable changes according to the degree of neutralization α. The model slurries with low α (acidic condition) showed a low-viscosity liquid-like behavior and stable dispersion of particles. On the contrary, the slurry with high α (basic condition) showed a gel-like rheological behavior accompanied by the aggregation of CB. It was revealed that the changes are attributed to the α-dependent adsorption of PAA on the particles. The rheological behavior according to α exhibited a sharp transition for CB and a gradual transition for graphite. The difference in dispersion quality accompanied by the rheological change was particularly apparent for CB and consequently contributed to the homogeneity of CB distribution in the

electrode.

The findings in this research demonstrate the importance of a proper degree of neutralization. In the viewpoint of viscosity control, low α is suitable for the uniform coating due to the constant viscosity. Moreover, it can be suggested that α should not be too high with regard to the homogeneity of the electrode since the aggregation of CB in the electrode slurry with $\alpha \geq 1.1$ leads to the inhomogeneous distribution of CB. Though correlation of the microstructure and the electrochemical performance was not shown in the current work, it is already known that the aggregate in the slurry and inhomogeneous electrodes have many demerits. Therefore, we expect that the proper adjustment of α will contribute to the quality control in the electrode manufacturing processes.

5. ORTHOGONAL SUPERPOSITION RHEOLOGY OF CARBON BLACK GELS

OVERVIEW

It is commonly accepted that the colloidal gels liquify when subsjected to flow, nevertheless, little is known on the dynamics of the gels under flow. In this chapter, we explore the relaxation behavior of model CB gels and fumed silica gels under steady shear flow by means of orthogonal superposition rheometry. As shear rate increases, the frequency dependent orthogonal moduli of the gels shift along the frequency axis without changing their shape, which finally can be superimposed to yield a single master curve. This indicates that the shear rate tunes a master clock for overall relaxation modes in the sheared colloidal gels to produce a "time-shear rate superposition".

5.1. Introduction: orthogonal superposition rheology

Colloidal gels composed of attractive nanoparticles are characterized by a sample-spanning network that results in a solid-like rheological behavior at rest, but yields and flows when subjected to external stresses. This yield stress and the flowability make such gels attractive for a wide range of applications, such as flowable electrodes and electrode slurries.[11,79–81] Colloidal gels experience steady shear flow in various applications such as coating or painting,[82,83] in which the material experiences also a variety of flow fields, resulting in microstructural changes at several different length scales.[16] While it is therefore important to characterize and understand the structure and property in the steady shear flow, there have been only few studies on the 'fluidized' state of the colloidal gel using rheological methods, mainly due to limitations in the measurement techniques: viscosity and normal stress measurements provide only a macroscopic response to the steady shear flow.[41] There has been a substantial amount of studies describing the microstructure of colloidal gels and its evolution under steady shear, using a variety of approaches such as simulations,[84,85] scattering techniques[86,87] and direct observation[85,88–90] that directly investigate the microstructure of the gel under steady shear flow. However, there has been limited information on the time-dependent viscoelastic response of the gels under steady shear, whose time scale is associated with the length scale of the

microstructure of the material.

Probing the viscoelastic response of colloidal gels while *simultaneously* subjecting the sample to a steady shear flow could provide necessary information to understand the link between microstructure development and macroscopic flow properties. One possibility to probe the evolution of relaxation modes under steady shear flow is the superposition of an oscillatory deformation onto a steady shear flow[91,92]. This method enables to analyze the mechanical response in a non-linear flow based on concepts used in linear viscoelasticity. In particular, the superposition of an oscillatory deformation in the direction orthogonal to the steady shear flow results in only a weak coupling of the two flow fields, hence the corresponding moduli can be directly related to the microstructure under flow.[91–96] Utilizing orthogonal superposition rheometry (OSR), dynamics of the flow behavior in steady shear flows of various complex fluids including associative polymers,[92] wormlike micelles,[93,94] colloidal glasses[95] and colloidal gels[96] have been studied.

In this study, we present the linear viscoelastic properties of colloidal gels under steady shear flow measured simultaneously using OSR. We could identify the relaxation behavior of fumed silica gels and carbon black gels in a Newtonian matrix during 'fluidization' by an applied steady shear flow. To investigate how the relaxation timescale depends on the flow, we analyzed the frequency-dependent orthogonal viscoelastic moduli $G'_{\perp}(\omega)$ and $G''_{\perp}(\omega)$ with respect to the increase in shear rate. A master curve was obtained by shifting the orthogonal moduli along the frequency axis in a similar manner to time-temperature superposition of polymeric liquids.[97]

From the shear rate-dependence of the shift factor, the microscopic mechanism of the relaxation behavior of the colloidal gel under shear flow will be discussed in perspective to that of a Brownian suspension.

5.2. Materials and methods

In this study, we used carbon black gels and fumed silica gels in Newtonian media with different viscosities, which is a well-known model system widely utilized to study the rheological behavior of colloidal gel with high reproducibility.[2,13,96,98] The carbon black gels were composed of carbon black particles (Cabot Vulcan XC72R) dispersed in Newtonian matrices with three different viscosities. For this two polybutenes (PB320; M_n = 320 g/mol and PB920; M_n = 920 g/mol) were mixed in different ratios to adjust the Newtonian viscosities for three matrices (0.04, 0.4, 4 Pa·s). The fumed silica gel was prepared by mixing hydrophobic fumed silica particles (Evonik Aerosil R972) in a mixture of 80% nonpolar oligomeric polybutene (M_n = 920 g/mol, Sigma-Aldrich) and 20% paraffin oil (Sigma-Aldrich) as the matrix. The viscosity of the mixture of polybutene and paraffin oil was determined as 0.3 Pa·s at 25 ˚C with Newtonian behavior over the accessible and relevant range of shear rates. All the samples were dispersed with an Ultra Turrax T18 disperser (IKA, Germany) at 8000 rpm for 5 min. Subsequently, bubbles in the suspensions were removed using a vacuum desiccator.

Orthogonal superposition rheometry measurements were performed

using an ARES-G2 rheometer (TA Instrument) with a modification of the normal force control board to perform orthogonal oscillations in the shear flow field of a custom built double wall Couette geometry (shown in Figure 5.1a) as described in previous works.[93–96] The double wall Couette geometry features openings in the inner wall of the cup to minimize pumping flow effects. The oscillatory motion can be imposed perpendicular ($\dot{\gamma}_{\perp}$, *orthogonal superposition*) to the direction of the steady or transient shear flow ($\dot{\gamma}$) as schematically shown in Figure 5.1b. The oscillatory shear deformation orthogonal to the main flow is obtained by moving the Couette bob axially, whereas the main steady shear flow is achieved by rotating the Couette cup (see Figure 5.1a). Detailed information on the orthogonal setup can be found in earlier work.[93] Steady shear flow is applied over a shear rate range of 0.01 to 100 s^{-1}. During steady state shear flow, small-amplitude oscillations were superimposed in the axial direction with a variable frequency. The orthogonal measurements are highly reproducible if the same experimental protocol is applied.

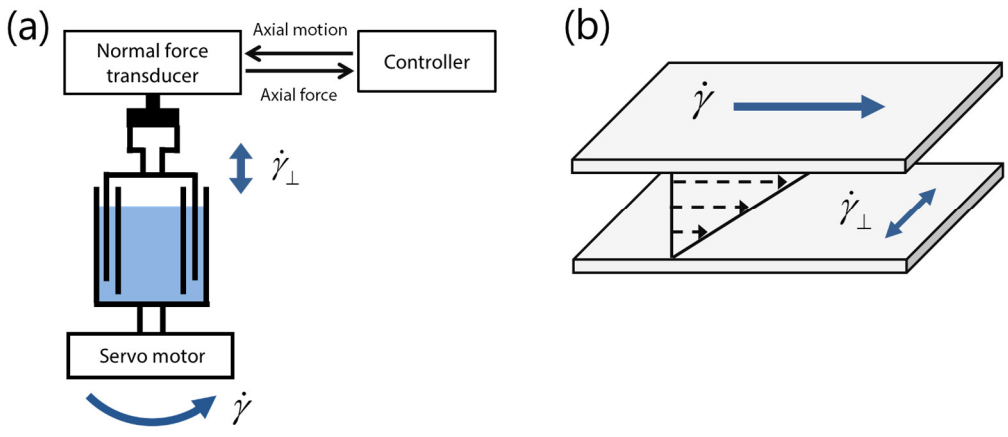

Figure 5.1 (a) Schematic diagram of the orthogonal superposition setup with a double wall Couette cell. An opening is made in the inner wall of the cup that connects with a liquid reservoir in the center of the cup. (b) Superposition flows: orthogonal superposition is achieved by superposing the oscillatory flow in the vorticity direction ($\dot{\gamma}_{\perp}$) onto the steady shear flow ($\dot{\gamma}$).

Colloidal gels do not exhibit absolute (rest) values for the moduli due to aging effects. Moreover, the linear viscoelastic moduli of the colloidal gels at rest are strongly dependent on shear history. To minimize the effect of shear history and obtain reproducible measurements, the following preconditioning protocols were applied before all measurements of frequency dependent moduli of the materials at rest: (1) preshear at 300 s^{-1} for 120 s followed by 0.1 s^{-1} for 300 s, and a rest time of 7200 s for the fumed silica gel. (2) preshear at 300 s^{-1} for 120 s, followed by 0.1 s^{-1} for 60 s, and a rest time of 3600 s.

5.3. Results

5.3.1. Fumed silica gel

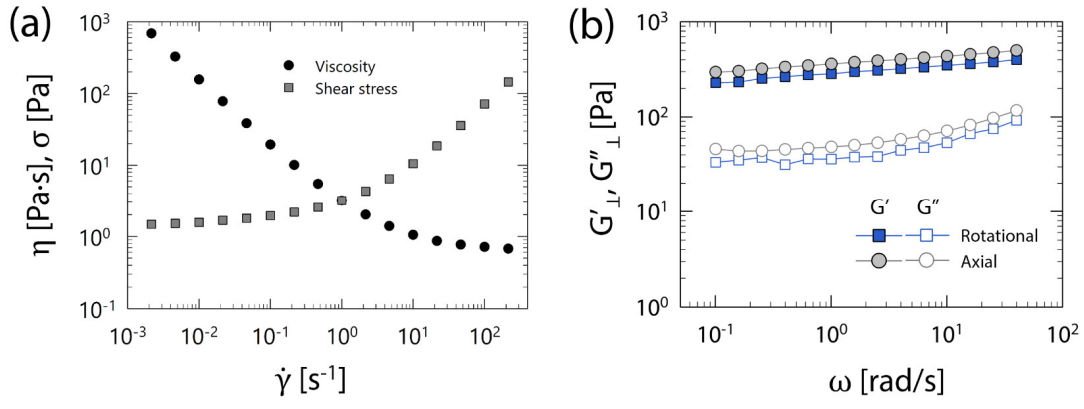

Figure 5.2 (a) Steady state flow curve and (b) frequency dependent linear viscoelastic moduli at rest of a 2.5 vol% fumed silica dispersion.

Figure 5.2a shows the steady shear viscosity curve of the fumed silica gel, which exhibits a power law slope of -0.97 at $\dot{\gamma} < 0.01$ s^{-1}, indicating a typical yielding behavior. The fumed silica gel shows a shear thinning behavior as shear rate increases, and a nearly-Newtonian plateau at $\dot{\gamma} > 100$ s^{-1}. Figure 5.2b shows the frequency dependency of the linear viscoelastic moduli G' and G'', measured both in the rotational and axial direction without the application of a steady shear flow. G' is nearly independent of ω and much larger than G'' for the whole range of the measured ω. Such an elastic behavior indicates a solid-like character of the particle network at rest.[99] With increasing ω the viscous modulus G'' is eventually increasing above its plateau value when approaching the high frequency regime that is controlled by the thickness of lubrication boundary layers and diffusion of the primary particle aggregates of size *a*,[100] and thus related to the matrix viscosity η_m. It can be said that G'' is controlled by an oscillatory Peclet number $Pe_\omega = 6\pi a^3 \eta_m \omega / k_B T$. Colombo *et al.*[96] recently showed that this particle network of colloidal gels exhibits a mechanical anisotropy depending on preshear conditions. The similar values of the moduli in rotational and axial direction obtained in Figure 5.2b indicate that this assures a sufficiently isotropic state of the material for our investigations. It should be noted that with the current experimental setup of an opened double wall Couette the measured axial moduli are always larger than the rotational moduli, which can be attributed to an increased resistance caused by pumping flows. Recent numerical

simulation of the actual flow field in this opened Couette geometry by Colombo et al.[96] indicated that this error amounts for Newtonian fluids to at least 10%, in agreement with our observations in Figure 5.2b. This inherent difference prevents a direct comparison between axial and rotational moduli. Nevertheless, the difference due to this inherent measurement error ($G'_{axi}/G'_{rot} < 2$ for all the experiments in the current study) is much smaller than the difference due to the shear-induced anisotropy of the colloidal gels ($G'_{axi}/G'_{rot} > 100$ for high $\dot{\gamma}_{preshear}$).[96]

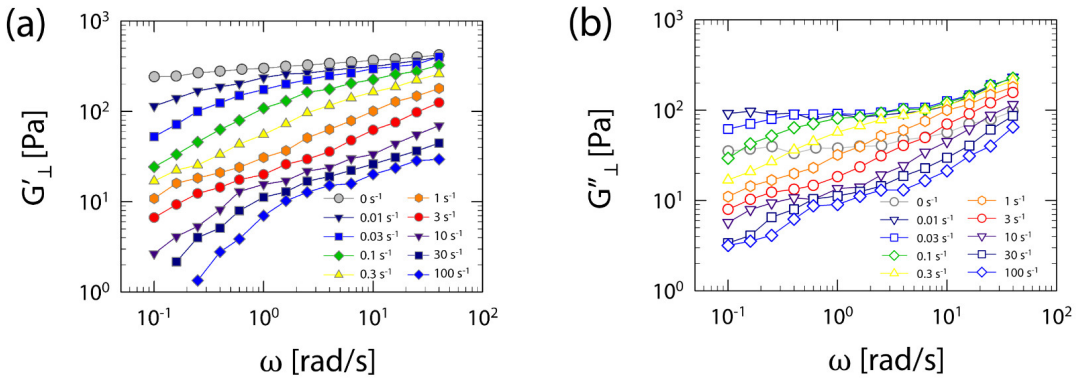

Figure 5.3 Orthogonal superposition moduli $G'_{\perp}$ (a) and $G''_{\perp}$ (b) as a function of frequency for different shear rates of a 2.5 vol% fumed silica dispersion.

To understand the relaxation behavior of the fumed silica gel under the steady shear flow, we determined the orthogonal superposition moduli $G'_{\perp}(\omega)$ and $G''_{\perp}(\omega)$ at different steady shear rates as shown in Figure 5.3. At $\dot{\gamma} < 0.1$ s^{-1}, corresponding to the yielding regime in the flow curve (Figure 5.2a), the curves in Figure 5.3 are still similar in shape to the moduli at rest, with a plateau for both moduli, and an upturn for G'' when approaching the matrix viscosity η_m controlled high frequency regime. However, an

increase in shear rate in this regime leads eventually to a shortening of the initial plateaus and a reduction of the moduli at low frequencies as the shear rate increases, indicative of the gradual loss of connectivity in the network structure.[3] At 0.1 $s^{-1} < \dot{\gamma} < 3\ s^{-1}$, where a shear thinning behavior is observed in the flow curve in Figure 5.2a, the initial plateaus in the moduli in Figure 5.3 disappear and the moduli increase continuously with frequency. Further increasing the shear rate, the absolute moduli values decrease evenly over the whole frequency range. Eventually in this regime with increasing rate the decreasing moduli develop a second plateau at lower frequencies, which is roughly an order of magnitude below the initial plateau at rest. For $\dot{\gamma} > 10\ s^{-1}$, where a nearly-Newtonian plateau is observed in the flow curve (Figure 5.2a), both $G'_{\perp}(\omega)$ and $G''_{\perp}(\omega)$ start to deviate from the second plateau with the appearance of a terminal relaxation regime at low frequencies.

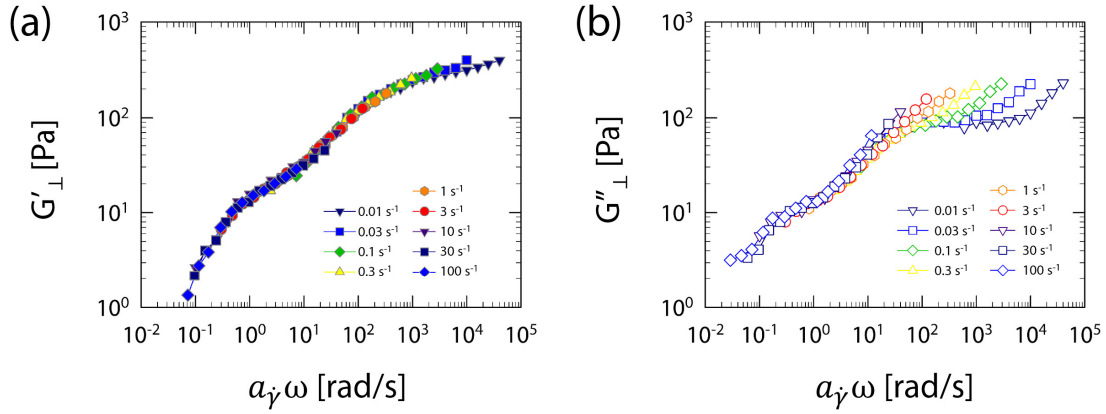

Figure 5.4 Orthogonal superposition moduli $G'_{\perp}$(a) and $G''_{\perp}$(b) as a function of scaled frequency $a_{\dot{\gamma}}\omega$ for different shear rates of a 2.5 vol% fumed silica dispersion.

On closer inspection the $G'_{\perp}(\omega)$ and $G''_{\perp}(\omega)$ curves in Figure 5.3 appear similar in shape over the whole range of the shear rate, indicating

that it should be possible to shift $G'_{\perp}(\omega)$ and $G''_{\perp}(\omega)$ along the ω axis via a shift factor $a_{\dot{\gamma}}$ to obtain a single master curve (as demonstrated in Figure 5.4, using the moduli at $\dot{\gamma} = 10\ s^{-1}$ as the reference point). The superposition of the moduli, which can be termed as 'time-shear rate superposition (TSS)', is reminiscent of the effect of temperature on polymeric materials where a time–temperature superposition (TTS) applies. The TSS behavior has been previously observed for a colloidal glass, where the horizontal shift factor was reported to vary linearly with the shear rate, suggesting a shear-induced relaxation behavior of the materials.[95] Horizontal shifting alone was sufficient to reasonably collapse the orthogonal moduli, contrary to the case of colloidal glasses, where also a vertical shifting is necessary. A possible reason for this difference can be that the vertical shift required for the glasses reflects the effect of shear on the free volume due to the cage deformation, similar to TTS where the scaling factor represents the temperature dependence of the density. In contrast to this, there is no equivalent to a free volume in our colloidal gel systems.

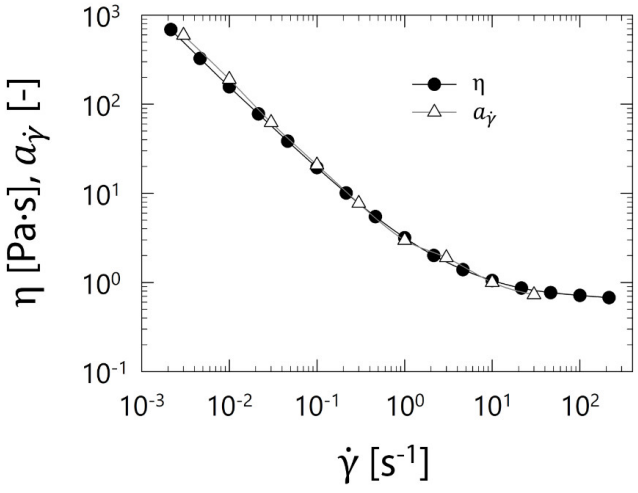

Figure 5.5 Horizontal shift factor $a_{\dot{\gamma}}$ and steady shear viscosity η as a function of shear

rate of a 2.5 vol% fumed silica dispersion.

In Figure 5.5, the shift factor $a_{\dot{\gamma}}$ is plotted as a function of $\dot{\gamma}$ and compared to the steady shear viscosity $\eta(\dot{\gamma})$, and a remarkable similarity between the two over the entire range of investigated $\dot{\gamma}$ is observed. Furthermore, in Figure 5.4b we observe a deviation from the master curve for the $G_{\perp}''$ data at $a_{\dot{\gamma}}\omega$ > 10 rad·s^{-1} for shear rates $\dot{\gamma}$ < 10 s^{-1}. This is not surprising since, as pointed out above, in this high frequency regime it is not the steady shear viscosity $\eta(\dot{\gamma})$, but rather the matrix viscosity η_m, which is represented by an oscillatory Peclet number $Pe_{\omega} = 6\pi a^3\eta_m\omega/k_BT$ that controls the moduli increase above the initial plateau regime for the unshifted data in Figure 5.3b for $\dot{\gamma}$ < 10 s^{-1}. The nice collapse and rate independency of the $G_{\perp}''$ in this regime in Figure 5.3b will thus lead to a spreading of the data when scaling the frequency with an $a_{\dot{\gamma}}$ that equals the rate dependent steady shear viscosity $\eta(\dot{\gamma})$. A further investigation of this apparent viscosity control of the TSS will be shown in the next section.

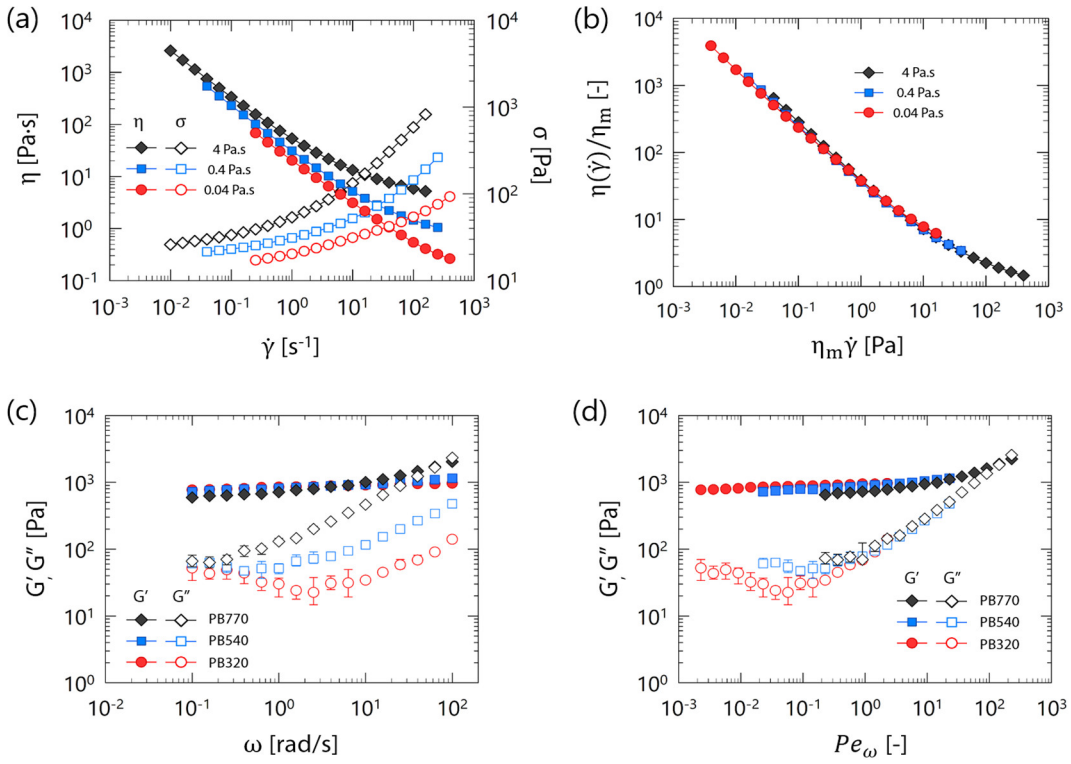

Figure 5.6 (a) Steady state flow curves, (b) the flow curves normalized by the matrix viscosity (the relative viscosity as a function of the hydrodynamic stress) and (c) frequency dependent linear viscoelastic moduli (d) viscoelastic moduli versus Pe_{ω} of 3.0 vol% dispersions of carbon black in matrices with 3 different viscosities (0.04, 0.4, 4 Pa s).

5.3.2. Carbon black gel

To see if the TSS is a general behavior that can be observed in other material systems, and to further understand the discrepancy of $G''_{\perp}$ in the high frequency regime (Figure 5.4b), we performed OSR measurement also for a different model system, carbon black gels, in which the viscosity of the matrix fluid could be systematically varied. Carbon black particles are dispersed in Newtonian matrices of three different viscosities.

The flow curves of carbon black gels in Figure 5.6a exhibit a yielding

behavior, followed by a shear thinning behavior as shear rate increases. These features are qualitatively similar with the fumed silica gel. An increase in the viscosity of the matrix hardly affects the viscosity at low rates and the yield stress level. Also, viscosities coincide into nearly a single curve when they are normalized by matrix viscosities (Figure 5.6b). The frequency dependency of the linear viscoelastic moduli G' and G'' is shown in Figure 5.6. Similar to the fumed silica experiments the plateau modulus G' is frequency-independent and higher than G'' for all three carbon black samples, indicating a solid-like behavior that is expected to be originating from the particle networks.[6] It seems that the upturn of $G''_{\perp}$ is happening at lower frequencies as η_m increases. This agrees with the picture that an increasing matrix viscosity increases the Brownian time of particles, as if we are looking at larger time scales. Similar to the case of viscosity, G' and G''overlap when plotted against the frequency reduced by the matrix viscosity in form of the oscillatory Peclet number $Pe_\omega = 6\pi a^3 \eta_m \omega / k_B T$ (Figure 5.6d). For the calculation of Pe_ω, we assumed a diameter of the carbon black particles or primary aggregates of a = 50 nm (which is obtained from the following discussion part). It should be noted that the moduli of carbon black gels at rest are particularly sensitive to the preshear. For this reason, small difference in the moduli at rest among the three samples still exists despite the well-controlled experimental protocol. In comparison to this, orthogonal superposition moduli under steady shear flow show a much lower history dependence.

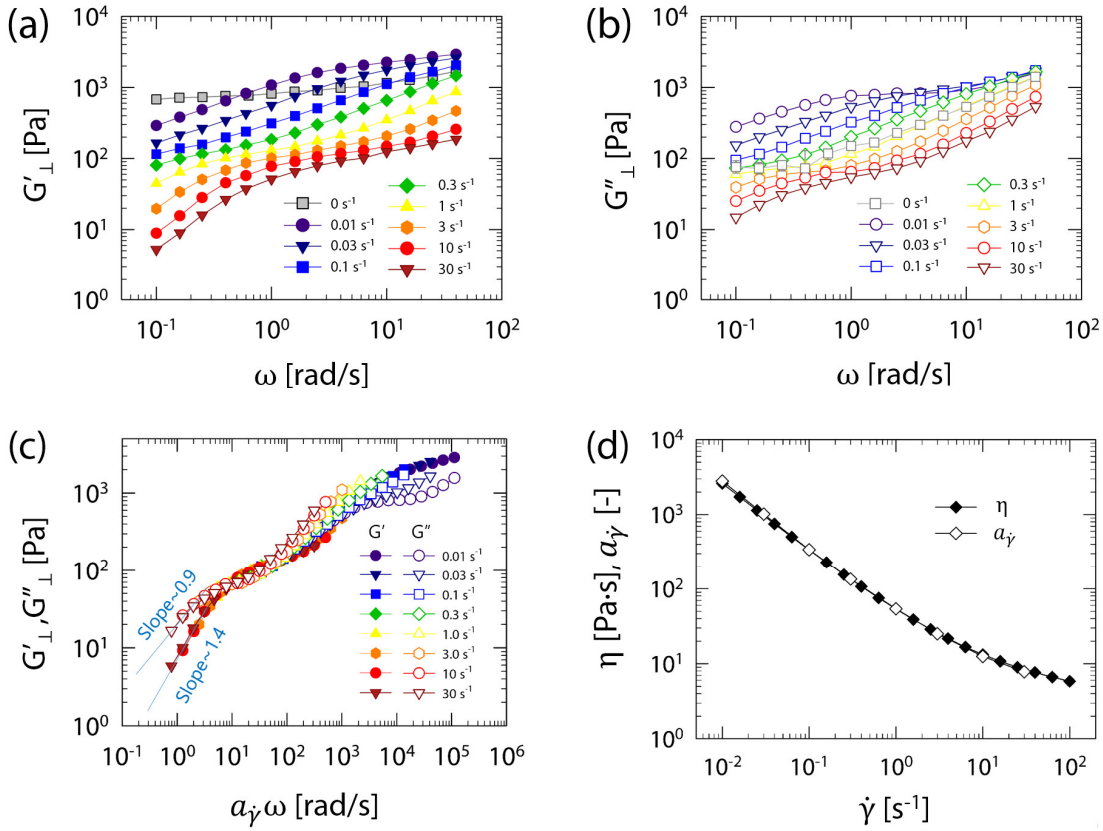

Figure 5.7 Orthogonal superposition measurements at varied shear rates of 3.0 vol% dispersions of carbon black in a matrix with η_m = 4 Pa s: orthogonal moduli as a function of frequency (a, b) and as a function of scaled frequency $a_{\dot{\gamma}}\omega$ (c). The corresponding shift factor is shown together with the viscosity of the suspension (d).

In a similar way as for the fumed silica gel, OSR measurements are performed also for the carbon black gels. Figure 5.7 shows the results for the 3.0 vol% dispersion of carbon black in the matrix with η_m = 4 Pa·s. The orthogonal moduli of the carbon black gels (Figure 5.7a, b) show a similar dependency on shear rate as the fumed silica gel (Figure 5.3): a reduction of the moduli and shortening of the plateaus at low frequencies ($\dot{\gamma}$ ~0.01 s^{-1}), followed by a reduction over the whole frequency range (0.03 $s^{-1} < \dot{\gamma} < 1$ s^{-1}), and again the appearance of a second plateau and then a second

relaxation at low frequencies as shear rate increases ($\dot{\gamma}$ > 3 s^{-1}).

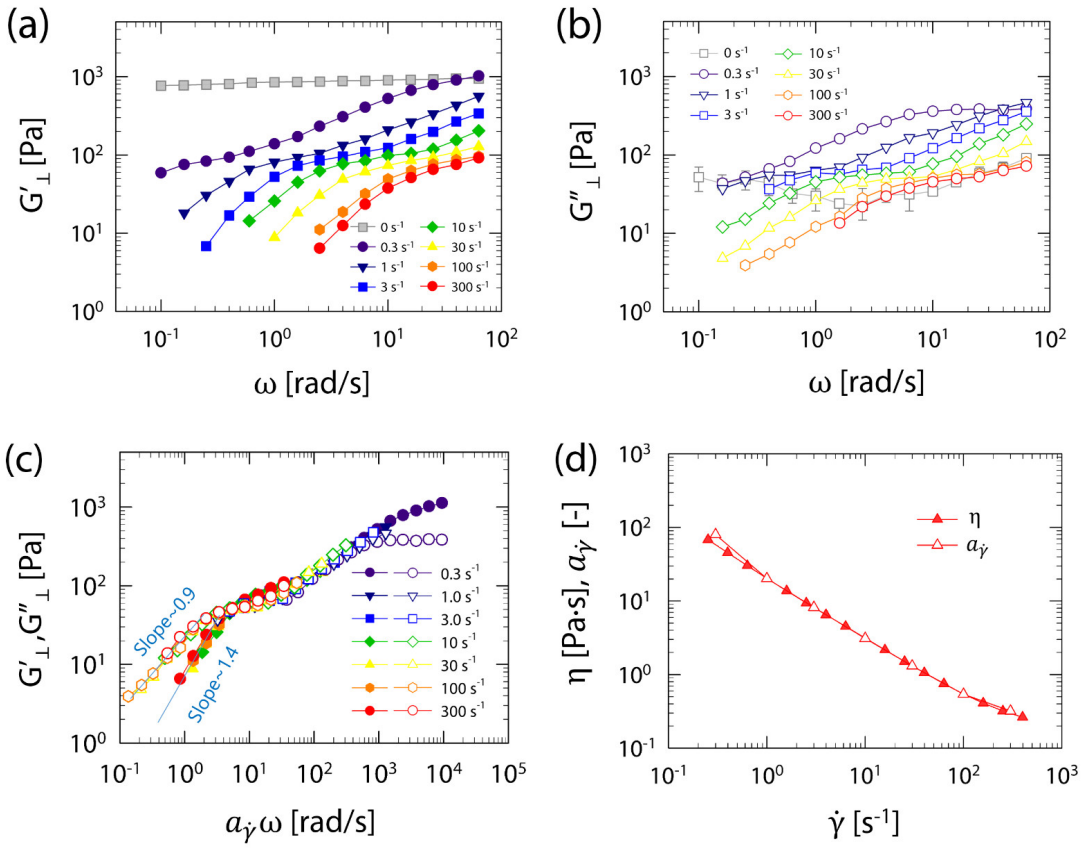

Figure 5.8 Orthogonal superposition measurements at varied shear rates of 3.0 vol% dispersion of carbon black in a matrix with η_m=0.04 Pa·s: orthogonal moduli as a function of frequency (a, b) and as a function of scaled frequency $a_{\dot{\gamma}}\omega$ (c). The corresponding shift factor is shown together with the viscosity of the suspension (d).

Again, the orthogonal moduli curves measured at different shear rates can be shifted along the frequency axis so that they overlap onto a single curve, as shown in Figure 5.7. And also, the carbon black gel in the matrix with η_m = 4 Pa·s shows deviations from a master curve for $G''_{\perp}(a_{\dot{\gamma}}\omega)$ above the initial plateau at high frequency, similar to the fumed silica gel, whereas the $G'_{\perp}(a_{\dot{\gamma}}\omega)$ data overlap perfectly over the whole frequency range. The

shift factors $a_{\dot{\gamma}}(\dot{\gamma})$ used for scaling of the orthogonal moduli were again nearly identical to the steady state viscosity $\eta(\dot{\gamma})$ as seen in Figure 5.7d. Figure 5.8 shows the results of the OSR measurements of the carbon black gel in the lowest-viscosity matrix (η_m = 0.04 Pa·s). The overall observations are equivalent to the case of carbon black in the highest-viscosity matrix (η_m = 4 Pa·s) (Figure 5.7c), a master curve of orthogonal moduli could be obtained (Figure 5.8c), by means of the steady shear viscosity $\eta(\dot{\gamma})$ as the shift factor $a_{\dot{\gamma}}(\dot{\gamma})$ (Figure 5.8d). Compared to carbon black dispersed in the highest-viscosity matrix (η_m = 4 Pa·s), the deviation of the $G_\perp''$ data from the master curve at high frequencies is not observed, which is due to the fact that the upturn of $G_\perp''$ above the initial plateau is happening only at even higher frequencies. To further compare the effect of the matrix viscosity to that of the steady shear viscosity, the orthogonal moduli $G_\perp'$ and $G_\perp''$ for all carbon black gels and the three different matrix viscosities η_m (i.e. 0.04, 0.4 and 4 Pa·s) are plotted together in Figure 5.9 as a function of the frequency scaled with the respective steady shear viscosity $a_{\dot{\gamma}}\omega$. The elastic moduli $G_\perp'$ nicely superpose onto a single curve over a wide frequency range (Figure 5.9a), confirming that the matrix viscosity has little influence on the general relaxation behavior of the system. On the other hand, $G_\perp''$ shows a discrepancy for the high frequency data above the initial plateau in the high $a_{\dot{\gamma}}\omega$ range (Figure 5.9b).

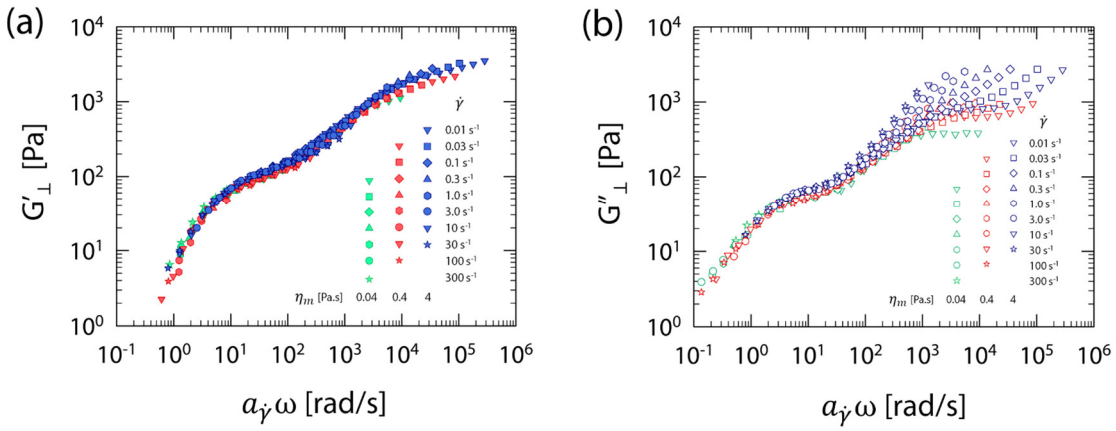

Figure 5.9 Orthogonal superposition moduli $G'_\perp$ (a) and $G''_\perp$ (b) as a function of scaled frequency $a_{\dot{\gamma}}\omega$ of 3.0 vol% dispersions of carbon black in 3 matrices with different viscosities (0.04, 0.4, 4 Pa·s).

The direct comparison of the three different matrix viscosity data shows that the scaled data for $G''_\perp$ starts to deviate already in between the first and second plateau and is not as nicely superposing as $G'_\perp$. A similar discrepancy was observed in the OSR measurement of a colloidal glass.[95] In case of the colloidal glass, the origin of high frequency deviation in $G''_\perp$ was interpreted as shear-induced slowing down of in-cage dynamics.[101] However, the colloidal gels do not exhibit a cage-like structure as the glass, it is thus not likely that in the current case the discrepancy at high frequencies can be attributed to a slowing down of the short time dynamics. A more likely explanation of the deviation is an instantaneous viscous response that would simply scale with the frequency and does not shift with shear rate.

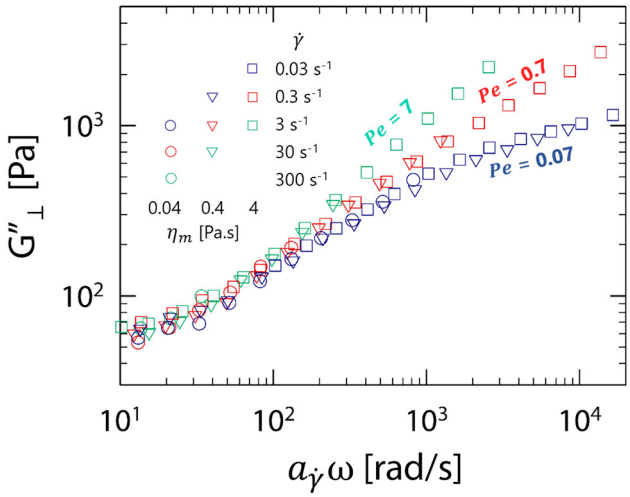

Figure 5.10 Re-plotted selected data of Figure 5.9b. The shear rates are selected to match three different Peclet numbers as indicated in the legend. The same color of the symbols indicates the same Peclet number.

To understand the $G''_\perp$ deviation regime more clearly, part of the data from Figure 5.9b were chosen and three shear rates for each sample were selected, such that the Peclet numbers $Pe = 6\pi a^3 \eta_m \dot{\gamma}/k_B T$ of the flow are matched as 0.07, 0.7 and 7 (Figure 5.10). For the calculation of the diffusivity entering *Pe*, we assumed a diameter of the carbon black particles or primary aggregates of a = 50 nm (which is obtained from the following discussion part) and the viscosity of the respective matrix fluid η_m. As it can be seen in Figure 5.10, $G''_\perp$ measured for samples of different matrix viscosities but under the same *Pe* overlapped when plotted against $a_{\dot{\gamma}}\omega$, indicating that the discrepancy can indeed be associated to the Peclet number. Again, this supports the interpretation that the deviation is due to an increasing contribution of the instantaneous viscous response on $G''_\perp$. The highest Pe samples (for example the CB 3 vol% sample in matrix with η_m = 4 Pa·s under a rate of 30 s^{-1}) exhibit indeed a high frequency slope for

$G''_{\perp}$ that approaches one, similar to the slope observed for the neat Newtonian matrix.

Time-shear rate superposition of the CB dispersion is also explored with some variation of the composition (Figure 5.11). The volume fraction of CB is varied from 1.8 vol% to 3.6 vol%. All samples exhibit time shear rate superposition, and the orthogonal moduli curves are very similar in shape. These self-similar viscoelastic spectra over a wide range of compositions imply a self-similar microstructure of the colloidal gels[13], even when subjected to shear flow.

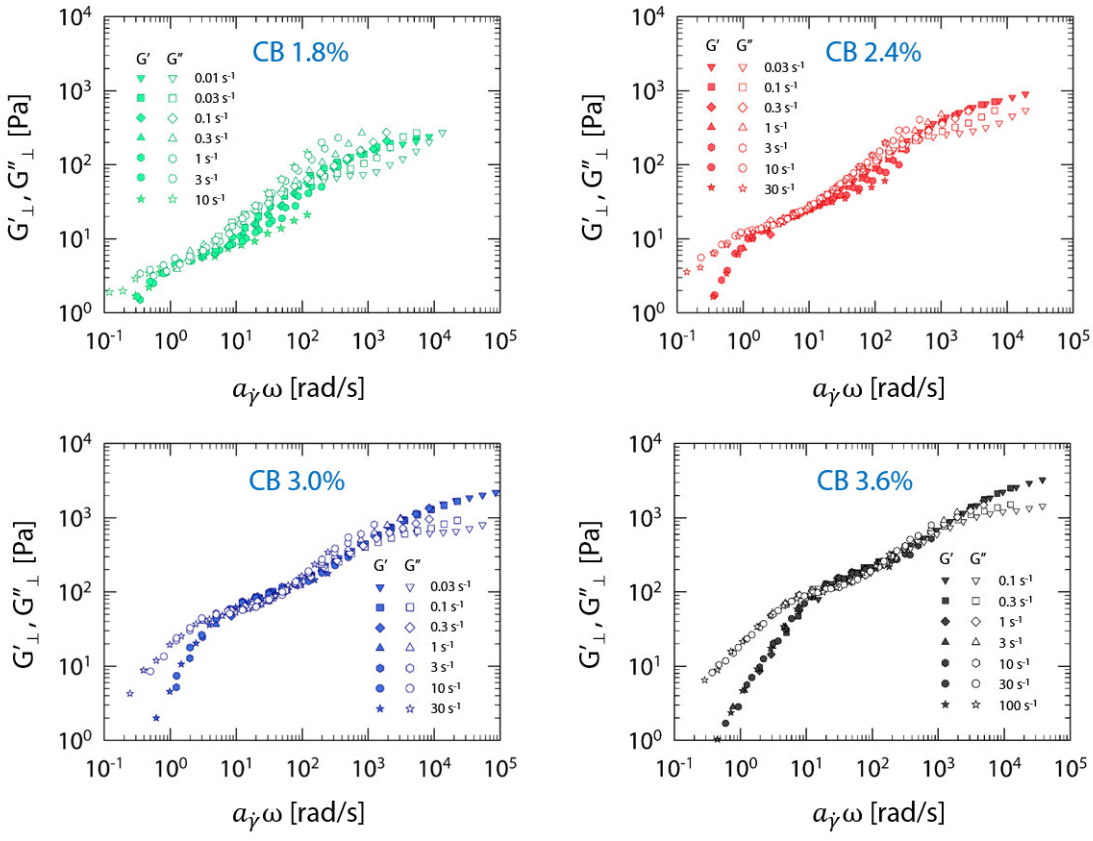

Figure 5.11 Orthogonal superposition moduli as a function of scaled frequency $a_{\dot{\gamma}}\omega$ of carbon black dispersions with different volume fractions in a matrix with η_m=0.4 Pa·s: 1.8 vol%, 2.4 vol%, 3.0 vol% and 3.6 vol%.

5.4. Discussion

In this study, we found that orthogonal moduli of colloidal gels can be shifted along the frequency axis to collapse onto a single master curve, when using a shift factor in form of the steady shear viscosity of the suspension at the shear rate $\dot{\gamma}$ of the main flow for the OSR measurement. Such behavior is reminiscent of the effect of temperature on polymeric liquids, for which a time-temperature superposition (TTS) applies. This suggests that $\dot{\gamma}$ tunes a single master clock for overall relaxation modes in the system, similar as temperature does for relaxation spectra of fluids that have the same internal friction dependence of all modes on T. In the following, we discuss the physical mechanism of this 'time-shear rate superposition' in the colloidal gels of the present study and suggest a possible explanation why the shift factor becomes equivalent to the steady shear viscosity of the suspension.

Before discussing the microstructure of the colloidal gels subjected to different $\dot{\gamma}$, it should be noted that sheared colloidal gels display a significant mechanical anisotropy between the orthogonal and the parallel direction to the main flow, as reported recently[96], caused by a spatially anisotropic breakup of the gel. Bonds in the velocity-velocity gradient plane are more easily broken, while less affected in the other planes in which the gel retains significant elasticity[96]. The frequency dependent orthogonal moduli in the present study can therefore be translated into the relaxation behavior of the gel in the velocity-vorticity plane where the

microstructure is less affected by the steady shear flow.

We are starting from this viewpoint of an analogy to TTS, which is described using a friction coefficient ζ_0 that defines the relaxation time and its temperature dependence.[102] Except specific cases where TTS does not suffice,[103–105] the same microscopic frictional process operates at all length and time scales.[106,107] In a similar fashion, a shear rate-dependent parameter that determines all relaxation times in the colloidal gel under flow can be suggested. Two hypotheses can explain the rate-dependent time scale, which is associated with the microstructure in the velocity-vorticity plane.

The first is that the shear flow changes the relaxation time of the aggregates by progressively changing the length scale of the aggregate in the velocity-vorticity plane, which has been previously suggested by Colombo et al.[96] The main point of this hypothesis is that the length scale in the neutral direction of shear also breaks down gradually, though the breakdown of the aggregates mainly occurs in the velocity-velocity gradient plane. Assuming that the slow Brownian relaxation of aggregates is responsible for the viscoelastic response of the material[108] and that the diffusion of the aggregates follows the Stokes–Einstein relation, rate dependent hydrodynamic radii of the aggregates $a(\dot{\gamma})$ can be calculated using the following equation (1)

$$\lambda(\dot{\gamma}) \approx \frac{\pi a(\dot{\gamma})^3}{k_B T} \eta_m \qquad (1)$$

However, this hypothesis has a shortcoming: Since it assumes that the Brownian relaxation of aggregates is responsible for the viscoelastic

response of the material, the change in aggregate size should affect the magnitude of the viscoelastic moduli as well as the relaxation time. As elasticity arises from the Brownian force, the change of aggregate size r should result in a significant change of $G'_{\perp}$ and $G''_{\perp}$, e.g. proportional to r^{-3} for Brownian hard spheres.[109,110] However, the orthogonal moduli only shifts along the frequency axis with negligible change in their magnitude, which is inconsistent with the case where the length scale changes.

In the second approach, we hypothesize that the Brownian relaxation of the smallest unit aggregate is responsible for the orthogonal moduli. Considering that the horizontal shift factor was found to be directly proportional to the suspension viscosity at each shear rate, the viscosity can be pointed out as the parameter that determines the relaxation time of the system. Since the relaxation time of Brownian suspensions can be described by the diffusion time[111–114] $\lambda \approx \frac{\pi a l^2}{k_B T}\eta_{sus}$, where l represents a characteristic length scale, a the particle radius and η_{sus} the suspension viscosity, we can now replace the fixed suspension viscosity η_{sus} with the rate-dependent suspension viscosity $\eta(\dot{\gamma})$, and use the particle radius as the characteristic length scale for simplicity. Here, it should be noted that $\eta(\dot{\gamma})$ is the viscosity measured in the flow direction while the orthogonal moduli are associated with the viscoelastic response in the velocity-vorticity plane that is less affected by the steady flow. As a result, the rate-dependent relaxation time $\lambda(\dot{\gamma})$ can be expressed as

$$\lambda(\dot{\gamma}) \approx \frac{\pi a^3}{k_B T}\eta(\dot{\gamma}) \qquad (2)$$

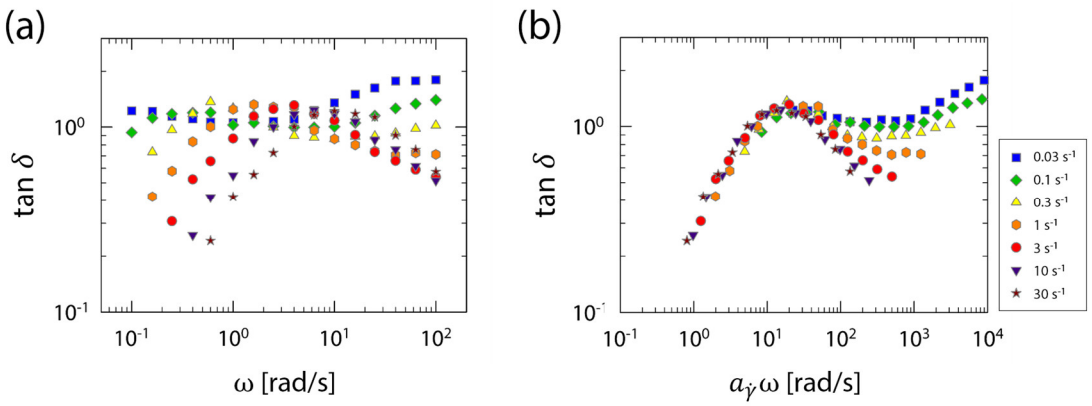

Figure 5.12 Orthogonal superposition tan(δ) versus (a) unscaled and (b) scaled frequency, at varied shear rates. The frequency at the minimum of unscaled data are used as inverse Brownian diffusion time to obtain the relaxation time of the gels under flow.

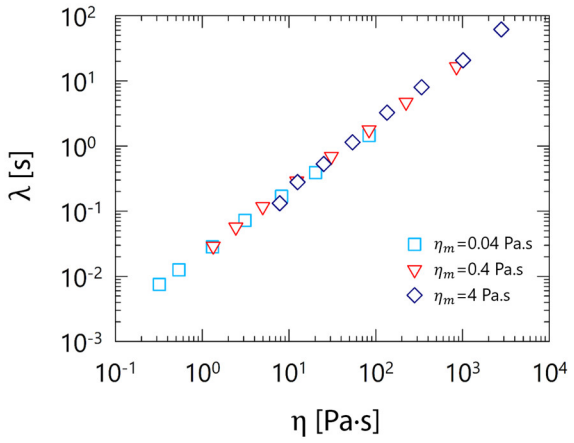

Figure 5.13 Relaxation time $\lambda(\dot{\gamma})$ as a function of the suspension viscosity $\eta(\dot{\gamma})$ of the carbon black 3.0vol% dispersions in matrices with 3 different viscosities (0.04, 0.4, 4 Pa·s).

We calculate the relaxation time of the system from the inverse of the frequency at the minimum phase angle (or maximum $tan(\delta)$) of the orthogonal measurements data (Figure 5.12). This relaxation time as a

function of the suspension viscosity for the three carbon black samples is shown in Figure 5.13. It can be clearly seen that the suspension viscosity and relaxation time are indeed linearly related. This explanation, that the rate-dependent suspension viscosity $\eta(\dot{\gamma})$ determines the relaxation of the colloidal gel under shear, is consistent with a previous study that showed a direct proportionality between suspension viscosity and Brownian relaxation times by theoretical[111,112] and phenomenological[113] considerations. In addition, the radius of the particles can be calculated from equation (2) as ~40 nm for the primary aggregates of the fumed silica and ~50 nm for the carbon black, which is a reasonable value previously published dimensions for these materials.[115,116]

5.5. Conclusion

Utilizing orthogonal superposition rheology (OSR), we found that the orthogonal moduli of colloidal gels under steady shear flow exhibit a time-shear rate superposition (TSS), indicating that the time scales for all the relaxation modes are equally dependent on the shear rate. From this result it can be concluded that the relaxation mechanism itself of the colloidal gel does not change with the applied shear rate, but rather the associated time scale, which is similar to a colloidal glass under flow. The horizontal shift factor for TSS is directly proportional to the rate-dependent suspension viscosity $\eta(\dot{\gamma})$. Though it will require further investigation to entirely understand the mechanism, it is suggested that $\eta(\dot{\gamma})$ determines the

relaxation time of the units constituting the colloidal gel under steady shear flow. Given that the orthogonal superposition rheometry only provides mechanical information in the orthogonal direction, additional techniques such as rheo-SAXS can be utilized to assist the results. Our findings provide valuable insights for the understanding of physics controlling the flow of colloidal gels, which is difficult to directly observe otherwise. The observations also open a possibility to investigate the low-frequency behavior of weakly attractive colloidal gels that is so far limited, as aging effects usually prevent to assess the long-time scale behavior associated with the low-frequency response. While we could not measure reproducible and reliable data at very low $\dot{\gamma}$ for the materials used in the present study, it would be intriguing to examine the connection between orthogonal moduli at very low $\dot{\gamma}$ and that at rest in the future work.

6. CONCLUSIONS AND OUTLOOK

Carbon black dispersions are very well-known and have been studied over several decades. Nevertheless, there are surprisingly a lot of features unknown for the dispersions containing carbon black particles. This thesis includes studies related with the carbon black dispersions, focusing on the correlation between the aggregating behavior of the particles and the unusual rheological behaviors.

First, a critical difference in rheological behavior or NMP-based and water-based slurries was demonstrated in chapter 2. In a similar manner, a study on water-based slurries using PAA as a binder was also conducted in chapter 3. I showed that the slurries show gel-like and liquid-like rheology according to the difference in the interaction between particles and binders. Furthermore, it is shown that the influence CB is dominant in all slurries despite its small fraction. The results can be utilized to formulate the electrode slurries in the industrial as well as in the lab; I believe that the slurry formulation for the better processing will be received more importantly in the industrial field. The concept is very simple and straightforward so that the engineers in the field of battery industry can easily refer to.

The results shown in the chapter 2 and 3 also draws that many of the electrode slurries, especially cathode slurries can be regarded as colloidal

gels. Motivated from the complex shear history-dependence of the cathode slurries, I tried to thoroughly investigate more simplified version of the cathode slurry: CB/PVDF/NMP suspension, which is a model cathode slurry where micron-sized active material particles are removed for the simplicity. It was found that the carbon black dispersions in PVDF/NMP solutions shows universal scaling behavior similar to the model CB gels in various other suspending media. Comparison of many suspending media also lead to the fact that CB forms colloidal gel in broad scope of suspending media with different polarity and viscosities, which may be counterintuitive in a classical viewpoint of "affinity".

It should be mentioned that even though many interesting and important findings are shown on the CB suspensions in chapter 5, there are more ways to go, especially a study on the full cathode slurry where a combination of the micron-sized active material and the attractive carbon black particles are leading to a unique shear history-dependence. In addition, a combination of rheology with the other techniques such as electrical measurements are expected to broaden a sight to blind spots of the dispersion quality assessment due to the extremely high light absorption of the carbon black dispersions.

Bibliography

[1] K. Dullaert, J. Mewis, A structural kinetics model for thixotropy, Journal of Non-Newtonian Fluid Mechanics. 139 (2006) 21–30. doi:10.1016/j.jnnfm.2006.06.002.

[2] K. Dullaert, J. Mewis, A model system for thixotropy studies, Rheol Acta. 45 (2005) 23–32. doi:10.1007/s00397-005-0439-2.

[3] K. Dullaert, J. Mewis, Stress jumps on weakly flocculated dispersions: Steady state and transient results, Journal of Colloid and Interface Science. 287 (2005) 542–551. doi:10.1016/j.jcis.2005.02.018.

[4] T. Amari, K. Watanabe, Flow properties and electrical conductivity of carbon black–linseed oil suspension, Journal of Rheology. 34 (1990) 207–221. doi:10.1122/1.550124.

[5] Y. Aoki, Rheology of carbon black suspensions. IV. Effect of suspending media on the sol-gel transition behavior, Rheologica Acta. 50 (2011) 779–785. doi:10.1007/s00397-011-0583-9.

[6] Y. Aoki, A. Hatano, H. Watanabe, Rheology of carbon black suspensions. I. Three types of viscoelastic behavior, Rheologica Acta. 42 (2003) 209–216.

[7] Y. Aoki, A. Hatano, H. Watanabe, Rheology of carbon black suspensions. II. Well dispersed system, Rheologica Acta. 42 (2003) 321–325.

[8] Y. Aoki, H. Watanabe, Rheology of carbon black suspensions. III. Sol-gel transition system, Rheologica Acta. 43 (2004) 390–395. doi:10.1007/s00397-004-0355-x.

[9] Y. Aoki, Rheological characterization of carbon black/polystyrene solution systems, Journal of Applied Polymer Science. 108 (//) 2660–2666.

[10] K.M. Yearsley, M.R. MacKley, F. Chinesta, A. Leygue, The rheology of multiwalled carbon nanotube and carbon black suspensions, Journal of Rheology. 56 (2012) 1465–1490.

[11] M. Youssry, L. Madec, P. Soudan, M. Cerbelaud, D. Guyomard, B. Lestriez, Non-aqueous carbon black suspensions for lithium-based redox flow batteries: rheology and simultaneous rheo-electrical behavior, Phys. Chem. Chem. Phys. 15 (2013) 14476–14486. doi:10.1039/C3CP51371H.

[12] M.J. Armstrong, A.N. Beris, S.A. Rogers, N.J. Wagner, Dynamic shear rheology and structure kinetics modeling of a thixotropic carbon black suspension, Rheol Acta. 56 (2017) 811–824. doi:10.1007/s00397-017-1038-8.

[13] V. Trappe, D.A. Weitz, Scaling of the viscoelasticity of weakly attractive particles, Physical Review Letters. 85 (2000) 449–452. doi:10.1103/PhysRevLett.85.449.

[14] D. Mohanty, E. Hockaday, J. Li, D.K. Hensley, C. Daniel, D.L. Wood, Effect of electrode manufacturing defects on electrochemical performance of lithium-ion batteries: Cognizance of the battery failure sources, Journal of Power Sources. 312 (2016) 70–79. doi:10.1016/j.jpowsour.2016.02.007.

[15] T. Yim, S.J. Choi, Y.N. Jo, T.-H. Kim, K.J. Kim, G. Jeong, Y.-J. Kim, Effect of binder properties on electrochemical performance for silicon-graphite anode: Method and application of binder screening, Electrochimica Acta. 136 (2014) 112–120. doi:10.1016/j.electacta.2014.05.062.

[16] J. Lee, S. Sung, Y. Kim, J.D. Park, K.H. Ahn, A new paradigm of materials processing—heterogeneity control, Current Opinion in Chemical Engineering. 16 (2017) 16–22. doi:10.1016/j.coche.2017.04.002.

[17] C.C. Li, Y.S. Lin, Interactions between organic additives and active powders in water-based lithium iron phosphate electrode slurries, Journal of Power Sources. 220 (2012) 413–421. doi:10.1016/j.jpowsour.2012.07.125.

[18] Z. Zhang, T. Zeng, Y. Lai, M. Jia, J. Li, A comparative study of different binders and their effects on electrochemical properties of LiMn2O4 cathode in lithium ion batteries, Journal of Power Sources. 247 (2014) 1–8. doi:10.1016/j.jpowsour.2013.08.051.

[19] C.-C. Li, J.-T. Lee, X.-W. Peng, Improvements of Dispersion Homogeneity and Cell Performance of Aqueous-Processed LiCoO2 Cathodes by Using Dispersant of PAA – NH4, J. Electrochem. Soc. 153 (2006) A809–A815. doi:10.1149/1.2177071.

[20] W. Porcher, B. Lestriez, S. Jouanneau, D. Guyomard, Optimizing the surfactant for the aqueous processing of LiFePO4 composite electrodes, Journal of Power Sources. 195 (2010) 2835–2843. doi:10.1016/j.jpowsour.2009.11.088.

[21] J.-H. Lee, J.-S. Kim, Y.C. Kim, D.S. Zang, U. Paik, Dispersion properties of aqueous-based LiFePO4 pastes and their electrochemical performance for lithium batteries, Ultramicroscopy. 108 (2008) 1256–1259. doi:10.1016/j.ultramic.2008.04.027.

[22] A.Z. Weber, M.M. Mench, J.P. Meyers, P.N. Ross, J.T. Gostick, Q. Liu, Redox flow

batteries: a review, J Appl Electrochem. 41 (2011) 1137. doi:10.1007/s10800-011-0348-2.

[23] K. Lin, Q. Chen, M.R. Gerhardt, L. Tong, S.B. Kim, L. Eisenach, A.W. Valle, D. Hardee, R.G. Gordon, M.J. Aziz, M.P. Marshak, Alkaline quinone flow battery, Science. 349 (2015) 1529–1532. doi:10.1126/science.aab3033.

[24] M. Duduta, B. Ho, V.C. Wood, P. Limthongkul, V.E. Brunini, W.C. Carter, Y.-M. Chiang, Semi-Solid Lithium Rechargeable Flow Battery, Advanced Energy Materials. 1 (2011) 511–516. doi:10.1002/aenm.201100152.

[25] V. Presser, C.R. Dennison, J. Campos, K.W. Knehr, E.C. Kumbur, Y. Gogotsi, The Electrochemical Flow Capacitor: A New Concept for Rapid Energy Storage and Recovery, Advanced Energy Materials. 2 (2012) 895–902. doi:10.1002/aenm.201100768.

[26] H. Zheng, R. Yang, G. Liu, X. Song, V.S. Battaglia, Cooperation between active material, polymeric binder and conductive carbon additive in lithium ion battery cathode, Journal of Physical Chemistry C. 116 (2012) 4875–4882. doi:10.1021/jp208428w.

[27] F.A. Çetinel, W. Bauer, Processing of water-based LiNi1/3Mn1/3Co1/3O2 pastes for manufacturing lithium ion battery cathodes, Bull Mater Sci. 37 (2014) 1685–1690. doi:10.1007/s12034-014-0733-7.

[28] S.-L. Chou, Y. Pan, J.-Z. Wang, H.-K. Liu, S.-X. Dou, Small things make a big difference: binder effects on the performance of Li and Na batteries, Physical Chemistry Chemical Physics. (2014). doi:10.1039/C4CP02475C.

[29] S. Lim, S. Kim, K.H. Ahn, S.J. Lee, The effect of binders on the rheological properties and the microstructure formation of lithium-ion battery anode slurries, Journal of Power Sources. 299 (2015) 221–230. doi:10.1016/j.jpowsour.2015.09.009.

[30] S. Lim, S. Kim, K.H. Ahn, S.J. Lee, Stress Development of Li-Ion Battery Anode Slurries during the Drying Process, Ind. Eng. Chem. Res. 54 (2015) 6146–6155. doi:10.1021/acs.iecr.5b00878.

[31] W. Bauer, D. Nötzel, Rheological properties and stability of NMP based cathode slurries for lithium ion batteries, Ceramics International. 40 (2014) 4591–4598. doi:10.1016/j.ceramint.2013.08.137.

[32] Y.I. Kwon, J.D. Kim, Y.S. Song, Agitation Effect on the Rheological Behavior of Lithium-Ion Battery Slurries, Journal of Elec Materi. 44 (2014) 475–481.

doi:10.1007/s11664-014-3349-1.

[33] K.Y. Cho, Y.I. Kwon, J.R. Youn, Y.S. Song, Interaction analysis between binder and particles in multiphase slurries, Analyst. 138 (2013) 2044–2050. doi:10.1039/C3AN36720G.

[34] K.Y. Cho, Y.I. Kwon, J.R. Youn, Y.S. Song, Evaluation of slurry characteristics for rechargeable lithium-ion batteries, Materials Research Bulletin. 48 (2013) 2922–2926. doi:10.1016/j.materresbull.2013.04.026.

[35] Z. Chen, G.-T. Kim, D. Chao, N. Loeffler, M. Copley, J. Lin, Z. Shen, S. Passerini, Toward greener lithium-ion batteries: Aqueous binder-based LiNi0.4Co0.2Mn0.4O2 cathode material with superior electrochemical performance, Journal of Power Sources. 372 (2017) 180–187. doi:10.1016/j.jpowsour.2017.10.074.

[36] J.-T. Lee, Y.-J. Chu, X.-W. Peng, F.-M. Wang, C.-R. Yang, C.-C. Li, A novel and efficient water-based composite binder for LiCoO2 cathodes in lithium-ion batteries, Journal of Power Sources. 173 (2007) 985–989. doi:10.1016/j.jpowsour.2007.07.073.

[37] S. Morelly, M. Tang, N. Alvarez, S.L. Morelly, M.H. Tang, N.J. Alvarez, The Impotence of Non-Brownian Particles on the Gel Transition of Colloidal Suspensions, Polymers. 9 (2017) 461. doi:10.3390/polym9090461.

[38] S.H. Sung, S. Kim, J. Hendricks, C. Clasen, K.H. Ahn, Orthogonal Superposition Rheometry of Colloidal Gels: Time-Shear Rate Superposition, Soft Matter. (2018). doi:10.1039/C8SM01512K.

[39] J.C. Badot, E. Ligneel, O. Dubrunfaut, D. Guyomard, B. Lestriez, A multiscale description of the electronic transport within the hierarchical architecture of a composite electrode for lithium batteries, Advanced Functional Materials. 19 (2009) 2749–2758.

[40] B. Ludwig, Z. Zheng, W. Shou, Y. Wang, H. Pan, Solvent-Free Manufacturing of Electrodes for Lithium-ion Batteries, Scientific Reports. 6 (2016) 23150. doi:10.1038/srep23150.

[41] A. Negi, C. Osuji, New insights on fumed colloidal rheology—shear thickening and vorticity-aligned structures in flocculating dispersions, Rheol Acta. 48 (2009) 871–881. doi:10.1007/s00397-008-0341-9.

[42] C.O. Osuji, D.A. Weitz, Highly anisotropic vorticity aligned structures in a shear thickening attractive colloidal system, Soft Matter. 4 (2008) 1388–1392. doi:10.1039/B716324J.

[43] Z.P. Cai, Y. Liang, W.S. Li, L.D. Xing, Y.H. Liao, Preparation and performances of LiFePO4 cathode in aqueous solvent with polyacrylic acid as a binder, Journal of Power Sources. 189 (2009) 547–551. doi:10.1016/j.jpowsour.2008.10.040.

[44] J. Li, D.-B. Le, P.P. Ferguson, J.R. Dahn, Lithium polyacrylate as a binder for tin–cobalt–carbon negative electrodes in lithium-ion batteries, Electrochimica Acta. 55 (2010) 2991–2995. doi:10.1016/j.electacta.2010.01.011.

[45] Z. Zhang, W. Bao, H. Lu, M. Jia, K. Xie, Y. Lai, J. Li, Water-Soluble Polyacrylic Acid as a Binder for Sulfur Cathode in Lithium-Sulfur Battery, ECS Electrochem. Lett. 1 (2012) A34–A37. doi:10.1149/2.009202eel.

[46] A. Magasinski, B. Zdyrko, I. Kovalenko, B. Hertzberg, R. Burtovyy, C.F. Huebner, T.F. Fuller, I. Luzinov, G. Yushin, Toward Efficient Binders for Li-Ion Battery Si-Based Anodes: Polyacrylic Acid, ACS Appl. Mater. Interfaces. 2 (2010) 3004–3010. doi:10.1021/am100871y.

[47] S. Komaba, T. Ozeki, N. Yabuuchi, K. Shimomura, Polyacrylate as Functional Binder for Silicon and Graphite Composite Electrode in Lithium-Ion Batteries, Electrochemistry. 79 (2011) 6–9. doi:10.5796/electrochemistry.79.6.

[48] C. Erk, T. Brezesinski, H. Sommer, R. Schneider, J. Janek, Toward Silicon Anodes for Next-Generation Lithium Ion Batteries: A Comparative Performance Study of Various Polymer Binders and Silicon Nanopowders, ACS Appl. Mater. Interfaces. 5 (2013) 7299–7307. doi:10.1021/am401642c.

[49] D. Mazouzi, Z. Karkar, C. Reale Hernandez, P. Jimenez Manero, D. Guyomard, L. Roué, B. Lestriez, Critical roles of binders and formulation at multiscales of silicon-based composite electrodes, Journal of Power Sources. 280 (2015) 533–549. doi:10.1016/j.jpowsour.2015.01.140.

[50] L. Wei, C. Chen, Z. Hou, H. Wei, Poly (acrylic acid sodium) grafted carboxymethyl cellulose as a high performance polymer binder for silicon anode in lithium ion batteries, Scientific Reports. 6 (2016) 19583. doi:10.1038/srep19583.

[51] B. Koo, H. Kim, Y. Cho, K.T. Lee, N.-S. Choi, J. Cho, A Highly Cross-Linked Polymeric Binder for High-Performance Silicon Negative Electrodes in Lithium Ion Batteries, Angewandte Chemie International Edition. 51 (2012) 8762–8767. doi:10.1002/anie.201201568.

[52] Z.-J. Han, N. Yabuuchi, S. Hashimoto, T. Sasaki, S. Komaba, Cross-Linked Poly(acrylic acid) with Polycarbodiimide as Advanced Binder for Si/Graphite Composite Negative Electrodes in Li-Ion Batteries, ECS Electrochem. Lett. 2

(2013) A17–A20. doi:10.1149/2.005302eel.

[53] J. Song, M. Zhou, R. Yi, T. Xu, M.L. Gordin, D. Tang, Z. Yu, M. Regula, D. Wang, Interpenetrated Gel Polymer Binder for High-Performance Silicon Anodes in Lithium-ion Batteries, Advanced Functional Materials. 24 (2014) 5904–5910. doi:10.1002/adfm.201401269.

[54] S. Aoki, Z.-J. Han, K. Yamagiwa, N. Yabuuchi, M. Murase, K. Okamoto, T. Kiyosu, M. Satoh, S. Komaba, Acrylic Acid-Based Copolymers as Functional Binder for Silicon/Graphite Composite Electrode in Lithium-Ion Batteries, J. Electrochem. Soc. 162 (2015) A2245–A2249. doi:10.1149/2.0171512jes.

[55] C.-C. Li, J.-T. Lee, C.-Y. Lo, M.-S. Wu, Effects of PAA-NH4 Addition on the Dispersion Property of Aqueous LiCoO2 Slurries and the Cell Performance of As-Prepared LiCoO2 Cathodes, Electrochem. Solid-State Lett. 8 (2005) A509–A512. doi:10.1149/1.2012287.

[56] S. Komaba, K. Okushi, T. Ozeki, H. Yui, Y. Katayama, T. Miura, T. Saito, H. Groult, Polyacrylate Modifier for Graphite Anode of Lithium-Ion Batteries, Electrochem. Solid-State Lett. 12 (2009) A107–A110. doi:10.1149/1.3086262.

[57] J. Dong, Y. Ozaki, K. Nakashima, Infrared, Raman, and Near-Infrared Spectroscopic Evidence for the Coexistence of Various Hydrogen-Bond Forms in Poly(acrylic acid), Macromolecules. 30 (1997) 1111–1117. doi:10.1021/ma960693x.

[58] T.S. Shim, J.M. Kim, Soft-, shape changing materials toward physicochemically powered actuators, Korean J. Chem. Eng. 34 (2017) 2355–2365. doi:10.1007/s11814-017-0199-6.

[59] Z.-J. Han, N. Yabuuchi, K. Shimomura, M. Murase, H. Yui, S. Komaba, High-capacity Si–graphite composite electrodes with a self-formed porous structure by a partially neutralized polyacrylate for Li-ion batteries, Energy Environ. Sci. 5 (2012) 9014–9020. doi:10.1039/C2EE22292B.

[60] Z.-J. Han, K. Yamagiwa, N. Yabuuchi, J.-Y. Son, Y.-T. Cui, H. Oji, A. Kogure, T. Harada, S. Ishikawa, Y. Aoki, S. Komaba, Electrochemical lithiation performance and characterization of silicon–graphite composites with lithium, sodium, potassium, and ammonium polyacrylate binders, Phys. Chem. Chem. Phys. 17 (2015) 3783–3795. doi:10.1039/C4CP04939J.

[61] J.C. Grunlan, L. Liu, Y.S. Kim, Tunable Single-Walled Carbon Nanotube Microstructure in the Liquid and Solid States Using Poly(acrylic acid), Nano Lett. 6 (2006) 911–915. doi:10.1021/nl052486t.

[62] K. Saint-Aubin, P. Poulin, H. Saadaoui, M. Maugey, C. Zakri, Dispersion and Film-Forming Properties of Poly(acrylic acid)-Stabilized Carbon Nanotubes, Langmuir. 25 (2009) 13206–13211. doi:10.1021/la9018822.

[63] P.J. Kay, F.E. Treloar, The intrinsic viscosity of poly(acrylic acid) at different ionic strengths: Random coil and rigid rod behaviour, Die Makromolekulare Chemie. 175 (1974) 3207–3223. doi:10.1002/macp.1974.021751114.

[64] G. Staikos, G. Bokias, The intrinsic viscosity of poly(acrylic acid) and partially neutralized poly(acrylic acid) by isoionic dilution, Polymer International. 31 (1993) 385–389. doi:10.1002/pi.4990310412.

[65] Z. Adamczyk, A. Bratek, B. Jachimska, T. Jasiński, P. Warszyński, Structure of Poly(acrylic acid) in Electrolyte Solutions Determined from Simulations and Viscosity Measurements, The Journal of Physical Chemistry B. 110 (2006) 22426–22435. doi:10.1021/jp063981w.

[66] B.R. Alves, W.D. Cooper, Colloid stabilisation by polyelectrolytes. Dispersions of carbon black in aqueous poly(acrylic acid) solution, J. Chem. Soc., Faraday Trans. 1. 77 (1981) 889–896. doi:10.1039/F19817700889.

[67] M. Wiśniewska, A. Nosal-Wiercińska, I. Ostolska, D. Sternik, P. Nowicki, R. Pietrzak, A. Bazan-Wozniak, O. Goncharuk, Nanostructure of Poly(Acrylic Acid) Adsorption Layer on the Surface of Activated Carbon Obtained from Residue After Supercritical Extraction of Hops, Nanoscale Research Letters. 12 (2017) 2. doi:10.1186/s11671-016-1772-3.

[68] J.C. Grunlan, L. Liu, O. Regev, Weak polyelectrolyte control of carbon nanotube dispersion in water, Journal of Colloid and Interface Science. 317 (2008) 346–349. doi:10.1016/j.jcis.2007.08.057.

[69] S. Biggs, T.W. Healy, Electrosteric stabilisation of colloidal zirconia with low-molecular-weight polyacrylic acid. An atomic force microscopy study, J. Chem. Soc., Faraday Trans. 90 (1994) 3415–3421. doi:10.1039/FT9949003415.

[70] I. Szilagyi, G. Trefalt, A. Tiraferri, P. Maroni, M. Borkovec, Polyelectrolyte adsorption, interparticle forces, and colloidal aggregation, Soft Matter. 10 (2014) 2479–2502. doi:10.1039/C3SM52132J.

[71] N. Tsukida, H. Muranaka, M. Ide, Y. Maeda, H. Kitano, Effect of Neutralization of Poly(acrylic acid) on the Structure of Water Examined by Raman Spectroscopy, J. Phys. Chem. B. 101 (1997) 6676–6679. doi:10.1021/jp971210+.

[72] P.S. Bhosale, J.C. Berg, The dynamics of polymer bridge formation and disruption

and its effect on the bulk rheology of suspensions, Langmuir. 28 (2012) 16807–16811.

[73] A. Lee, K. Sudau, K.H. Ahn, S.J. Lee, N. Willenbacher, Optimization of Experimental Parameters to Suppress Nozzle Clogging in Inkjet Printing, Ind. Eng. Chem. Res. 51 (2012) 13195–13204. doi:10.1021/ie301403g.

[74] J.-B. Donnet, ed., Carbon Black: Science and Technology, Second Edition, 2 edition, CRC Press, New York, 1993.

[75] S. Kim, J. Sung, K. Ahn, S. Lee, Drying of the Silica/PVA Suspension: Effect of Suspension Microstructure, Langmuir. 25 (2009) 6155–6161. doi:10.1021/la804112b.

[76] S. Kim, J.H. Sung, K. Hur, K.H. Ahn, S.J. Lee, The effect of adsorption kinetics on film formation of silica/PVA suspension, Journal of Colloid and Interface Science. 344 (2010) 308–314. doi:10.1016/j.jcis.2009.12.046.

[77] W. Bauer, D. Nötzel, V. Wenzel, H. Nirschl, Influence of dry mixing and distribution of conductive additives in cathodes for lithium ion batteries, Journal of Power Sources. 288 (2015) 359–367. doi:10.1016/j.jpowsour.2015.04.081.

[78] S.L. Morelly, N.J. Alvarez, M.H. Tang, Short-range contacts govern the performance of industry-relevant battery cathodes, Journal of Power Sources. 387 (2018) 49–56. doi:10.1016/j.jpowsour.2018.03.039.

[79] S. Jeon, H. Park, J. Yeo, S. Yang, C.H. Cho, M.H. Han, D.K. Kim, Desalination via a new membrane capacitive deionization process utilizing flow-electrodes, Energy Environ. Sci. 6 (2013) 1471–1475. doi:10.1039/C3EE24443A.

[80] F.Y. Fan, W.H. Woodford, Z. Li, N. Baram, K.C. Smith, A. Helal, G.H. McKinley, W.C. Carter, Y.-M. Chiang, Polysulfide Flow Batteries Enabled by Percolating Nanoscale Conductor Networks, Nano Lett. 14 (2014) 2210–2218. doi:10.1021/nl500740t.

[81] G.-W. Lee, J.H. Ryu, W. Han, K.H. Ahn, S.M. Oh, Effect of slurry preparation process on electrochemical performances of LiCoO2 composite electrode, Journal of Power Sources. 195 (2010) 6049–6054. doi:10.1016/j.jpowsour.2009.12.101.

[82] S.J. Weinstein, K.J. Ruschak, Coating Flows, Annual Review of Fluid Mechanics. 36 (2004) 29–53. doi:10.1146/annurev.fluid.36.050802.122049.

[83] M. Schmitt, M. Baunach, L. Wengeler, K. Peters, P. Junges, P. Scharfer, W. Schabel, Slot-die processing of lithium-ion battery electrodes—Coating window characterization, Chemical Engineering and Processing: Process Intensification. 68 (2013) 32–37. doi:10.1016/j.cep.2012.10.011.

[84] J.D. Park, K.H. Ahn, N.J. Wagner, Structure-rheology relationship for a homogeneous colloidal gel under shear startup, Journal of Rheology. 61 (2016) 117–137. doi:10.1122/1.4971993.

[85] N. Koumakis, E. Moghimi, R. Besseling, W.C.K. Poon, J.F. Brady, G. Petekidis, Tuning colloidal gels by shear, Soft Matter. 11 (2015) 4640–4648. doi:10.1039/C5SM00411J.

[86] A.T.J.M. Woutersen, R.P. May, C.G. de Kruif, The shear-distorted microstructure of adhesive hard sphere dispersions: A small-angle neutron scattering study, Journal of Rheology. 37 (1993) 71–88. doi:10.1122/1.550437.

[87] H. Hoekstra, J. Mewis, T. Narayanan, J. Vermant, Multi length scale analysis of the microstructure in sticky sphere dispersions during shear flow, Langmuir. 21 (2005) 11017–11025.

[88] K. Masschaele, J. Fransaer, J. Vermant, Flow-induced structure in colloidal gels: direct visualization of model 2D suspensions, Soft Matter. 7 (2011) 7717–7726. doi:10.1039/C1SM05271C.

[89] B. Rajaram, A. Mohraz, Steady shear microstructure in dilute colloid–polymer mixtures, Soft Matter. 8 (2012) 7699–7707. doi:10.1039/C2SM25936B.

[90] L.C. Hsiao, H. Kang, K.H. Ahn, M.J. Solomon, Role of shear-induced dynamical heterogeneity in the nonlinear rheology of colloidal gels, Soft Matter. 10 (2014) 9254–9259. doi:10.1039/C4SM01375A.

[91] J. Vermant, L. Walker, P. Moldenaers, J. Mewis, Orthogonal versus parallel superposition measurements1, Journal of Non-Newtonian Fluid Mechanics. 79 (1998) 173–189. doi:10.1016/S0377-0257(98)00105-0.

[92] J. Mewis, B. Kaffashi, J. Vermant, R.J. Butera, Determining Relaxation Modes in Flowing Associative Polymers Using Superposition Flows, Macromolecules. 34 (2001) 1376–1383. doi:10.1021/ma000987p.

[93] S. Kim, J. Mewis, C. Clasen, J. Vermant, Superposition rheometry of a wormlike micellar fluid, Rheol Acta. 52 (2013) 727–740. doi:10.1007/s00397-013-0718-2.

[94] S. Khandavalli, J. Hendricks, C. Clasen, J.P. Rothstein, A comparison of linear and branched wormlike micelles using large amplitude oscillatory shear and orthogonal superposition rheology, Journal of Rheology. 60 (2016) 1331–1346. doi:10.1122/1.4965435.

[95] A.R. Jacob, A.S. Poulos, S. Kim, J. Vermant, G. Petekidis, Convective Cage Release in Model Colloidal Glasses, Phys. Rev. Lett. 115 (2015) 218301.

doi:10.1103/PhysRevLett.115.218301.

[96] G. Colombo, S. Kim, T. Schweizer, B. Schroyen, C. Clasen, J. Mewis, J. Vermant, Superposition rheology and anisotropy in rheological properties of sheared colloidal gels, Journal of Rheology. 61 (2017) 1035–1048.

[97] J.D. Ferry, Viscoelastic properties of polymers, Wiley, New York, 1980.

[98] V. Grenard, T. Divoux, N. Taberlet, S. Manneville, Timescales in creep and yielding of attractive gels, Soft Matter. 10 (2014) 1555–1571. doi:10.1039/C3SM52548A.

[99] S.A. Khan, N.J. Zoeller, Dynamic rheological behavior of flocculated fumed silica suspensions, Journal of Rheology. 37 (1993) 1225–1235.

[100] R.A. Lionberger, W.B. Russel, High frequency modulus of hard sphere colloids, Journal of Rheology. 38 (1994) 1885–1908. doi:10.1122/1.550530.

[101] N. Koumakis, M. Laurati, S.U. Egelhaaf, J.F. Brady, G. Petekidis, Yielding of Hard-Sphere Glasses during Start-Up Shear, Phys. Rev. Lett. 108 (2012) 098303. doi:10.1103/PhysRevLett.108.098303.

[102] R.G. Larson, The Structure and Rheology of Complex Fluids, 1 edition, Oxford University Press, New York, 1998.

[103] R.H. Colby, Breakdown of time-temperature superposition in miscible polymer blends, Polymer. 30 (1989) 1275–1278. doi:10.1016/0032-3861(89)90048-7.

[104] Y. Ding, A.P. Sokolov, Breakdown of Time–Temperature Superposition Principle and Universality of Chain Dynamics in Polymers, Macromolecules. 39 (2006) 3322–3326. doi:10.1021/ma052607b.

[105] S. Seiffert, J. Sprakel, Physical chemistry of supramolecular polymer networks, Chem. Soc. Rev. 41 (2012) 909–930. doi:10.1039/C1CS15191F.

[106] M. Doi, S.F. Edwards, The Theory of Polymer Dynamics, Oxford University Press, Oxford, New York, 1988.

[107] A.P. Sokolov, K.S. Schweizer, Resolving the Mystery of the Chain Friction Mechanism in Polymer Liquids, Phys. Rev. Lett. 102 (2009) 248–301. doi:10.1103/PhysRevLett.102.248301.

[108] L.C. Hsiao, R.S. Newman, S.C. Glotzer, M.J. Solomon, Role of isostaticity and load-bearing microstructure in the elasticity of yielded colloidal gels, PNAS. 109 (2012) 16029–16034. doi:10.1073/pnas.1206742109.

[109] R.A. Lionberger, W.B. Russel, High frequency modulus of hard sphere colloids, Journal of Rheology. 38 (1994) 1885–1908. doi:10.1122/1.550530.

[110] T. Shikata, D.S. Pearson, Viscoelastic behavior of concentrated spherical suspensions, Journal of Rheology (1978-Present). 38 (1994) 601–616. doi:10.1122/1.550477.

[111] A.J. Banchio, G. Nägele, J. Bergenholtz, Viscoelasticity and generalized Stokes–Einstein relations of colloidal dispersions, The Journal of Chemical Physics. 111 (1999) 8721–8740. doi:10.1063/1.480212.

[112] I.S. Sohn, R. Rajagopalan, Microrheology of model quasi-hard-sphere dispersions, Journal of Rheology. 48 (2004) 117–142. doi:10.1122/1.1626678.

[113] R. Dannert, H.H. Winter, R. Sanctuary, J. Baller, Influence of suspension viscosity on Brownian relaxation of filler particles, Rheol Acta. 56 (2017) 615–622. doi:10.1007/s00397-017-1019-y.

[114] H. Watanabe, M.-L. Yao, K. Osaki, T. Shikata, H. Niwa, Y. Morishima, N.P. Balsara, H. Wang, Nonlinear rheology and flow-induced structure in a concentrated spherical silica suspension, Rheol. Acta. 37 (1998) 1–6. doi:10.1007/s003970050085.

[115] M.J. Lázaro, L. Calvillo, V. Celorrio, J. Pardo, S. Perathoner, R. Moliner, Study and application of Vulcan XC-72 in low temperature fuel cells, 2011.

[116] Z.Y. Liu, J.L. Zhang, P.T. Yu, J.X. Zhang, R. Makharia, K.L. More, E.A. Stach, Transmission Electron Microscopy Observation of Corrosion Behaviors of Platinized Carbon Blacks under Thermal and Electrochemical Conditions, J. Electrochem. Soc. 157 (2010) B906–B913. doi:10.1149/1.3391737.

카본블랙 나노입자를 포함하는 입자 분산계 재료의 유변학적 거동 연구

성상훈
서울대학교 화학생물공학부

국문초록

카본블랙 분산계의 유변학적 성질은 학술 및 산업의 관점에서 높은 중요성을 가지며, 최근에는 리튬이온전지 산업의 성장으로 인해 더욱 주목을 받고 있다. 카본블랙 분산계는 오랫 동안 수많은 연구가 이루어져 왔음에도 불구하고 아직 잘 알려지지 않거나 명확하게 이해되지 않은 부분이 있다. 본 논문에서는 카본블랙을 함유 한 다양한 현탁액의 유변학적 거동을 연구하였으며, 특히 상당 부분이 리튬이온전지의 전극 슬러리 공정을 중심에 둔 관점에서 진행되었다. 먼저, NMP계와 수계 슬러리 내에서 조성물간 상호작용에 어떠한 차이가 있는지를 연구하였고, 비슷한 관점에서 PAA를 바인더로 사용한 슬러리에서 중화도에 따른 유변물성과 분산성 차이를 확인하였다. 두 가지 경우에 모두 슬러리는 입자와 바인더간의 상호 작용 차이에 따라 젤 또는 액체에 가까운 유변학적 거동을 나타냈다. 또한 조성물간 상호작용에 대한 이해를 바탕으로, NMP 기반 양극슬러리의 독특한 유변학적 거동을 연구하였다. 유동 중 물성변화의 메커니즘은 카본블랙 입자의 응집에 기인하는 것으로 확인되었고, 응집의 발생 조건을 현탁 매질의 유체역학적 응력 측면에서 해석하였다. 이어지는 장에서는 카본블랙과 뉴턴유체 매질로 구성된 모델 콜로이드 젤을 사용하여, 카본블랙 분산계의 보편적인 스케일링 거동을 연구하였다. 특히, 직교 중첩 유변학을 이용하여 전단 하에서 콜로이드 젤이 전단 속도에 관계없이 보편적인 이완거동을 나타냄으로써 “시간 전단 속도 중첩”이 발생함을 최초로 보였다.

주요어: 유변학, 카본블랙, 콜로이드 젤, 리튬이온전지, 전극슬러리, 분산성

학번: 2011-21041